

Project: Reduced models in DIANA

A fast method for preliminary assessment of concrete structures with nonlinear finite element analysis

**Report #1**

**Calculation of benchmarks with a shear beam model**

Faculty of Civil Engineering and Geosciences  
Structural Mechanics Section  
Report number: TUD/CITG/B&I/CM-2015-13

*Author:*

Dr. Denise C. S. Ferreira

[D.C.SantosFerreira@tudelft.nl](mailto:D.C.SantosFerreira@tudelft.nl)

*Participants:*

Prof. dr.ir. Max A.N. Hendriks

[M.A.N.Hendriks@tudelft.nl](mailto:M.A.N.Hendriks@tudelft.nl)

Dr. ir. Ane de Boer

[Ane.de.Boer@rws.nl](mailto:Ane.de.Boer@rws.nl)

Prof. dr. ir. Jan Rots

[J.G.Rots@tudelft.nl](mailto:J.G.Rots@tudelft.nl)

DATE: April 2015



# CONTENTS

1.	INTRODUCTION .....	7
1.1	Background .....	7
1.2	Scope and objectives .....	7
1.3	Outline .....	8
2	SHEAR-SENSITIVE FIBRE BEAM MODEL. BASIS FORMULATION .....	9
2.1	Overview .....	9
2.2	Shear model .....	10
2.2.1	Constitutive model for concrete .....	10
2.2.2	Constitutive model for the reinforcement .....	12
2.2.3	Sectional model and fibre state determination .....	12
2.2.4	Element formulation .....	16
2.3	Longitudinal prestressing .....	18
2.4	Transversal prestressing .....	18
2.5	Time-dependent effects .....	19
2.6	Procedure for nonlinear, phased and time-dependent analysis .....	20
2.7	Simulation of repair and strengthening interventions .....	21
2.8	Representation of cracking .....	23
3	RECALCULATION OF PREVIOUS WORKS: REINFORCED CONCRETE BEAMS .....	25
3.1	Case RB1: Vecchio & Shim (2004) .....	25
3.1.1	Experimental setup and results .....	25
3.1.2	Finite element model CONSHEAR .....	26
3.1.3	Nonlinear finite element analysis .....	27
3.1.4	Analysis with beam models in DIANA 9.6 .....	30
3.1.5	Concluding remarks .....	34
3.2	Case RB2: Collins & Kuchma (1999) .....	35
3.2.1	Experimental setup and results .....	35
3.2.2	Finite element model .....	37
3.2.3	Nonlinear finite element analysis .....	37
3.2.4	Analysis with beam models in DIANA 9.6 .....	42
3.2.5	Concluding remarks .....	44
3.3	Case RB3: Grace (2001) .....	45
3.3.1	Experimental setup and results .....	45
3.3.2	Finite element model .....	46

3.3.3	Nonlinear finite element analysis.....	47
3.3.4	Concluding remarks.....	51
<b>3.4</b>	<b>Case RB3A: Grace (2001)</b> .....	<b>51</b>
3.4.1	Experimental setup and results.....	51
3.4.2	Finite element model.....	52
3.4.3	Nonlinear finite element analysis.....	52
3.4.4	Concluding remarks .....	56
<b>4</b>	<b>RECALCULATION OF PREVIOUS WORKS: PRESTRESSED CONCRETE BEAMS</b> .....	<b>57</b>
<b>4.1</b>	<b>Case PB1: Leonhardt, Koch et al. (1975)</b> .....	<b>57</b>
4.1.1	Experimental setup and results.....	57
4.1.2	Finite element model.....	59
4.1.3	Nonlinear finite element analysis.....	61
4.1.4	Concluding remarks .....	65
<b>4.2</b>	<b>Case PB2/NSEL: Sun and Kuchma (2007)</b> .....	<b>66</b>
4.2.1	Experimental setup and results.....	66
4.2.2	Finite element model.....	67
4.2.3	Nonlinear finite element analysis.....	69
4.2.4	Concluding remarks .....	73
<b>4.3</b>	<b>Case PB3/MnDOT: Runzell et al. (2007)</b> .....	<b>74</b>
4.3.1	Experimental setup and results.....	74
4.3.2	Finite element model.....	77
4.3.3	Nonlinear finite element analysis.....	78
4.3.4	Concluding remarks .....	82
<b>5</b>	<b>NEW CASE STUDIES</b> .....	<b>83</b>
<b>5.1</b>	<b>Cases of the DIANA User’s Contest: large T-shaped prestressed concrete girders tested at TU Delft (Tests A – original load position)</b> .....	<b>83</b>
5.1.1	Experimental test, contest and results.....	83
5.1.2	Finite element model.....	86
5.1.3	Nonlinear finite element analysis.....	89
5.1.4	Concluding remarks .....	91
<b>5.2</b>	<b>Cases of the DIANA User’s Contest: large T-shaped prestressed concrete girders tested at TU Delft (Tests B – new load position)</b> .....	<b>91</b>
<b>5.3</b>	<b>Case OA1: Vecchio &amp; Shim (2004)</b> .....	<b>92</b>
5.3.1	Experimental setup and results.....	92
5.3.2	Finite element model.....	93
5.3.3	Nonlinear finite element analysis.....	94
5.3.4	Concluding remarks .....	96
<b>5.4</b>	<b>Case OA3: Vecchio &amp; Shim (2004)</b> .....	<b>96</b>

5.4.1	Experimental setup and results.....	96
5.4.2	Finite element model.....	97
5.4.3	Nonlinear finite element analysis.....	98
5.4.4	Concluding remarks .....	100
6	CONCLUSIONS AND FUTURE WORK .....	101
6.1.1	Summary of results .....	101
6.1.2	Remarks .....	103
	Acknowledgments.....	104
	REFERENCES .....	105



## 1. INTRODUCTION

Fiber models for beam and shell elements allow for relatively rapid finite element analysis of concrete structures and structural elements. This project aims at the development of the formulation of such elements and a pilot implementation. This first report describes the preliminary analysis and validation of the layered beam formulation within the software developed at Universitat Politècnica de Catalunya (UPC) - CONSHEAR.

### 1.1 Background

In 2012, the document RTD 1016: 2012 "Guidelines for Nonlinear Finite Element Analysis of Concrete Structures. Scope: Girder Members" (RTD1016 2012) was completed. With these guidelines it is possible to perform sophisticated nonlinear finite element analyses (NLFEA) and determine, as far as possible, existing residual capacities in structures. In 2014, a document 'Validating the Guidelines for Nonlinear Finite Element Analysis of Concrete Structures' (authors: Max A.N. Hendriks, Beatrice Belletti, Cecilia Damoni, Ane de Boer) will be completed. It includes the validation of the guidelines by means of various benchmarks of RC beams, prestressed beams and slabs, involving different modelling variations. Numerical simulations were performed with 2D (plane stress) and 3D (solids) continuum nonlinear finite element models.

The present project will continue this work by extending the case studies analysed, expand the library of objects available, perform systematic studies with NLFEM, include a 1D nonlinear model for faster analysis that is advantageous for pre- and quick scan assessment stages.

Standard nonlinear fibre beam formulations do not account for shear effects and cannot capture all failure modes (like shear failure) and hence cannot be used in the assessment of structures with shear problems, as it may result in large overestimations of ultimate carrying capacities. This issue has been remedied by the new shear-sensitive fibre beam formulation developed by (Ferreira 2013) at UPC.

This 1D fibre beam model accounts for bending-shear force interactions in a computationally efficient manner enabling nonlinear, time-dependent and strengthening analysis of shear critical concrete frame structures. The model acts as an efficient alternative and/or reference to the more sophisticated 2D (plane stress) and 3D (solid) nonlinear FE models for usage in practical engineering. The reduction of calculation time and degrees of freedom and the few required input variables are advantages of the 1D model. Due to its simplified formulation, the 1D fibre beam model can be advantageous for blind structural assessment (Ferreira, Bairán and Marí 2014a), (Ferreira, Bairán and Marí 2014b).

In this project, this shear-sensitive fibre beam model will be inserted in the software DIANA and extended to plate/shell elements. The analysis with the new 1D model in DIANA will be compared with the 2D (plane stress). Experimental tests published national and internationally will be selected for validation purposes as benchmarks. The goal is to sharpen the existing guidelines and to insert the 1D quick scan model in the flow of evaluation and decision process regarding strengthening and dismantling of infrastructure.

This report relates to the preliminary analysis and validation of the fibre beam model with calculation of existing and new benchmarks and comparison with plane stress models in DIANA performed by (RTD1016b, Hendriks et al. 2015) and with beam elements in DIANA.

### 1.2 Scope and objectives

The initial phase of the project includes analysing existing benchmarks and a few new benchmarks with:

- The fibre beam formulation within the UPC software (CONSHEAR);

- Existing beam elements in DIANA and studying the performance of different beam types, number of integration points, constitutive laws and integration schemes (in some cases only);
- Existing published results of 2D plane stress analyses in DIANA performed by Hendriks and Belletti et al. (2014).

The objective is to compare the various analyses between them and with the available experimental results, cross-validate and conclude about the performance of the shear-sensitive beam element and set main goals of enhancements in the future implementation in DIANA.

### 1.3 Outline

The present report is divided into 6 chapters.

**Chapter 1** is the present introduction.

**Chapter 2** presents the theory of the shear-sensitive fibre beam model developed by Ferreira, Bairán and Marí at UPC. This chapter refers only to the fundamentals of the model as the detailed formulations are available in published works, included as references along the text.

**Chapter 3** presents the recalculation of previous cases of reinforced concrete beams. Here the results of the beam element model CONSHEAR are compared with the results of simulations with 2D plane stress analyses with DIANA performed by Hendriks and Belletti et al. (2014) and with experimental data. In two of these cases, analysis with beam elements in DIANA are presented and also some studies relating with the performance of different class of elements in DIANA, number of integration points along the height of the cross section, solution procedures and material constitutive approaches for cracking.

The existing studies for re-calculation include:

- Case RB1\*: Vecchio & Shim (2004) – bending failure mechanism
- Case RB2\*: Collins & Kuchma (1999) – diagonal shear-tension failure mechanism
- Case RB3: Grace (2001) – bending failure mechanism
- Case RB3A: Grace (2001) – shear failure mechanism  
(\* analysed with beam elements in DIANA)

**Chapter 4** presents the calculation of previous cases of prestressed concrete beams. The analyses performed with CONSHEAR are compared with the results of the simulations performed with 2D plane stress models in DIANA by Hendriks and Belletti et al. (2014) and with existent experimental data.

The existing studies for re-calculation include:

- Case PB1/IP1: Leonhardt, Koch et al. (1973) – flexural compressive failure mechanism
- Case PB2/NSEL: Sun and Kuchma (2007) – shear-compression failure mechanism
- Case PB3/MnDOT: Runzell et al. (2007) – diagonal tension failure mechanism

**Chapter 5** presents new examples calculated with the fibre beam model CONSHEAR and compared with existent experimental data.

The new case studies include:

- Cases of Diana User's Contest in Parma: large scale T-shaped prestressed concrete girders tested in TU Delft
- Cases OA1 & OA3: Vecchio & Shim (2004) / Bresler & Scordelis (1963) – RC beams with brittle shear failure

**Chapter 6** resumes the results and outlines the main conclusions. Guidelines and ambitions for future works are also stated.

## 2 SHEAR-SENSITIVE FIBRE BEAM MODEL. BASIS FORMULATION

### 2.1 Overview

In traditional fibre beam models, the Navier-Bernoulli plane section theory and the use of a fibre sectional discretization combined with adequate uniaxial constitutive laws, allows fairly accurate analyses of flexural dominant RC frames to be obtained (Marí 2000). When tangential forces are applied, the plane section hypothesis is no longer valid due to the appearance of distortion. In attempting to extend frame models to loading conditions that include shear effects, several theories for the sectional response under tangential and normal forces were developed with different levels of complexity and computational demanding (Bairán and Marí 2007).

The 1D fibre beam model CONSHEAR (Figure 2.1-1) accounts for axial force-bending-shear force interactions in the nonlinear structural response. It is a displacement-based fibre beam FE formulation for the nonlinear, time-dependent and strengthening analysis of reinforced concrete (RC) and prestressed concrete (PC) frame structures. It is based on the Timoshenko 3D beam theory with the cross section discretized into fibres, the longitudinal reinforcement simulated by means of steel filaments and transversal reinforcement considered smeared in the concrete fibres. At the sectional level, a shear-sensitive model accounts for the 2D interaction of axial force – bending moment – shear force (N-M-V). The Timoshenko beam theory is linked with a shear-sensitive sectional model that associates the Bernoulli-Navier plane section theory with an assumption of fixed shear stress pattern. Cracking is simulated through the smeared and rotating crack approach. The effects of shear and its interaction with normal forces are accounted in all levels of damage, from SLS and ULS. This allows including the effects of shear in deflections, strains in concrete and reinforcement and cracking behaviour in addition to capture shear failure mechanisms. The time step-by-step analysis allows the simulation of segmental construction procedures and subsequent later changes, in which repair and strengthening interventions are included. The nonlinear analysis is performed within a Newton-Raphson framework.

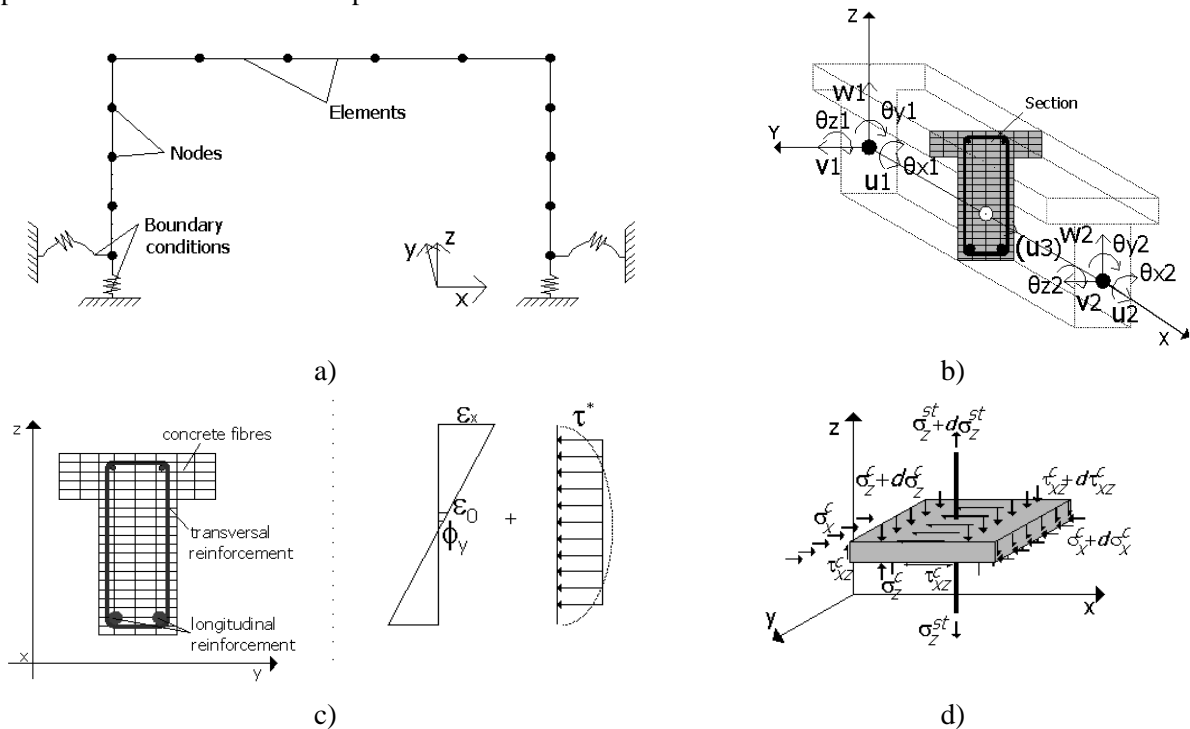


**Figure 2.1-1:** Fundamentals of CONSHEAR model: a) structural, b) element, c) section and d) fibre levels

The model, which detailed description is found in the publications (Ferreira 2013, Ferreira, Bairán et al. 2014), was validated and applied to several different studies of the concrete structural behaviour in which shear effects are relevant:

- Time-dependent response in (Ferreira, Bairán et al. 2015);
- Service analysis (Ferreira, Oller et al. 2015);
- Shear strengthening measures in (Ferreira, Bairán et al. 2013, Ferreira, Oller et al. 2013, Ferreira, Bairán et al. 2014);
- Linked to an thermo-mechanical model for early age behaviour of concrete to analyse the structural response since early ages in (Ferreira, Crespo et al. 2014);
- Assessment of existing structures in (Ferreira, Marí et al. 2013, Ferreira, Bairán et al. 2014).

In the following a brief description of the key characteristics of the model is presented.

## 2.2 Shear model

The proposed shear model is devised for the analysis of 3D frame concrete structures under combined axial, bending and shear forces. Nonlinear interaction of normal and tangential forces is accounted only at 2D level. In general, its main characteristics are: the Timoshenko beam theory is assumed at the element level; a hybrid sectional formulation, in which input variables comprises both kinematical and force quantities, links the plane section theory with the assumption of a constant shear stress flow. The multiaxial constitutive behaviour of concrete is assumed through a smeared crack approach with full rotating cracks; compression weakening (softening) and tensile tension stiffening effects are included. Longitudinal reinforcement is simulated through the use of steel filaments while transversal reinforcement is considered smeared in the concrete fibres.

### 2.2.1 Constitutive model for concrete

A smeared cracked approach is assumed to model the constitutive behaviour of concrete (Figure 2.2-1). The adopted concrete 2D constitutive law is a nonlinear uniaxial equivalent model formulated in terms of average principal strains  $\underline{\varepsilon}_{12}=[\varepsilon_1 \varepsilon_2]^T$  and stresses  $\underline{\sigma}_{12}=[\sigma_1 \sigma_2]^T$  in which the principal directions of strain and stress tensors are assumed to be coincident (subscript '1' represents the tensile principal strains and stresses – assumed as positive and subscript '2' represents the compressive strains and stresses – assumed as negative). The backbone equation for concrete in compression is the Hognestad parabola (Figure 2.2-2a)

$$\sigma_2 = f_p \left( 2 \left( \frac{\varepsilon_2}{\varepsilon_p} \right) - \left( \frac{\varepsilon_2}{\varepsilon_p} \right)^2 \right) \quad (1)$$

where  $\varepsilon_p$  is the strain at the peak stress  $f_p$ , being the latter a function of the 1D compressive strength of concrete  $f_c$  as

$$f_p = \beta k_{ci} f_c \quad (2)$$

$$\beta = \frac{1}{0.85 - 0.27 \frac{\varepsilon_1}{\varepsilon_2}} \leq 1.0 \quad (3)$$

$$k_{ci} = 1 + 0.92 \left( \frac{-\sigma_j}{f_c} \right) - 0.76 \left( \frac{-\sigma_j}{f_c} \right)^2 \geq 1.0 \quad (4)$$

Factor  $\beta$  (Vecchio and Collins 1986) accounts for the compression softening for biaxial tension-compression state, when tensile cracking exists in the orthogonal direction to the principal compression. Factor  $k_{ci}$  (Kupfer, Hilsdorf et al. 1969) takes into account the compression strength enhancement in biaxial compression state. The stiffness modulus  $E_2$  is taken as an approximation of tangent elasticity modulus which is determined through the derivation of the backbone curve for concrete in compression, neglecting the variations of both softening and strength enhancement factors as shown in Eq. (5). This allows a symmetric constitutive matrix of cracked concrete.

Possible errors of not having an “exact” tangent modulus are accounted for in the nonlinear iterations of the model.

$$E_2 = f_p \left( \frac{2}{\varepsilon_p} - 2 \left( \frac{\varepsilon_2}{\varepsilon_p} \right) \right) \quad (5)$$

The plastic behaviour of concrete in compression that takes place during loading is considered through the plastic strain  $\varepsilon_2^p$ :

$$\varepsilon_2^p = \varepsilon_2 - \frac{\sigma_2}{E_0} \quad (6)$$

Unloading and partial reloading is performed through straight lines parallel to the initial stiffness  $E_0$  which is the elasticity modulus of concrete.

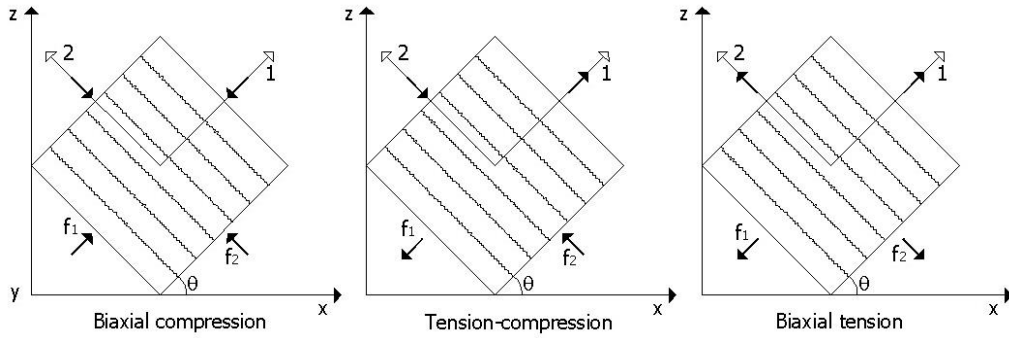


**Figure 2.2-1:** CONSHEAR model. Concrete stress states

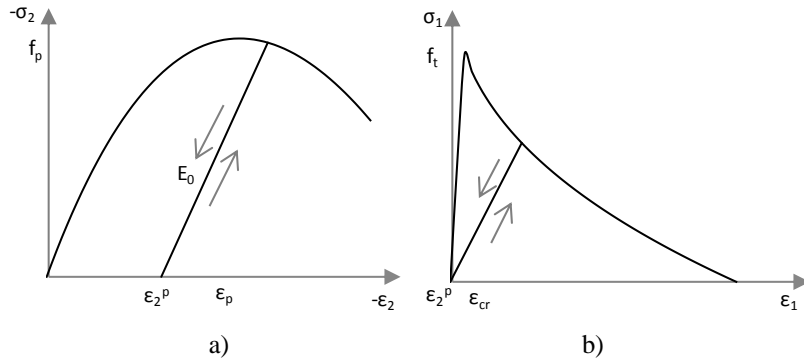


**Figure 2.2-2:** CONSHEAR model. Concrete constitutive behaviour: (a) in compression and (b) in tension

Before the beginning of cracking, concrete in tension (Figure 2.2-2b) has a linear elastic behaviour where  $\varepsilon_{cr}$  is the strain that corresponds to the peak tensile stress  $f_t$ . If the material has not been in compression before, the plastic strain  $\varepsilon_2^p$  is null, otherwise it acts like an offset. After cracking tension softening is represented by the (Cervenka 1985) curve; following recommendations of previous studies (Mohr, Bairán et al. 2010), its parameters are  $c=\varepsilon_{sy}$  and  $k_2=0.5$ , where  $\varepsilon_{sy}$  is the yielding strain of reinforcement, implying that tension stiffness is assumed to vanish after reinforcement yielding:

$$\sigma_1 = \begin{cases} E_0 (\varepsilon_1 - \varepsilon_2^p) & 0 \leq \varepsilon_1 \leq \varepsilon_{cr} \\ f_t \left[ 1 - \left( \frac{\varepsilon_1}{c} \right)^{k_2} \right] & \varepsilon_1 \geq \varepsilon_{cr} \end{cases} \quad (7)$$

Softening is taken into account through the use of the damage variable  $d_{tI}$

$$dt_1 = \begin{cases} 0 & 0 \leq \varepsilon_1 \leq \varepsilon_{cr} \\ 1 - \frac{\sigma_1}{E_0(\varepsilon_1 - \varepsilon_2^p)} \leq 1 & \varepsilon_1 \geq \varepsilon_{cr} \end{cases} \quad (8)$$

The secant elasticity modulus  $E_I$  is determined through the use of the damage variable as

$$E_I = (1 - dt_1)E_0 \quad (9)$$

Unloading and partial reloading performs by the straight line function:

$$\sigma_1 = (1 - dt_1)E_0(\varepsilon_1 - \varepsilon_2^p) \quad (10)$$

with the damage variable  $dt_1$  remaining constant during these phases.

In the principal axes, the 2D stress-strain state of concrete can be written as

$$\begin{Bmatrix} \sigma_1 \\ \sigma_2 \\ \tau_{12} \end{Bmatrix} = D_{12} \begin{Bmatrix} \varepsilon_1 \\ \varepsilon_2 \\ \gamma_{12} \end{Bmatrix} \quad \text{with} \quad D_{12} = \begin{pmatrix} E_1 & 0 & 0 \\ 0 & E_2 & 0 \\ 0 & 0 & G_{12} \end{pmatrix} \quad (11)$$

where the shear modulus is determined accordingly to the requirement that the angles of the principal directions of the stresses and strains are the same (Bazant 1983):

$$G_{12} = \frac{\sigma_1 - \sigma_2}{2(\varepsilon_1 - \varepsilon_2)} \quad (12)$$

### 2.2.2 Constitutive model for the reinforcement

Steel reinforcement is modelled with a bilinear 1D constitutive relationship in which  $f_{sy}$  and  $\varepsilon_{sy}$  are the yielding stress and strain and  $f_{su}$  and  $\varepsilon_{su}$  are the ultimate stress and strain, respectively (Figure 2.2-3). Unloading and partial reloading are performed along straight lines parallel to the initial elastic branch given by the elasticity modulus  $E_s$ .

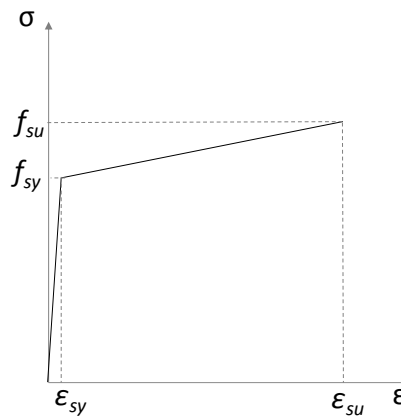


**Figure 2.2-3:** CONSHEAR model. Steel constitutive behaviour

### 2.2.3 Sectional model and fibre state determination

The model uses a simplified sectional formulation that links the plane section theory with the assumption of fixed shear stress along the cross section. This assumption results into a hybrid approach as the input variables comprises both kinematical quantities, in terms of curvature and axial beam's strain, and the applied shear force. The output of the sectional model is the axial force, bending moment and shear deformation. Figure 2.2-4 presents a scheme of the inputs and outputs of the sectional model in CONSHEAR. The fixed stress approach used in the model, although not guaranteeing compatibility between the fibres, gives satisfactory results in the simulation of the shear-resistant mechanism of reinforced cracked concrete cross-sections at a low computational and modelling cost, as concluded in (Bairán and Marí 2007).

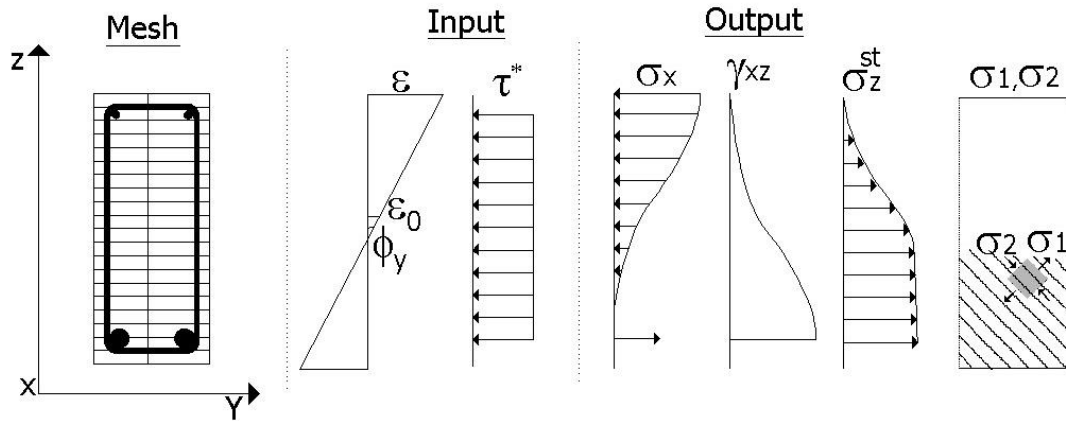


Figure 2.2-4: CONSHEAR model. Sectional model

The cross-section is discretized into two types of fibres as presented in Figure 2.2-5: a) non shear resistant ones, submitted only to 1D axial stresses, and b) shear resistant fibres submitted to a multiaxial stress-strain state (see Figure 2.2-6). This division is performed considering the following criteria:

- i) for traditional cross section geometries, such as, rectangular, T-shape and I-shape, it is considered that the fibres that pertain to the web (disregarding the cover area) are 2D fibres;
- ii) particularly for the T-shape and I-shapes cross sections, an effective area of the compressive flanges can be considered to contribute to the shear-resistance mechanism and assigned as 2D fibres - the effective width of the flange  $b_{ef}$  can be determined accordingly to (Zararis, Karaveziroglou et al. 2006);
- iii) for complex geometries a more sophisticated analysis with the model TINSA (Bairán and Marí 2006, Bairán and Marí 2006) is required in order to determine the portion of section that is preponderant for resisting shear forces; however in these cases, existent recommendations in some design codes (for example, the parameter  $b_w$  in EC2 (Zwicky and Vogel 2000)) can be used as a simplified criterion.

Option *i*) is the default in the model.

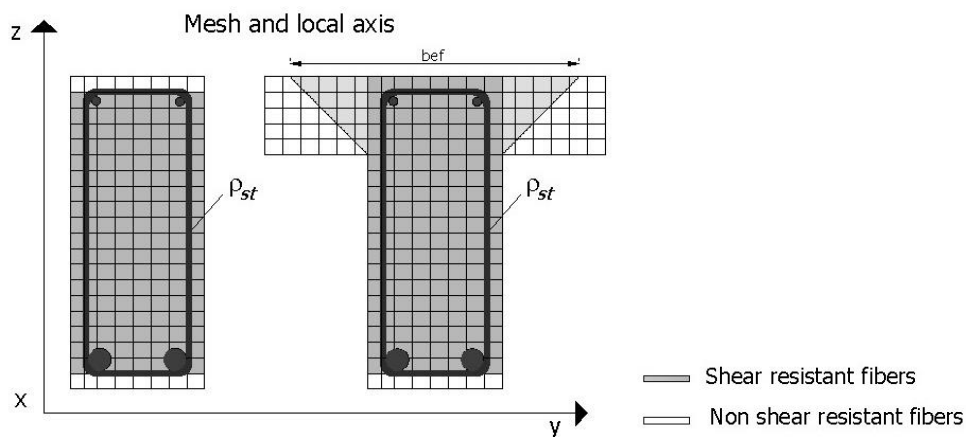
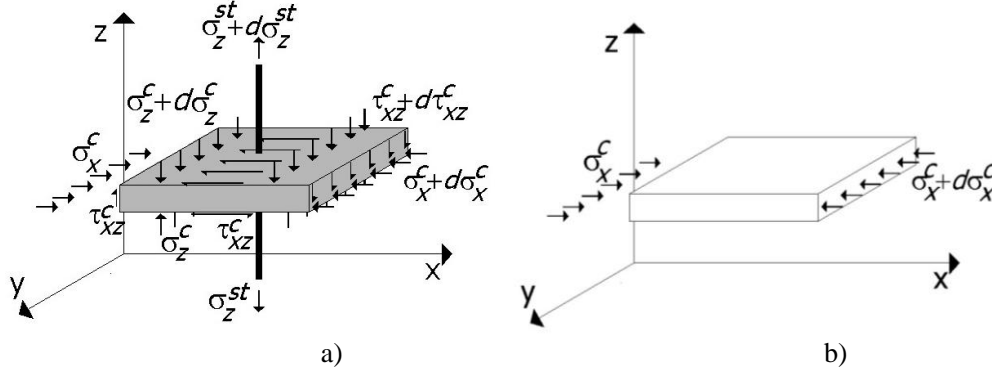


Figure 2.2-5: CONSHEAR model. Types of fibres in the sectional level



**Figure 2.2-6:** CONSHEAR model. Stress state in the fibres: a) shear resistant and b) non shear resistant

Axial strain orthogonal to the cross-section ( $\varepsilon_x$ ) is computed, in all fibres, by means of the Navier-Bernoulli plane section assumption:

$$\varepsilon_x(z) = \varepsilon_0 + \phi_y \cdot z \quad (13)$$

where  $\varepsilon_0$  is the axial strain of the reference axis of the section and  $\phi_y$  is the curvature of the cross-section with respect to the y-axis. In the shear resistant fibres a constant shear stress  $\tau^*$  flow along the section is assumed as:

$$\tau^* = G^* A^* \gamma_0 \quad (14)$$

where  $G^*$  is the transversal modulus,  $\gamma_0$  is the distortion at the neutral axis and the effective shear area  $A^*$  is given by the summation of the areas of the shear resistant fibres. By these means and using the equilibrium, compatibility and constitutive equations, the complete 2D stress-strain state and the stiffness matrix of the fibre are determined.

The concrete part of the shear resistant fibre is submitted to a 2D stress-strain state (Eq. 15); after rotating the principal stiffness to the local referential, a  $3 \times 3$  stiffness matrix  $D_c$  is obtained. A concrete fibre can have different  $n_k$  configurations of transversal steel (and different material properties) that are accounted for in the model through its volumetric ratio  $\rho_{st,k}$  and are submitted to axial stresses  $\sigma_{z,k}^{st}$  (along direction z). According to Eq. (16) the total transversal steel is taken into account by the summation of the contributions of the different stirrups configurations ( $A_{st,k}$  is the area of transversal steel,  $b_k$  is the width of the cross-section and  $s_k$  is the longitudinal spacing of each configuration of stirrups  $k$ ). Compatibility requirements impose that the vertical strain  $\varepsilon_z$  in concrete is equal to the strain in the transversal reinforcement.

$$\begin{pmatrix} \Delta \sigma_x \\ \Delta \sigma_z \\ \Delta \tau_{xz} \end{pmatrix}^c = D_c \begin{pmatrix} \Delta \varepsilon_x \\ \Delta \varepsilon_z \\ \Delta \gamma_{xz} \end{pmatrix} \quad D_c = \begin{pmatrix} D_{11} & D_{12} & D_{13} \\ D_{21} & D_{22} & D_{23} \\ D_{31} & D_{32} & D_{33} \end{pmatrix} \quad (15)$$

$$\begin{pmatrix} 0 \\ \Delta \sigma_z \\ 0 \end{pmatrix}^{st} = D_{st} \begin{pmatrix} 0 \\ \Delta \varepsilon_z \\ 0 \end{pmatrix} \quad D_{st} = \begin{pmatrix} 0 & 0 & 0 \\ 0 & \rho_{st} E_{st} & 0 \\ 0 & 0 & 0 \end{pmatrix} \quad \rho_{st} E_{st} = \sum_{k=1}^{n_k} \left( \frac{A_{st,k}}{s_k b_k} E_{st,k} \right) \quad (16)$$

Along the z direction the incremental tensile stresses in the transversal steel  $\Delta \sigma_z^{st}$  must equilibrate the incremental compression stresses in concrete  $\Delta \sigma_z^c$ :

$$\Delta\sigma_z^c + \rho_{st}\Delta\sigma_z^{st} = 0, \quad \rho_{st}\Delta\sigma_z^{st} = \sum_{k=1}^{n_k} \left( \frac{A_{st,k}}{s_k b_k} \Delta\sigma_{z,k}^{st} \right) \quad (17)$$

In addition to this equilibrium requirement, the other condition to be fulfilled in order to determine the fibre state is: the computed increment of shear stress  $\Delta\tau_{xz}$  must equate the impose shear stress given by the fixed stress constraint  $\Delta\tau^*$  as

$$\Delta\tau^* - \Delta\tau_{xz} = 0 \quad (18)$$

By solving the the system composed by Eqs. (17) and (18) – and making use of Eqs. (15) and (16) - the unknown increments of vertical axial strain  $\Delta\varepsilon_z$  and shear strain  $\Delta\gamma_{xz}$  are determined as functions of the increments of the longitudinal axial strain  $\Delta\varepsilon_x$ , the shear stress  $\Delta\tau^*$  and the material stiffness matrix  $D_{fibre}$ .

$$\Delta\varepsilon_z = f(\Delta\varepsilon_x, \Delta\tau^*, D_{fibre}) = \frac{(D_{23}D_{31} - D_{33}D_{21})\Delta\varepsilon_x - D_{23}\Delta\tau^*}{\overline{D_{22}D_{33}} - D_{23}D_{32}} \quad (19)$$

$$\Delta\gamma_{xz} = f(\Delta\varepsilon_x, \Delta\tau^*, D_{fibre}) = \frac{(D_{23}D_{21} - \overline{D_{22}D_{31}})\Delta\varepsilon_x + \overline{D_{22}}\Delta\tau^*}{\overline{D_{22}D_{33}} - D_{23}D_{32}} \quad (20)$$

To achieve both requirements along the vertical and transversal directions (Eqs. (17) and (28), respectively), an innermost iterative procedure within the fibre level is needed. After computation of the 2D fibre strain and stress states, Eqs. (17) and (18) are checked and the unbalanced vertical  $\delta\sigma_z$  and tangential  $\delta\tau_{xz}$  stresses are respectively computed as

$$\delta\sigma_z = -\rho_{st}\Delta\sigma_z^{st} + \Delta\sigma_z^c \quad (21)$$

$$\delta\tau_{xz} = \Delta\tau^* - \Delta\tau_{xz} \quad (22)$$

The increment of longitudinal axial strain  $\Delta\varepsilon_x$  is kept fixed and the iteration goes through the correction of the vertical  $\delta\varepsilon_z$  and transversal  $\delta\gamma_{xz}$  strains, which are computed through the following expressions as functions of the unbalanced stresses  $\delta\sigma_z$  and  $\delta\tau_{xz}$ :

$$\delta\varepsilon_z = f(\delta\tau_{xz}, \delta\sigma_z, D_{fibre}) = \frac{\delta\sigma_z D_{33} - D_{23}\delta\tau_{xz}}{D_{22}D_{33} - D_{32}D_{23}} \quad (23)$$

$$\delta\gamma_{xz} = f(\delta\tau_{xz}, \delta\sigma_z, D_{fibre}) = \frac{\delta\tau_{xz} \overline{D_{22}} - D_{32}\delta\sigma_z}{D_{22}D_{33} - D_{32}D_{23}} \quad (24)$$

The complete mathematic derivations of the fibre state determination are presented in (Ferreira, Bairán et al. 2014). The strain corrections ( $\Delta\varepsilon_z^{it}$ ,  $\Delta\gamma_{xz}^{it}$ ) are introduced in the next iteration until both the unbalanced vertical  $\delta\varepsilon_z$  and tangential stresses  $\delta\tau_{xz}$  vanish:

$$\Delta\varepsilon_z^{it} = \Delta\varepsilon_z + \delta\varepsilon_z \quad (25)$$

$$\Delta\gamma_{xz}^{it} = \Delta\gamma_{xz} + \delta\gamma_{xz} \quad (26)$$

Once this iteration procedure is finished and convergence is achieved (i.e.  $\delta\varepsilon_z \approx 0$  and  $\delta\tau_{xz} \approx 0$ ) the state determination of the fibre is accomplished. As stress  $\sigma_z$  is null and the section model does not include  $\varepsilon_z$ , a static condensation may be applied:

$$\begin{pmatrix} \sigma_x \\ 0 \\ \tau_{xz} \end{pmatrix} = \begin{pmatrix} D_{11} & D_{12} & D_{13} \\ D_{21} & \overline{D_{22}} & D_{23} \\ D_{31} & D_{32} & D_{33} \end{pmatrix} \begin{pmatrix} \varepsilon_x \\ \varepsilon_z \\ \gamma_{xz} \end{pmatrix} \quad (27)$$

and thus

$$\begin{pmatrix} \sigma_x \\ \tau_{xz} \end{pmatrix} = K_{fibre} \begin{Bmatrix} \varepsilon_x \\ \gamma_{xz} \end{Bmatrix} ; K_{fibre} = \begin{pmatrix} D_{11} - \frac{D_{12}D_{21}}{D_{22}} & D_{13} - \frac{D_{12}D_{23}}{D_{22}} \\ D_{31} - \frac{D_{32}D_{21}}{D_{22}} & D_{33} - \frac{D_{32}D_{23}}{D_{22}} \end{pmatrix} \quad (28)$$

where  $K_{fibre}$  is the condensed stiffness matrix of the fibre. The shear modulus in Eq. (14) is given by

$$G^* = D_{33} - \frac{D_{32}D_{23}}{D_{22}} \quad (29)$$

#### 2.2.4 Element formulation

A 2-noded Timoshenko 3D FE with linear shape functions is implemented (Figure 2.2-7). Nonlinear interaction of axial force and bending moment is accounted at the full 3D level. Nonlinear interaction of normal and tangential forces is accounted only at 2D level. In the Timoshenko beam theory it is assumed that non-deformed plane sections perpendicular to the beam axis remain plane but not necessarily normal to the longitudinal axis after deformation. An average rotation of the section due to distortion  $\gamma_0$  is considered in order to maintain valid the plane-section assumption.

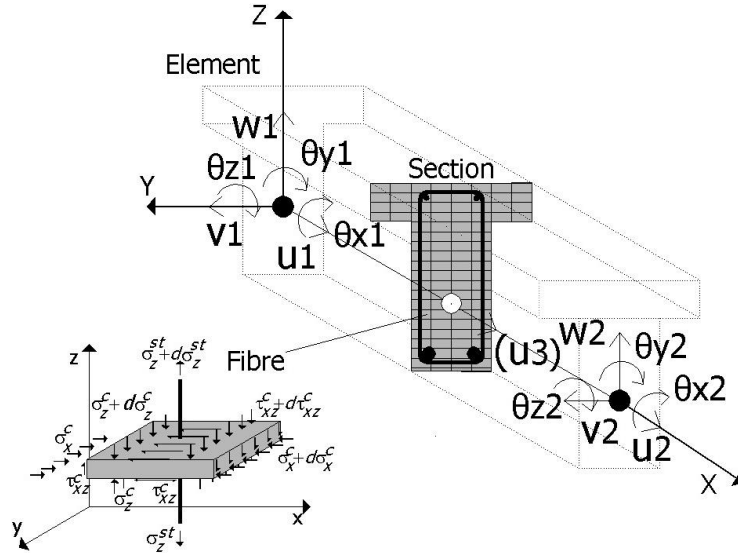


**Figure 2.2-7:** CONSHEAR model. Element level

Considering the 2D case, the kinematic equations that relate the nodal displacements  $a_j = [u_j \ w_j \ \theta_{y_j}]^T$  on each node  $j$  to the generalized strains in the Gauss points  $\underline{\varepsilon}_0 = [\varepsilon_0 \ \gamma_0 \ \phi_y]^T$  are given by the transformation matrix B:

$$\begin{pmatrix} \varepsilon_0 \\ \gamma_0 \\ \phi_y \end{pmatrix} = [B_1 \ B_2] \begin{pmatrix} a_1 \\ a_2 \end{pmatrix}, \quad [B_i] = \begin{pmatrix} \frac{\partial N_i}{\partial x} & 0 & 0 \\ 0 & \frac{\partial N_i}{\partial x} & N_i \\ 0 & 0 & \frac{\partial N_i}{\partial x} \end{pmatrix} \quad (30)$$

where  $\varepsilon_0$  is the axial strain,  $\gamma_0$  is the shear rotation,  $\phi_y$  is the curvature of the cross-section and  $N_i$  are the shape functions.

At the sectional level, the relationship between the generalized strains  $\underline{\varepsilon}_0$  determined in the axis of the element and the strains in each fibre  $\underline{\varepsilon}_{fibre} = [\varepsilon_x \ \gamma_{xz}]^T$  is given by the transformation matrix  $T$ ,

accordingly to Eq. (31). Filaments of longitudinal steel are assumed to be submitted only to axial strains as set by the transformation matrix  $T_{sl}$  given by Eq. (32).

$$\begin{pmatrix} \varepsilon_x \\ \gamma_{xz} \end{pmatrix}_{\text{fibre}} = T \begin{pmatrix} \varepsilon_0 \\ \gamma \\ \phi_y \end{pmatrix}, \quad T = \begin{bmatrix} 1 & 0 & z \\ 0 & 1 & 0 \end{bmatrix} \quad (31)$$

$$\begin{pmatrix} \varepsilon_x \end{pmatrix}_{sl} = T_{sl} \begin{pmatrix} \varepsilon_0 \\ \gamma_0 \\ \phi_y \end{pmatrix}, \quad T_{sl} = \begin{bmatrix} 1 & 0 & z \\ 0 & 0 & 0 \end{bmatrix} \quad (32)$$

After the state determination of the fibres (concrete and transversal steel - denoted as  $c+st$ ) and the filaments (longitudinal steel - denoted as  $sl$ ), the section stiffness matrix  $K_{sec}$  and the internal load vector  $\underline{S}_{sec} = [M \ V_z \ M_y]^T$  are given by the summation of both contributions:

$$K_{sec} = K_{sec}^{c+st} + K_{sec}^{sl} : K_{sec}^{c+st} = \int T^T K_{\text{fiber}} T dA, \quad K_{sec}^{sl} = \int T_{sl}^T E^{sl} T_{sl} dA_{sl} \quad (33)$$

$$\underline{S}_{sec} = \underline{S}_{sec}^{c+st} + \underline{S}_{sec}^{sl} : \underline{S}_{sec}^{c+st} = \int T^T \underline{S}_{\text{fiber}} dA, \quad \underline{S}_{sec}^{sl} = \int T_{sl}^T \sigma_x^{sl} dA_{sl} \quad (34)$$

where  $A$  represents the area of each fibre and  $A_{sl}$  the area of each filament.

Due to the hybrid nature of the sectional formulation which implies both kinematic (axial strains  $\varepsilon_0$  and curvatures  $\phi_y$ ) and force (shear stresses  $\tau^*$ ) quantities, there is a difference between the average distortion of the Timoshenko finite element  $\gamma_0$  (determined in Eq. (31) and used in Eq. (30)) and the average of the shear strains in each fibre  $\gamma_{xz}$  (determined in Eq. (20)). Consequently, to accomplish compatibility between the two types of distortions, a residual force  $V_{z,ul}$  is determined as

$$\begin{Bmatrix} 0 \\ V_{z,ul} \\ 0 \end{Bmatrix} = K_{sec} \begin{Bmatrix} 0 \\ \gamma_{ul} \\ 0 \end{Bmatrix}, \quad V_{z,ul} = (K_{sec}(1,2) + K_{sec}(2,2) + K_{sec}(3,2)) \gamma_{ul} \quad (35)$$

where the unbalanced shear strain is given by

$$\gamma_{ul} = \gamma_0 - \gamma_{xz,m} \quad (36)$$

and  $\gamma_{xz,m}$  is the average of the shear strains of each fibre in a cross-section weighted by its correspondent area  $A$ . The residual shear force is included in the internal force vector of the section

$$\underline{S}_{sec} = \begin{bmatrix} N \\ V_z + V_{z,ul} \\ M_y \end{bmatrix} \quad (37)$$

Making use of the presented sectional concept, the classical FEM equations (Zienkiewicz and Taylor 2004) of the element stiffness matrix  $K_{elem}$  and the internal resistant load vector  $F_{elem}$  can be written as:

$$K_{elem} = \int B K_{sec} B dx \quad (38)$$

$$F_{elem} = \int B^T \underline{S}_{sec} dx \quad (39)$$

The former integrals are solved through the Gaussian Quadrature Method using a reduced integration rule in order to avoid shear locking, in this case one integration point is considered.

### 2.3 Longitudinal prestressing

Prestressing (in pre- and post-tensioned structures) is considered in the model as an equivalent load vector that is in equilibrium with the forces of the prestressing tendons, in the same manner as in (Marí 2000). On the one hand, the contribution of prestress to the element end forces is determined by the transformation of the prestress force into equivalent nodal loads and bending moments. On the other hand, the prestress steel contribution to the stiffness of the element is added (after bonding in the case of post-tensioning) assuming an average eccentricity of the tendon segment. A multilinear stress-strain curve is used for prestressing steel. The prestressing losses due to friction and anchorage slip are considered in the determination of the prestressing forces acting at each time-step, as in (Marí 2000).

### 2.4 Transversal prestressing

When vertical prestress is applied at a given time-step, the prestressed transversal reinforcement is activated with a given stress as schematically represented in Figure 2.4-1. The equilibrium of stresses in concrete and transversal steel in the vertical direction at the fibre level are rewritten as

$$\Delta\sigma_z^c + \rho_{st}\Delta\sigma_z^{st} + \rho_{sp}\Delta\sigma_z^{sp} = 0 \quad (40)$$

where  $\rho_{sp}$  is the volumetric ratio and  $\Delta\sigma_z^{sp}$  is the increment of axial stresses (along direction  $z$ ) of the transversal prestressing. The prestressing force is accounted as an offset strain  $\varepsilon_z^p$  and the increment of axial stresses  $\Delta\sigma_z^{sp}$  is given by:

$$\Delta\sigma_z^{sp} = E_{sp} \left( \Delta\varepsilon_z^p + \varepsilon_z^{p,0} \right) \quad (41)$$

where  $E_{sp}$  is the elasticity modulus of the prestressing steel. The determination of the increment of strain in the active stirrups  $\Delta\varepsilon_z^p$  depends of the bond conditions of the tendons:

i) for bonded prestressed vertical reinforcement (Figure 2.4-1a)  $\Delta\varepsilon_z^p$  is equal to the vertical strain in concrete  $\varepsilon_z$ :

$$\Delta\varepsilon_z^p = \Delta\varepsilon_z \quad (42)$$

ii) for unbonded prestressed vertical reinforcement  $\Delta\varepsilon_z^p$  depends on the cross section distortion or elongation between the two anchorage points ( $u_{p,top}$  and  $u_{p,bot}$ ). By neglecting friction losses (acceptable because tendons are usually short and straight),  $\Delta\varepsilon_z^p$  is determined by:

$$\Delta\varepsilon_z^p = \frac{u_p}{L_p} = \frac{u_{p,top} - u_{p,bot}}{L_p} \quad (43)$$

$$u_p = u_{p,top} - u_{p,bot} = \int_{L_p} \varepsilon_z dz \square \sum_{L_p} \Delta\varepsilon_{zi} h_i = \bar{\Delta\varepsilon}_z L_p$$

where  $\bar{\Delta\varepsilon}_z$  is equal to the mean vertical strain of the prestressing reinforcement given by the integral of vertical strains along the fibres of the web  $\Delta\varepsilon_{zi}$  divided by the anchorage length of the tendons  $L_p$  (Figure 2.4-1b), where  $h_i$  is the width of each fibre  $i$ .

The stress state of a fibre with prestressing is schematically represented in Figure 2.4-2.

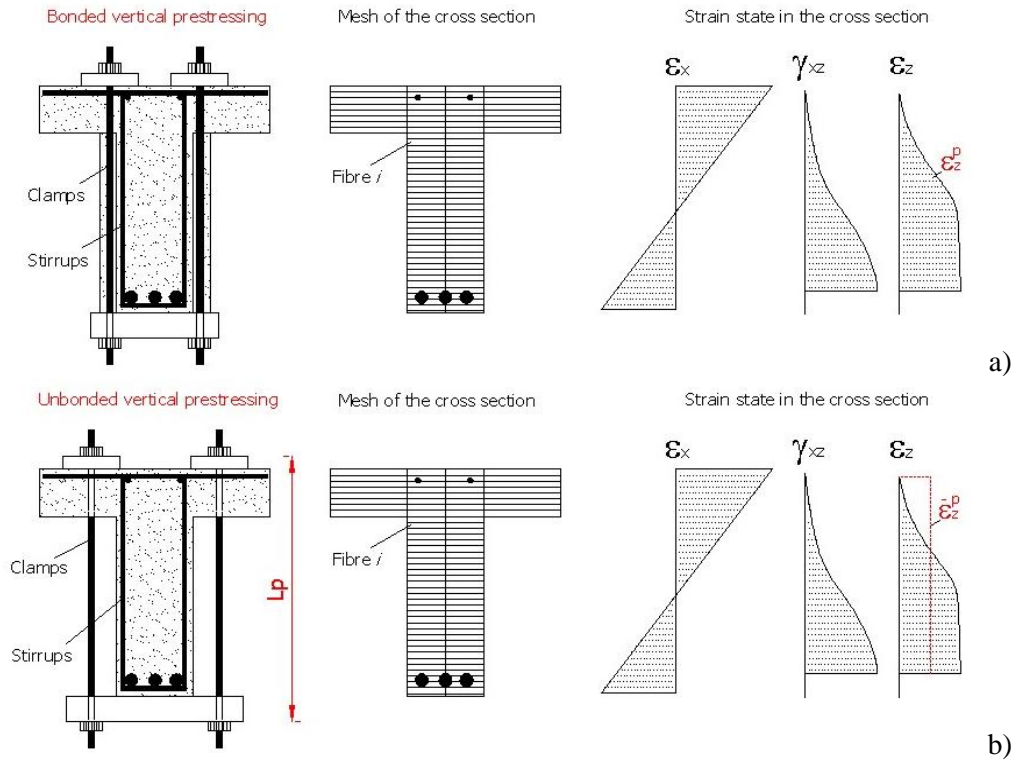


**Figure 2.4-1:** CONSHEAR model. Prestressed vertical reinforcement: a) bonded and b) unbonded

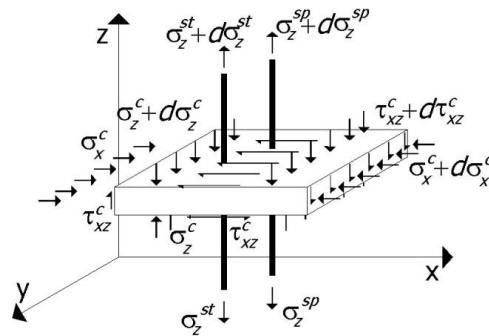


**Figure 2.4-2:** CONSHEAR model. Stress state in a fibre with active and passive stirrups

Through the equilibrium requirement on the vertical direction between concrete and steel, the concrete fibre is submitted to an active confinement when the vertical prestress is applied and passive stirrups will be pre-compressed.

The original fibre state determination explained in point 2.2.3 is then adapted to this case and performed in an analogous manner. Details of this formulation are presented in (Ferreira, Bairán et al. 2014)

## 2.5 Time-dependent effects

In order to compute the time-dependent response of structures the period of analysis is divided into time steps, and the non-mechanical strains are continuously updated. In terms of strains, a step-forward integration scheme in the time domain is performed by continuously adding the results obtained at each previous time step (Marí 2000). Each component of strain is determined separately and summed afterwards, assuming valid the principle of superposition of strains. It is inherent to this assumption, that during each time step, the stress state is kept constant. The validity of this hypothesis is ensured by a small enough size of the time steps during the analysis. Creep and shrinkage are treated in a decoupled manner. The creep response in compression and tension are

assumed to be equal before cracking, after cracking no creep strain is considered in tension. Concerning to the range of typical service stress levels applied in structures, experimental data on biaxial creep supports the assumption of adding the various creep strains due to multiaxial stresses (Bazant 1988), by considering that the principles of isotropy, linearity and superposition are valid. The effects of temperature variations are also considered in an independent fashion. The principle of superposition of creep strains.

The time-dependent approach presented in (Van Greunen 1979) for the nonlinear analysis of RC slabs and panels by means of 2D plane stress elements is adapted to 1D fibre beam elements with consideration of biaxial strain-stress state in the fibres. The 2D non-mechanical strain vector  $\underline{\varepsilon}^{nm}$  depends on time  $t$  and is divided into two types of strains – the stress-dependent  $\underline{\varepsilon}^c$  and the stress-independent  $\underline{\varepsilon}^0$  – as,

$$\underline{\varepsilon}^{nm}(t) = \underline{\varepsilon}^c(t) + \underline{\varepsilon}^0(t) \quad (44)$$

The strain tensor of creep strains  $\underline{\varepsilon}^c$  is stress-dependent and is written as,

$$\underline{\varepsilon}^c(t) = \begin{Bmatrix} \varepsilon_x^c \\ \varepsilon_z^c \\ \gamma_{xz}^c \end{Bmatrix} \quad (45)$$

and, the tensors of strains due to shrinkage and temperature variations, considered as stress-independent, are treated as volume changes  $\underline{\varepsilon}^0$ , and for this reason, do not contemplate shear deformations:

$$\underline{\varepsilon}^0(t) = \begin{Bmatrix} \varepsilon_x^0 \\ \varepsilon_z^0 \\ 0 \end{Bmatrix} = \begin{Bmatrix} \varepsilon_x^{sh} \\ \varepsilon_z^{sh} \\ 0 \end{Bmatrix} + \begin{Bmatrix} \varepsilon_x^T \\ \varepsilon_z^T \\ 0 \end{Bmatrix} \quad (46)$$

This format of biaxial shrinkage strain vector, with null distortion, was also used in (Chong, Foster et al. 2008).

The biaxial creep strain tensor is determined through a series of Dirichlet. The parameters are determined by applying the least square method to a creep empirical expression (MC90 expression is used). The approximation of the Dirichlet series is performed by means of the hidden variables formulation (Bazant and Wu 1973) which does not require the storage of all previous stress states for the determination of the creep strain increment in a step-by-step time integration algorithm.

Details of the time-dependent formulation in the shear-sensitive fibre beam model are found in (Ferreira, Bairán et al. 2014).

## 2.6 Procedure for nonlinear, phased and time-dependent analysis

The shear model was implemented into the existent flexural model CONS (Marí 2000), maintaining and adapting the time-dependent and evolutionary construction features available. The model has three global loops: constructive phases, time steps and load steps (Figure 2.6-1).

The phased analysis allows the simulation of most modifications that may take place during the construction process and along the service life of a structure. This includes changes in the longitudinal and transversal geometry, adding or removal of reinforcements, changes of support conditions, links between the elements, etc.

The time-dependent analysis allows including the effects of time-dependent phenomena, such as, creep, shrinkage, ageing, prestress relaxation, temperature changes. A time period is divided into time steps (intervals). The increment of non-mechanical strains  $\Delta \underline{\varepsilon}^{nm}$  that occurs during the time interval  $\Delta t_n$  is given by the summation of the different contributions (creep  $\underline{\varepsilon}^c$ , shrinkage  $\underline{\varepsilon}^{sh}$  and thermal gradients  $\underline{\varepsilon}^T$ ). The equivalent nodal force vector in the element due to the non-mechanical strains  $\underline{F}_{elem}^{nm}$  is determined in the incremental form. Afterwards, this load vector is assembled into

the structural equivalent load vector. Load is then applied at time  $t_n$  and is kept constant for the time step  $\Delta t_n$ .

Within the load step phase, two iterative loops are marked: (i) an outermost one, which corresponds to the standard Newton-Raphson (NR) procedure for determination of the displacement increments through the global equilibrium equations, and (ii) the innermost iteration loop that corresponds to the fibres' state determination. The resultant increment of nodal displacements in the elements and strains in the sections are determined and the fibre state determination is performed. Subsequently, the determination of the current internal loads is made and convergence is checked. The residual forces are computed and the correspondent structural displacements are updated within the NR iteration loop. Considering the outermost iterative procedure, and in order to overcome intermediate limit points, an arc-length based on the Updated Normal Plane (UNP) (Crisfield 1996) is available in the code.

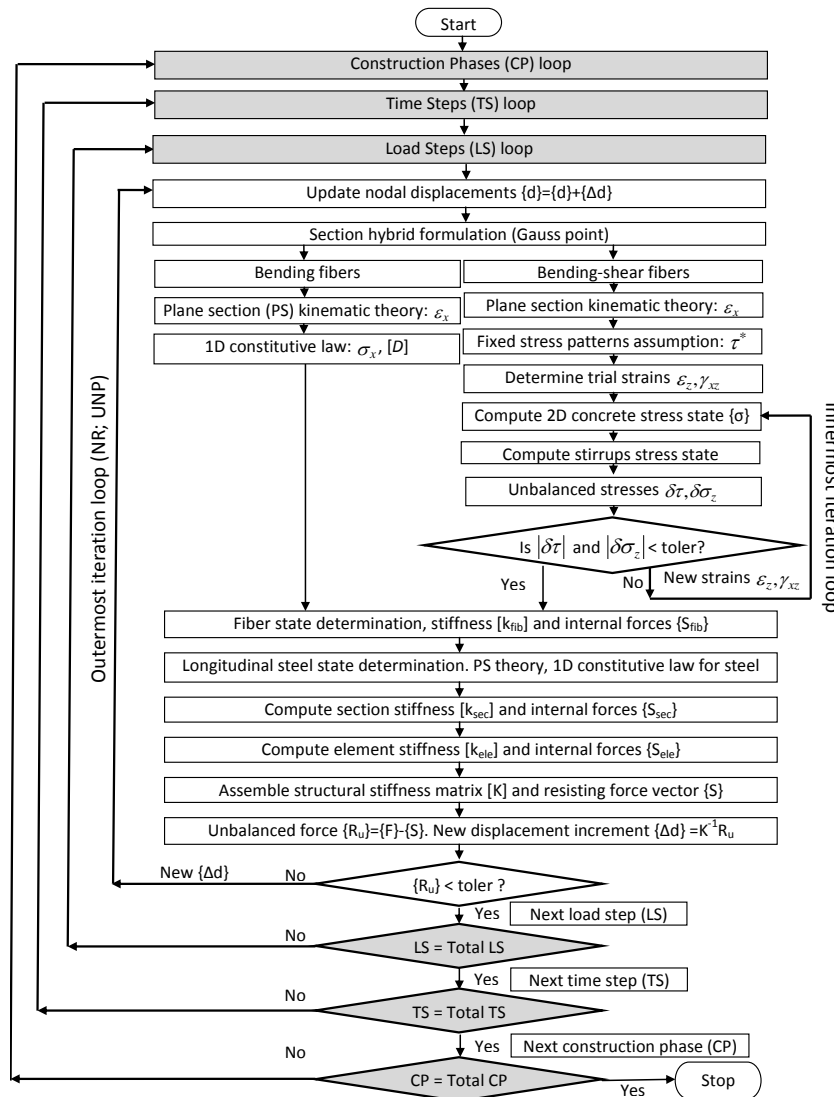


Figure 2.6-1: CONSHEAR model. Flow chart of the code

## 2.7 Simulation of repair and strengthening interventions

Most modifications that may take place during the construction process and along the service life of a structure can be simulated by the model, through the step-by-step solution scheme for the nonlinear problem. Deterioration and repair procedures are also possible to model due to the possibility to consider different concrete and steel types with different activation and removal timings for each

fibre and filament in a cross-section. Situations related to remodelling and strengthening of structures that can be simulated by the model include: substitution of damaged concrete parts, enlargement of concrete cross-section, placement of new reinforcement bars, steel plates or bond FRP laminates, placement or removal of temporary shores, imposed movements and application of external prestressing. With the phased analysis, the response of structures before and after the strengthening can be obtained, including the effects of previous damage and those of the repair, retrofit or strengthening operations.

For the case of strengthening in shear by means of adding extra concrete and transversal reinforcement, the assumptions of the evolutionary sectional model are represented in Figure 2.7-1: both original and strengthen fibers are assumed to comply with the plane section theory; before strengthening procedures, the constant shear force  $V$  is carried by the area of the shear resistant fibres ( $A^*$ ); after strengthening, the constant increment of shear stress  $\Delta V$  along the cross-section is equally distributed between the original and the strengthen fibres, but the effective shear area increases as it includes the strengthen shear resistant fibres ( $A^*_{stren}$ ). With this simplification hypothesis the differences between the distribution of shear stresses of the original and repair materials are neglected. This is aimed to be improved in future versions of the model, by accounting for the fact that more damaged fibres will absorb less shear force than undamaged ones.

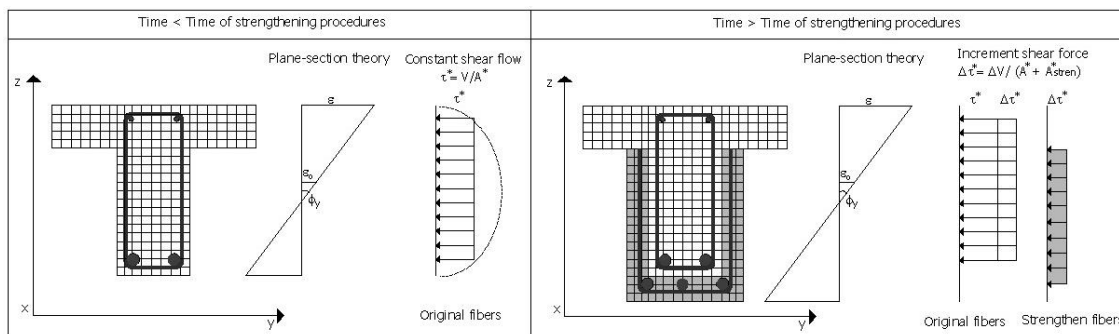


**Figure 2.7-1:** CONSHEAR model. Assumptions of the evolutionary sectional formulation

Regarding strengthening of RC elements in shear by means of externally bonded FRP shear reinforcement, only the wrapped configuration may be accounted by the model (Figure 2.7-2). FRP delamination phenomenon is not accounted; however, its incorporation is currently under development. The presence of FRP reinforcement modifies the cracks and strut inclinations, the concrete confinement stresses, and other parameters related to the shear response, producing an interaction between the concrete, internal steel and FRP contributions to the shear strength. FRP sheets are accounted as an extra configuration of stirrups in the fibres with their own material properties. More details on this option of the model is found in (Ferreira, Oller et al. 2013).

In the analysis of strengthened structures, the historical plasticity and damage variables of the original fibres are stored when the new strengthen fibres are activated. By these means, the influence of the previous damage in the behaviour of strengthened structures, which can be particularly relevant, is account for in the model.

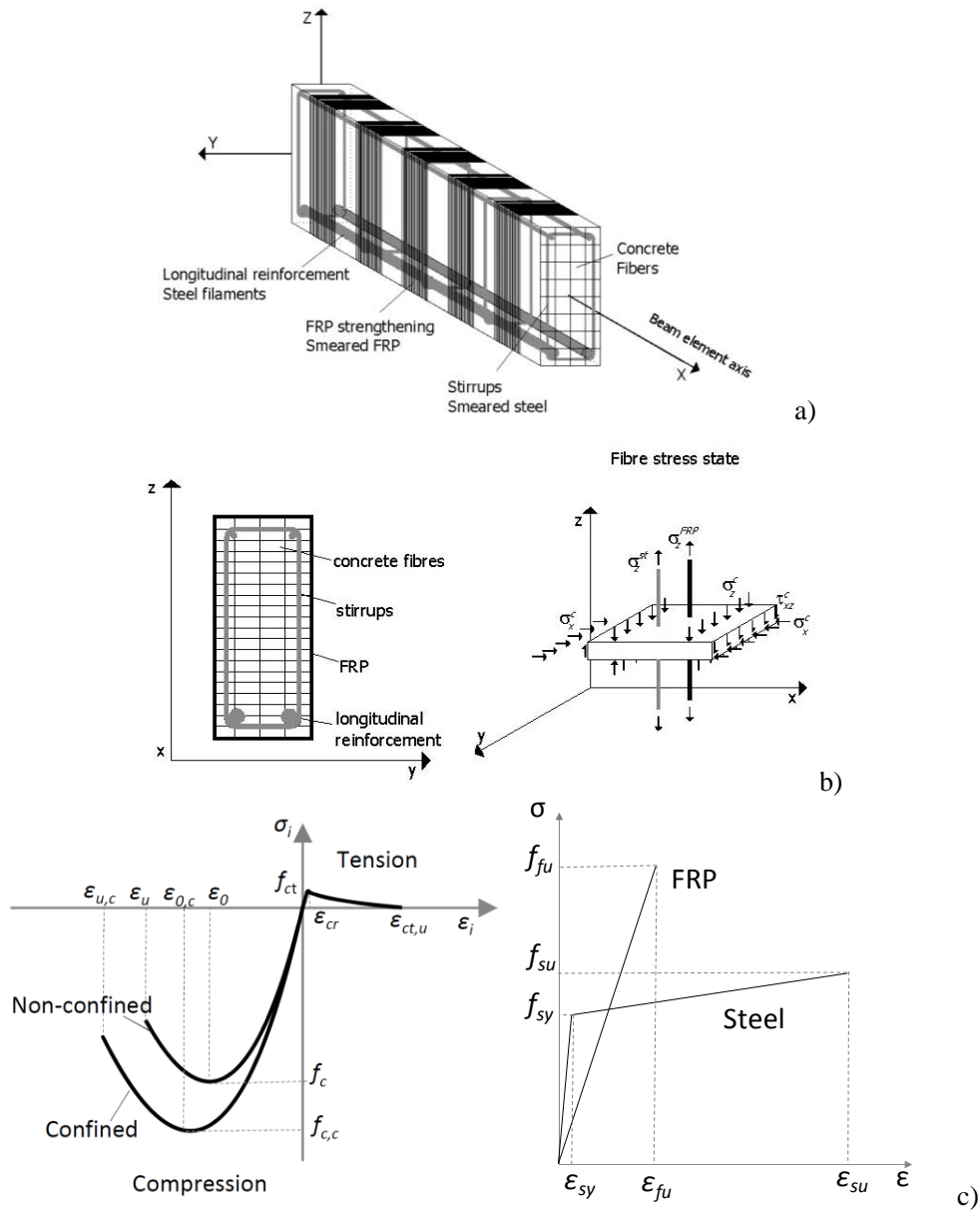


**Figure 2.7-2:** CONSHEAR model. Assumptions for FRP shear strengthening: a) element, b) section and fibre, c) material levels

## 2.8 Representation of cracking

As the constitutive model is based on a smeared crack assumption, discrete cracking patterns of concrete can be represented graphically only after a post-processing of the multiaxial strain tensor distribution, by means of an external algorithm. As for each Gauss point the principal strains and directions are known, as soon as the principle tensile strain of each concrete fiber reaches the critical value that corresponds to the material tensile strength ( $\epsilon_I = \epsilon_{cr}$ ) an orthogonal line to the corresponding principal direction is printed.

Due to the non-verticality of the cracks, the strain state in the location of the path of the crack does not correspond to a single Gauss point, being instead obtained via a linear interpolation between the strain states of the two close-most Gauss points (see Figure 2.8-1). In summary, for a given load step in which cracking has started the following procedure is followed:

- (i) the  $x$ - $z$  coordinates correspondent to the point that defines the crack tip settled in the previous load step are determined first;
- (ii) the strain state at the current crack tip is evaluated through interpolation;
- (iii) the existence of a new increment of the crack is checked and printed.

The  $x$ -coordinate where the first crack appears is a necessary input to this algorithm as well as the crack spacing which may be determined with the expression of some code (EC2, MC2012, etc.). This crack spacing is considered constant along the beam and throughout loading. The thickness of the lines that represent the discrete cracks may be proportional to the average crack width  $w_m$  as:

$$w_m = s_m \varepsilon_1 \tag{47}$$

where the principal tensile strain  $\varepsilon_1$  is an output of the numerical model for each fibre at each Gauss point.

As rotating cracking is assumed in the model, tensile strains rotate continuously with loading. In reality, cracks form at a given load level and do not rotate; only new cracks appear with distinct inclinations. The flow of principal tensile strains does not coincide with the cracking pattern at a given load level. This algorithm acts as a representation of cracks imitating reality and cannot be considered as a direct output result of the model.

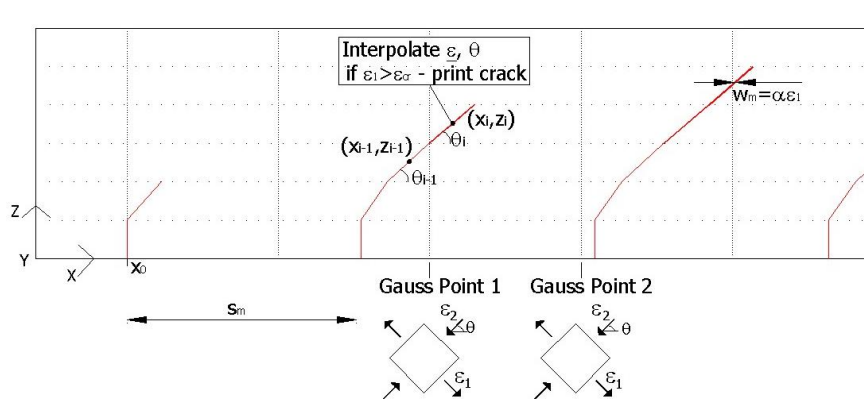


Figure 2.8-1: CONSHEAR model. Representation of cracking

### 3 RECALCULATION OF PREVIOUS WORKS: REINFORCED CONCRETE BEAMS

Four cases of experimental tests available in literature and calculated by Hendriks and Belletti et al. (2014) with plane stress models in DIANA were recalculated with the CONSHEAR model - Cases RB1, RB2, RB3 and RB4. These cases embrace different geometries, reinforcement, experimental setups and failure mechanisms. Two of these cases (RB1 and RB2) were also studied with beam models in DIANA.

The NLFEA performed by Hendriks and Belletti et al. (2014) considered for comparison in this work present the following characteristics:

- Model: 2D plane stress;
- FE: 8 node membrane elements for concrete plus embedded truss elements in reinforcement;
- Software: DIANA Release 9.4.4;
- Analysis: nonlinear static,
- Concrete: total strain rotating crack model.
- Solution: NR, norms of force (tolerance of 5E-2) and energy (tolerance of 1E-2), line search algorithms.

In order to attain a direct comparison, the mechanical properties of the materials used in the 2D plane stress DIANA models were, as far as possible, maintained equal in CONSHEAR and further beam simulations using DIANA.

#### 3.1 Case RB1: Vecchio & Shim (2004)

The series of beams tested by (Vecchio and Shim 2004) in Toronto were a reproduction of the experiments by (Bresler and Scordelis 1963). In total, four series of three beams with rectangular cross sections subjected to point loads were tested. They differed from each other in the amount of shear reinforcement, span length, cross-section dimensions and concrete compressive strength. The measured experimental data were the applied load and the displacement at mid-span.

From this set of experiments, specimen C3 is selected as this beam has the longest span (6400 mm) and a flexure-compressive failure mechanism. In addition to the simulation with CONSHEAR model, this case will be compared with DIANA beam elements and some parametric studies related.

##### 3.1.1 *Experimental setup and results*

The beam has a total length of 6.840 m, a depth of 0.552 m, and a width of 0.152 m. The characteristics of the beam in terms of geometry, reinforcement, loading, boundary conditions and experimental setup are presented in Figure 3.1-1. The bottom longitudinal reinforcement is extended outside the beam and welded to thick plates.

The beam exhibited a flexural-compressive failure mode (Figure 3.1-2) with a clear maximum in the load-deflection response. The experimental ultimate value of applied load was equal to  $P_{EXP} = 265$  kN at a deflection of 44.3 mm.

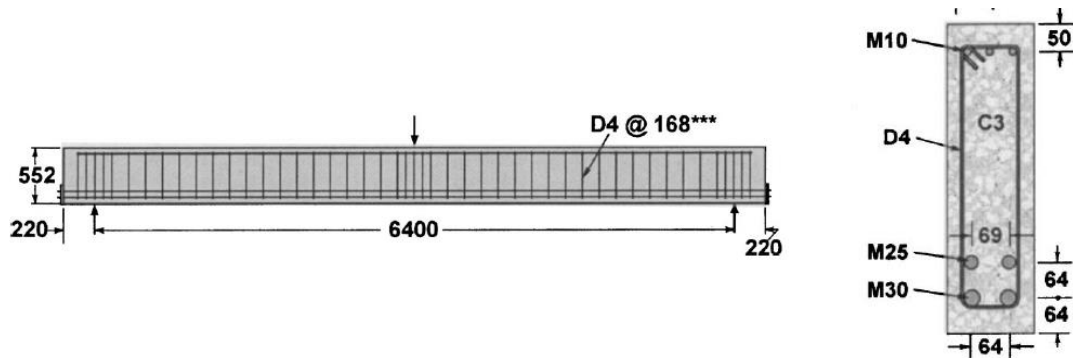


**Figure 3.1-1:** Case RB1. Dimensions (in m), reinforcements and experimental setup (Vecchio and Shim 2004)

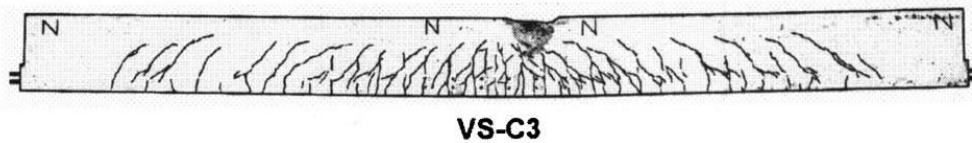


**Figure 3.1-2:** Case RB1. Failure mechanism observed at ultimate load (Vecchio and Shim 2004)

### 3.1.2 Finite element model CONSHEAR

The characteristics of the model are presented in Figure 3.1-3; the beam was discretized into 32 FEs and 33 nodes (constant length of the beam elements of 0.20 m). The cross section was divided into fibres with 0.013 – 0.016 m of width; steel filaments were simulated according to their positions in the beam (3xM10, 2xM25 and 2xM30) and shear reinforcement was considered smeared in the shear resistant fibres ( $\rho_{sw}=0.2\%$ ). Apart from the concrete cover, all the fibres were considered shear resistant.

Regarding the material properties, the values given in the paper for the concrete and steel mechanical properties were used in the model as resumed in Table 3.1-1 for concrete and in Table 3.1-2 for steel.

Load (P) was applied as a nodal force, in an incremental form until failure in 78 load steps. Energetic tolerance considered was  $1 \times 10^{-3}$  and updated normal plane switch on in the advanced loading steps. Computation time takes around 1-2 minutes.

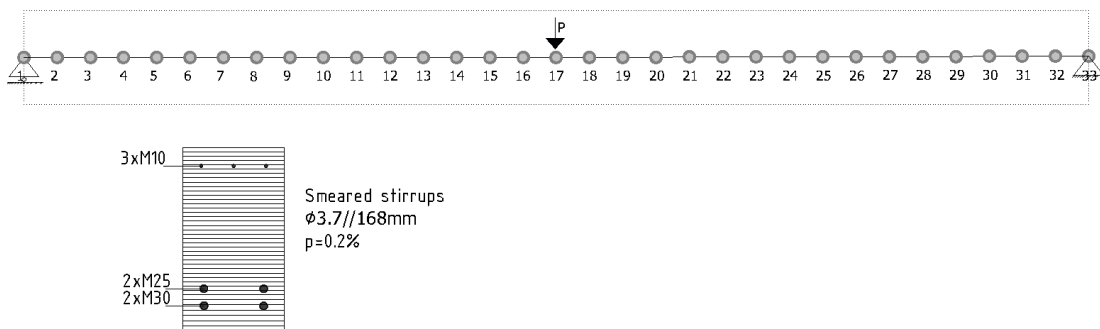


**Figure 3.1-3:** Case RB1. Mesh of the model

**Table 3.1-1:** Case RB1. Constitutive properties for concrete

	$f_{cm}$ (N/mm <sup>2</sup> )	$f_{ctm}$ (N/mm <sup>2</sup> )	$E_c$ (N/mm <sup>2</sup> )	$\epsilon_{cu}$
Mean measured values	43.5	3.13	34300	0.0035

**Table 3.1-2:** Case RB1. Reinforcement properties

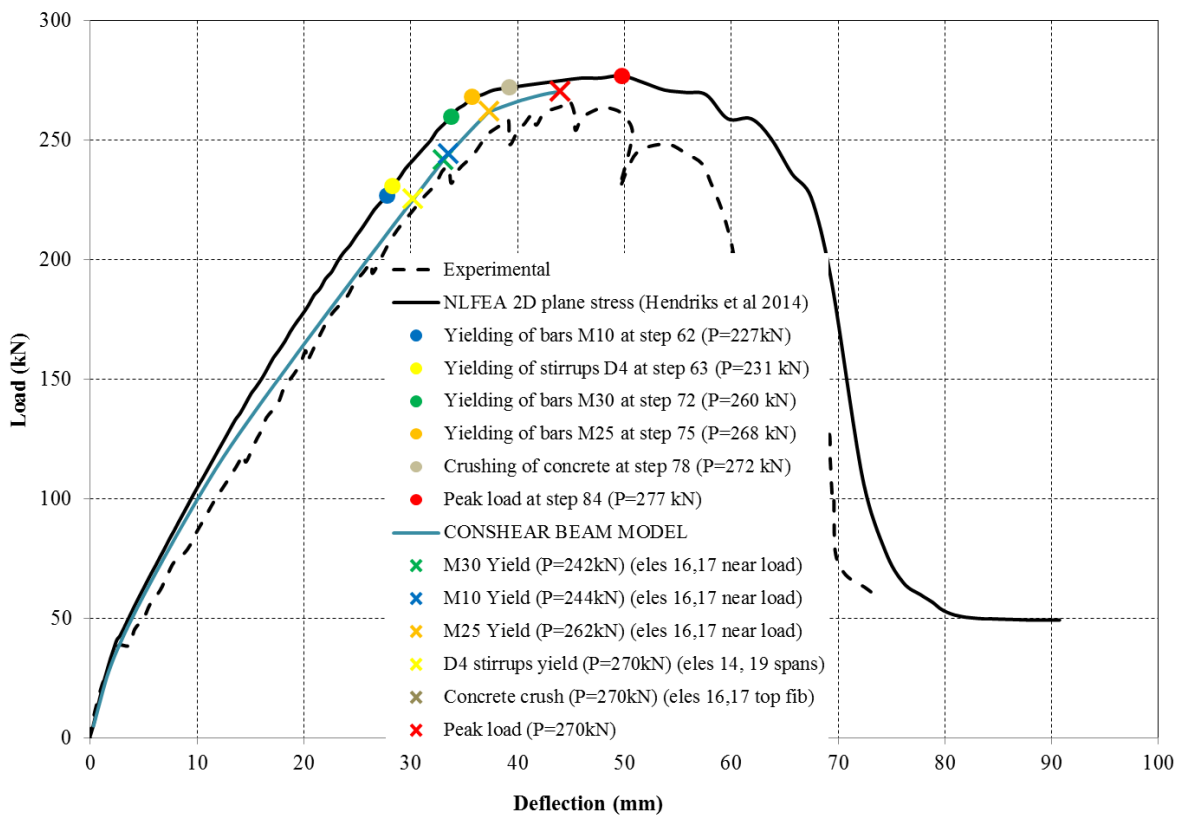
Bar	$\Phi$ (mm)	$A_s$ (mm <sup>2</sup> )	$E_s$ (N/mm <sup>2</sup> )	$f_{ym}$ (N/mm <sup>2</sup> )	$f_{um}$ (N/mm <sup>2</sup> )	$\epsilon_{su}^*$	$E_{sy}^*$ (N/mm <sup>2</sup> )
M10	11.3	100	200000	315	460	0.025	6000
M25	25.2	500	220000	445	680	0.05	6000
M30	29.9	700	200000	436	700	0.05	6000
D4	3.7	25.7	200000	600	651	0.0112	6000

\*assumed values

### 3.1.3 Nonlinear finite element analysis

#### Load – deflection response

The load – deflection curve is presented in Figure 3.1-4. The load values corresponding to the starting of yielding of the longitudinal bars (M30, M25 and M10), yielding of the stirrups (D4) and concrete crushing are indicated and compared with the 2D FE model performed by (RTD1016b, Hendriks et al. 2015). As in the same manner as in the 2D NLFEA, the load step in which the first integration point reaches a minimum principal strain value lower than  $-3.5 \times 10^{-3}$  is defined crushing of concrete. The experimental load-displacement curve is also included in the graphic. The results of the nonlinear analysis for the start of the different levels of damage determined by the beam model CONSHEAR and the 2D plane stress model DIANA are resumed and compared in Table 3.1-3.

**Figure 3.1-4:** Case RB1. Load-deflection curves and levels of damage

**Table 3.1-3:** Case RB1. Results of the NLFEAs (kN)

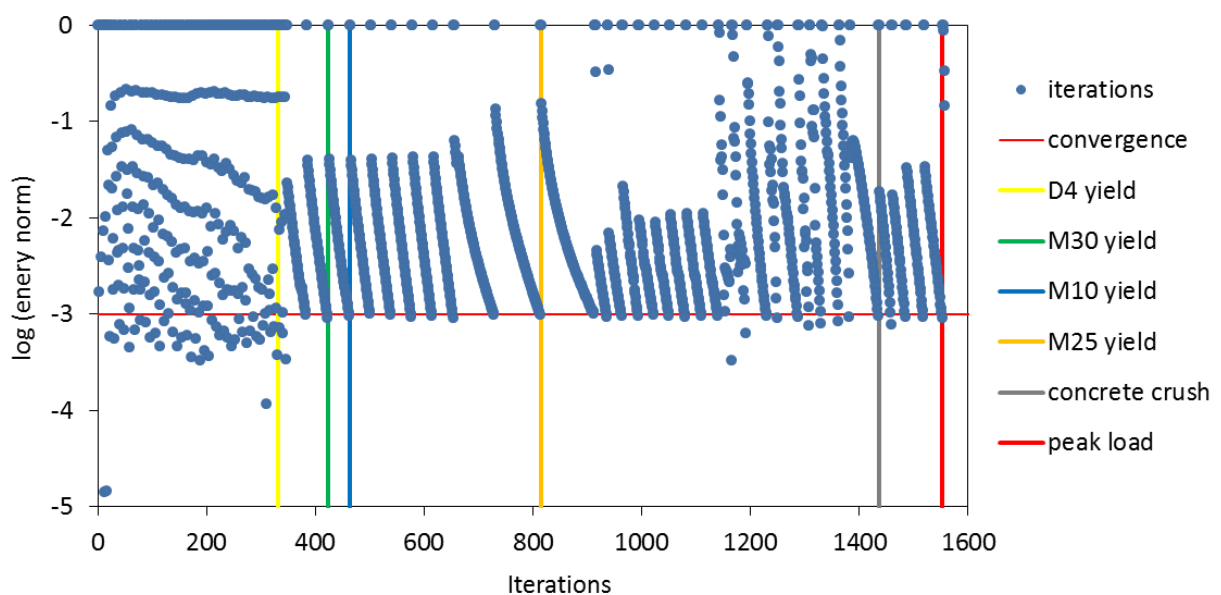
Level of damage	DIANA Plane stress	CONSHEAR	Comparison	Exp.
Peak Load	277	270	CONSHEAR <, similar	265
Start yielding long. reinforcement				
M30 (bottom 2nd layer reinf.)	260	242	CONSHEAR <	No data
M10 (top reinf.)	227	244	CONSHEAR >	No data
M25 (bottom 1st layer reinf.)	268	262	CONSHEAR < similar	No data
Start yielding stirrups D4	231	270	CONSHEAR >	No data
Start crushing of concrete	272	270	Similar	No data
Computation time	1h	1-2 minutes		

Consistently with the 2D model, CONSHEAR determined bending failure with yielding of the longitudinal and transversal reinforcement and crushing of concrete for a similar peak load level. There are some differences in the sequence of yielding of the reinforcement, as the top bars M10 reach yielding sooner in the 2D model in comparison with the 1D. Concerning the results of the fibre beam model, longitudinal reinforcement yielded in elements near load application point (elements 16 and 17); concrete crushed in these elements in the top fibres. Transversal reinforcement yielded in the elements in the span (elements 14 and 19); see mesh in Figure 3.1-3. These results are consistent with the ones from the 2D model (RTD1016b, Hendriks et al. 2015).

CONSHEAR presents problems with post-peak regime, which is a typical problem of the model, that is aimed to be fixed in the future of this project. CONSHEAR presents a less stiffer response than plane stress elements.

### Convergence behaviour

The energy criterion is used in the global NR iteration procedure with a tolerance of  $1 \times 10^{-3}$ . Whenever the energy norm reaches this value (represented by a red line in the graphic) the analysis proceeds to the next load step. Each load step starts with an energy norm of 1 ( $\log(1)=0$ ). In the graphic it can be observed that the first load steps reach fast convergence. The number of iterations needed for convergence increases near failure load. In the ultimate load step, convergence is not achieved. The key levels of damage identified in the load-displacement curve are marked with vertical lines.

**Figure 3.1-5:** Case RB1. Energy norm vs. global iterations at the NR level

**Strains**

The strains with increasing load are presented in the following graphics for the same points previously marked in the load-deflection curve.

In Figure 3.1-6, the strains in concrete in the top fibre located at mid-shear point show that crushing of concrete is attained in this point.

The strains in the different filaments of longitudinal reinforcement located at mid span, show that yielding is achieved for both bottom and top reinforcement at ultimate load (Figure 3.1-7).

Strains in transversal reinforcement (Figure 3.1-8) are presented for two fibres at different height (mid height of the section and at the location of the bottom longitudinal reinforcement) in the shear span, demonstrating how the stirrups are not activated until cracking occurs in each fibre (under the bottom fibre cracks sooner than the mid height fiber, hence is activated for a lower load level), and reach yielding.

These results represent the failure mechanism predicted by the model: bending related, with crushing of concrete and yielding of longitudinal reinforcement in the position of higher bending moment. Effects of shear are important also, because stirrups reach yielding in the shear span.

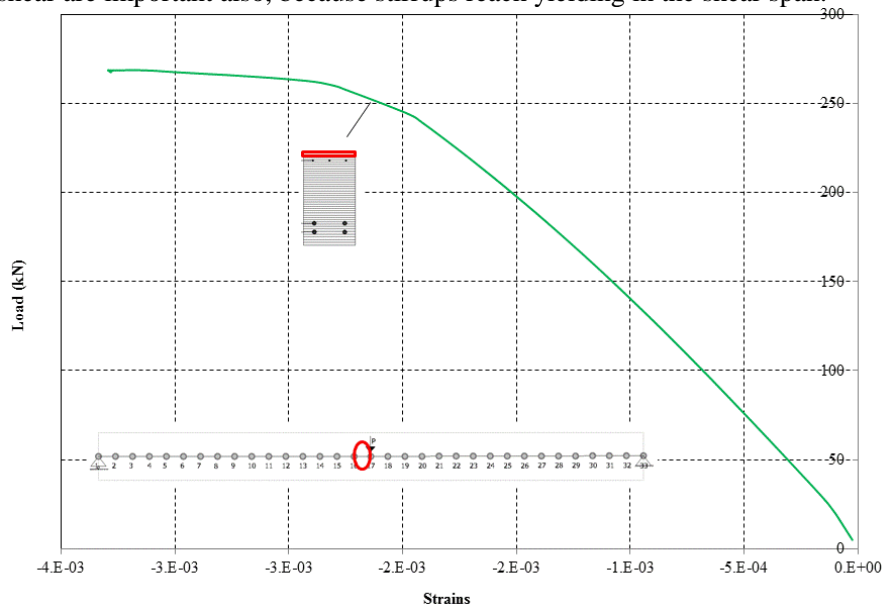


**Figure 3.1-6:** Case RB1. Load vs. longitudinal strains in concrete

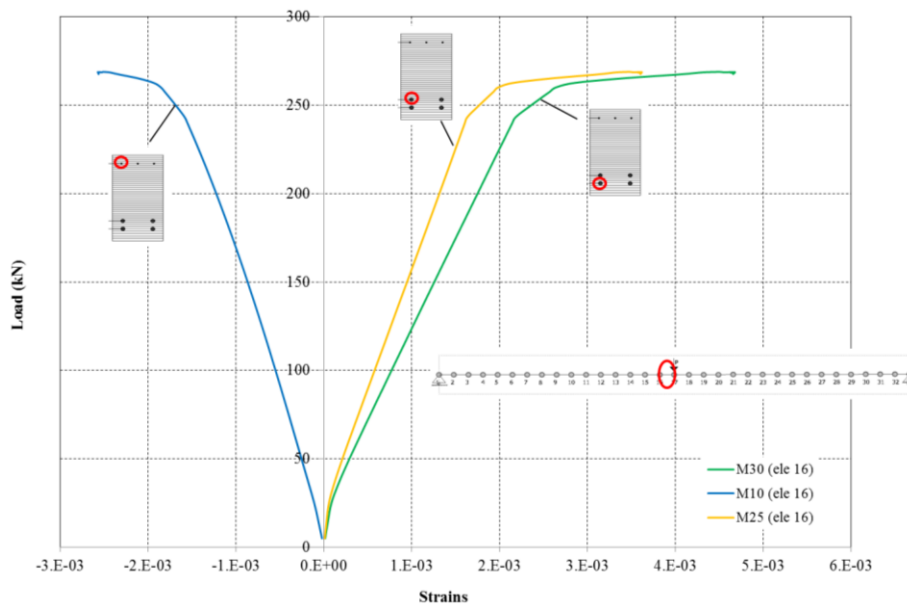


**Figure 3.1-7:** Case RB1. Load vs. longitudinal strains in the longitudinal reinforcement

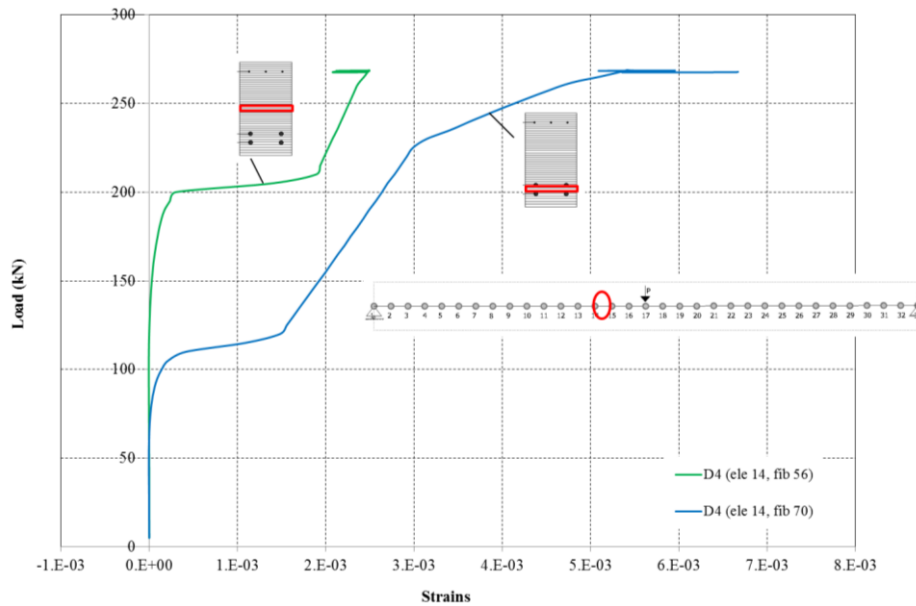


**Figure 3.1-8:** Case RB1. Load vs. longitudinal strains in the transversal reinforcement

### Crack patterns

The predicted crack patterns are represented in Figure 3.1-9 for the load levels of approximately 50%, 70%, 90% of the failure load and ultimate load. The average crack spacing is an input parameter of this post-processing algorithm for crack drawing and was determined using the expression of EC2:  $S_m(EC2) = 140$  mm.

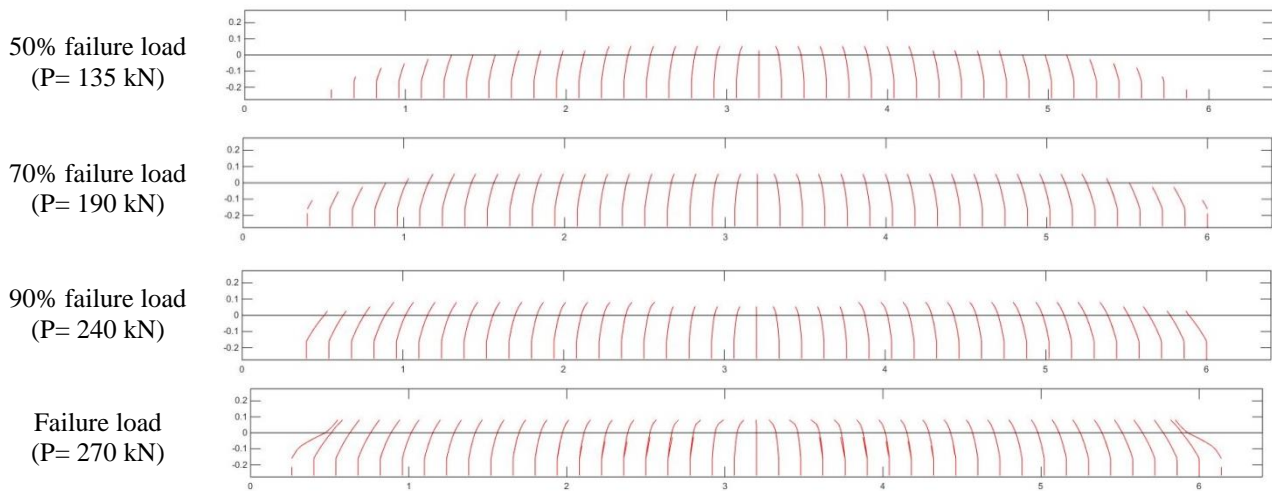


**Figure 3.1-9:** Case RB1. Predicted crack patterns

### 3.1.4 Analysis with beam models in DIANA 9.6

The analyses were performed with DIANA Release 9.6, using the Class II and Class III 2D beam elements.

The mesh is built with 32 FEs with a constant length of 0.20 m (equal to the CONSHEAR model) and the point load was inserted in node 17 as presented in Figure 3.1-10. The cross section was defined according to the geometric properties and the reinforcement was modelled with embedded

bar elements in their correspondent positions (7 bars in total correspondent to the top and bottom reinforcement) and own material properties.

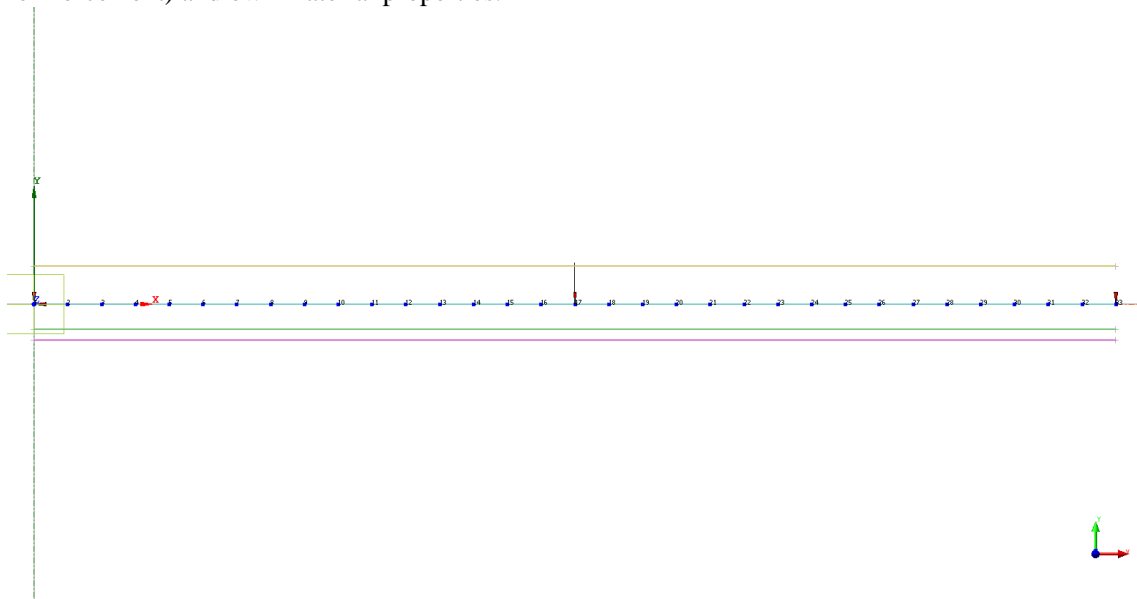


**Figure 3.1-10:** Case RB1. Beam model in DIANA

Regarding the material models in DIANA the following was considered:

#### Concrete

- Total strain crack model
- Rotating crack orientation

Tension: exponential curve

$$F_{ct}=3.13e6N/m^2$$

$G_f=0.1439e3 N/m$  (same as use in (RTD1016b, Hendriks et al. 2015))

Reducing due to lateral cracking  $k_c$ , (Vecchio and Collins 1993)

Lower bound reduction curve=0.2 ((RTD1016b, Hendriks et al. 2015) used 0.6, maybe is too high)

Poisson ratio reduction: damage based

Compression: parabolic curve

$$F_c=43.5e6N/m^2$$

$$G_c=1.5f_c \text{ (considered)}=68e3N/m$$

No stress confinement

The mechanical properties for concrete are summarized in Table 3.1-4, similarly to what was considered in CONSHEAR.

**Table 3.1-4:** Case RB1. Constitutive model parameters for concrete in DIANA beam models

	$f_{cm}$ ( $N/mm^2$ )	$f_{ctm}$ ( $N/mm^2$ )	$E_c$ ( $N/mm^2$ )	$\nu$	$G_F$ ( $Nmm/mm^2$ )
<b>Mean measured values</b>	43.5	3.13	34300	0.2	0.1439*

\*Not specified in reference; estimated according to MC2010 (fib, 2013).

#### Steel

Class: reinforcement and pile foundations

Material model: Von Mises plasticity

Plastic hardening: yield stress-plastic strain

Curves of steel (see Table 3.1-2, the same curves as considered in CONSHEAR model)

Several analyses were performed considering different class beam elements (Class II and Class III), integration points along the height of the section (3 and 11 points with Simpson integration scheme) and different solution procedures (force and displacement control and arc length with selection of degrees of freedom). All the convergence checks were considered with their default tolerances. The default integration along the beam's length, which corresponds to 2 points with Gauss integration for Class II and 3 points with Simpson integration for Class III, was considered in all the analysis. The characteristics of the 5 analysis performed in DIANA are resumed in Table 3.1-5. The load (or displacement) was applied in approximately 100 steps until failure.

**Table 3.1-5:** Case RB1. Nonlinear analyses performed with beam models available in DIANA 9.6

NLFEA	Class beam element	Integration beam length	Integration section height	Solution procedure NLA
DIANA Beam #1	II	2 points Gauss*	3 points Simpson*	Force control
DIANA Beam #2	II	2 points Gauss*	3 points Simpson*	Displacement control
DIANA Beam #3	II	2 points Gauss*	3 points Simpson*	Force control + Arc length <sup>±</sup>
DIANA Beam #4	II	2 points Gauss*	11 points Simpson	Force control + Arc length
DIANA Beam #5	III	3 points Simpson*	11 points Simpson	Force control + Arc length

\* Default integration scheme in DIANA

<sup>±</sup> Control  $u_y$  node 17 mid span

The results of the several NLFEAs with beam elements in DIANA are compared in Figure 3.1-11 with the CONShear model, with the 2D plane stress model in DIANA and with the experimental results. In other words, to the results of Figure 3.1-4 was added the correspondent load-deflection curves determined by the 5 analyses performed with the beam elements in DIANA. The most relevant results are resumed in Table 3.1-6.

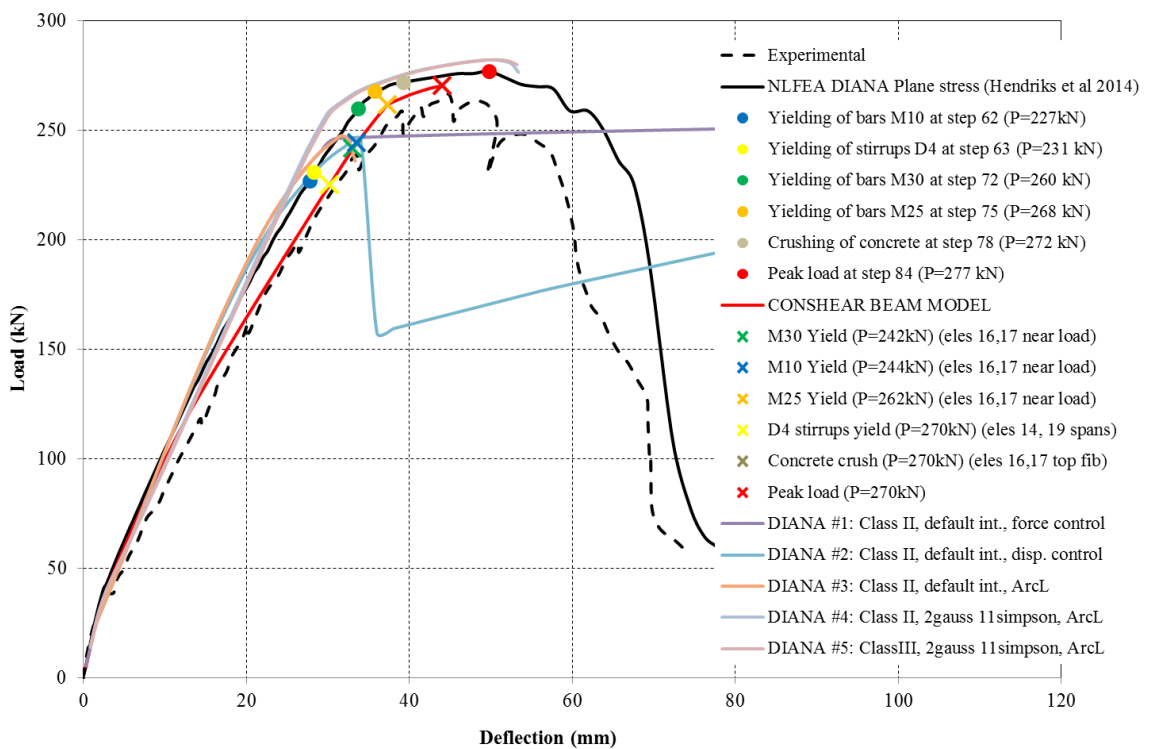


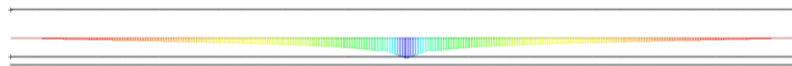
**Figure 3.1-11:** Case RB1. Load-deflection curves

**Table 3.1-6:** Case RB1. Results of the NLFEAs (kN)

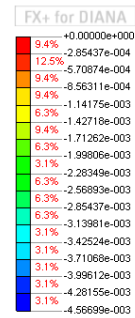
Level of damage	DIANA 2D FE Plane stress	CONSHEAR 3D Beam	DIANA 2D Beam Class II (3 Simpson int.)	DIANA 2D Beam Class II (11 Simpson int.)*	Exp.
Peak Load	277	270	247.7	282.2	265
Start yielding long. reinforcement					
M30 (bottom 2nd layer reinf.)	260	242	237.5	241.7	No data
M10 (top reinf.)	227	244	207	253.2	No data
M25 (bottom 1st layer reinf.)	268	262	245.5	265.3	No data
Start yielding stirrups D4	231	270	-	-	No data
Start crushing of concrete	272	270	247.7	275.5	No data
Computation time	1h	1-2 minutes	<1 minute	<1 minute	

\* very similar to Class III 2D beam element with 11 Simpson integration points in the height.

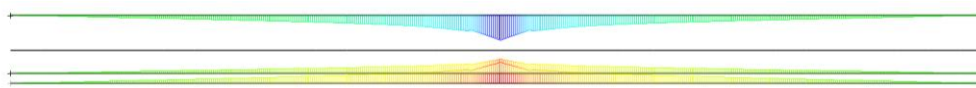
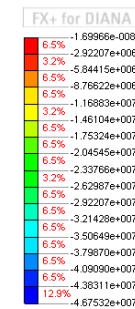
The failure mechanism in all the analyses was in bending with yielding of tensile longitudinal reinforcement and crushing of concrete, both occurring at mid span, as represented in Figure 3.1-12 for Analysis #1; similar results regarding the failure mechanism were observed for all the other analyses.



(a) Longitudinal strains  $E_{xx}$  in the top extreme fiber at peak load

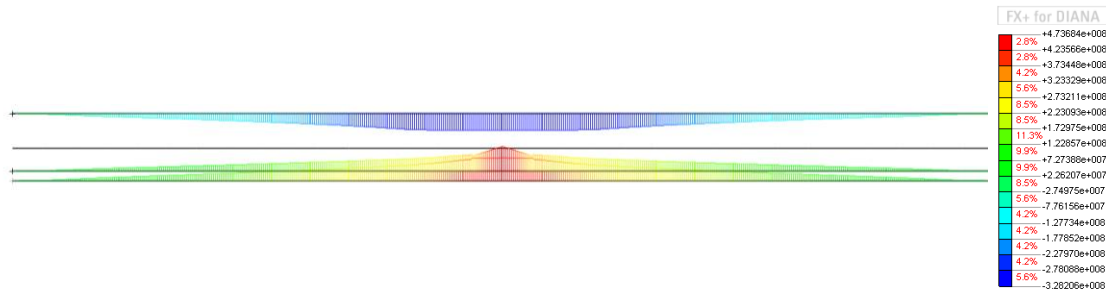


(b) Longitudinal stresses  $S_{xx}$  in the top extreme fiber at peak load – crushing of concrete



(c) Longitudinal strains  $E_{xx}$  in the longitudinal reinforcement





(d) Longitudinal stresses  $S_{xx}$  in the longitudinal reinforcement

**Figure 3.1-12:** Case RB1. Strain and stresses at failure for beam model in DIANA (Analysis #1)

In Class II 2D beam analyses and default integration along the height of the cross section (3 points with Simpson integration), which correspond to Analysis #1, #2 and #3 (see Table 3.1-5 and Table 3.1-6), peak load is underestimated and the several levels of damage (yielding of longitudinal reinforcement and crushing of concrete) starts earlier in comparison with CONSHEAR and DIANA plane stress analyses. The stirrups are not considered in the beam elements in DIANA. Changing the type of solution procedure did not influence the results, as the peak load and failure happened for similar load levels.

In Analysis #4 (Class II 2D) the number of integration points along the cross section was augmented to 11 points with Simpson integration; all the other model properties were maintained and the analysis was performed with force control plus arc length (Updated Normal Plane). As can be observed in Figure 3.1-11 and in Table 3.1-6, the results are very similar to the DIANA plane stress analysis in terms of load-deflection curve and in terms of damage propagation.

In analysis #5, the only parameter changed was the type of element (Class III 2D), all the other parameters and characteristics of the model were maintained as in Analysis #4. The results are very similar to Class II 2D, in terms of force – displacement curve, failure mechanism and peak load. Class III 2D is Mindlin element (with shear strain) and Class II 2D is Hermitian (without shear strain), but as the failure mechanism is bending, shear plays a secondary role in this example. In both simulations, post peak analysis could be carried out with changing of analysis parameter to help further convergence. However, the peak load is evident with the decrease of load captured by the arc-length, proving that failure happened in this point.

### 3.1.5 Concluding remarks

From the analysis of the RB1 test (benchmark failing in bending) with CONSHEAR and beam elements in DIANA and comparison with DIANA plane stress (Hendrik, Belletti et al. 2014) and experimental results (Vecchio and Shim 2004) the following conclusions are pointed out:

- CONSHEAR model presented similar results to DIANA plane stress in terms of peak load, failure mechanism and propagation of damage throughout the nonlinear analysis;
- CONSHEAR did not captured post-peak response;
- DIANA 2D beam elements with default integration points (3 points, Simpson integration) underestimated the peak load and the start of the levels of damage;
- DIANA 2D beam elements of Class II and Class III gave good results, very similar to DIANA plane stress, whenever a higher number of integration points along the height of the cross section is considered (11 points, Simpson integration);
- Solution procedure of load control plus arc length or displacement based presented good performances;
- The stirrups are not considered in the beam elements in DIANA, in this case does not influence the results because it is a bending test.
- No significant difference is observed between CONSHEAR and DIANA beam elements with higher integration points along the cross section; just a higher increment of deflections given by CONSHEAR in the advanced nonlinear stage, that must be related with the influence of shear effects.

Some notes in respect to future implementation of CONSHEAR in DIANA are:

- Fx+ only prints the results for the extreme fibres, whatever the number of integration points is. Extreme fibres are the most relevant for the bending analysis, but in the presence of shear effects, it will be required to see the response in all the integration points through the height of the section, as failure can happen in the web. There are ways to see in DIANA the information in all the integration points that will need to be used.
- Stirrups will be included in the beam elements in DIANA and the strains and stresses in the stirrups along the height of the cross section will be a new output.

### 3.2 Case RB2: Collins & Kuchma (1999)

Case RB2 considers beam SE-50A-45 of the experimental program of (Collins and Kuchma 1999) and was reported in (CEB Bulletin N0 237 1997). The beam was labelled beam 8 in an international workshop on shear force held in Rotterdam, the Netherlands in 2007. Beam RB2 has been selected because it is characterized by a diagonal-tension failure mechanism.

In addition to the simulation with CONSHEAR model, this case will be compared with DIANA beam elements and some parametric studies related.

#### 3.2.1 Experimental setup and results

The beam has a total length of 5.0 m, a depth of 0.5 m, and a width of 0.169 m. The geometry and reinforcement are presented in Figure 3.2-1 and Figure 3.2-2.

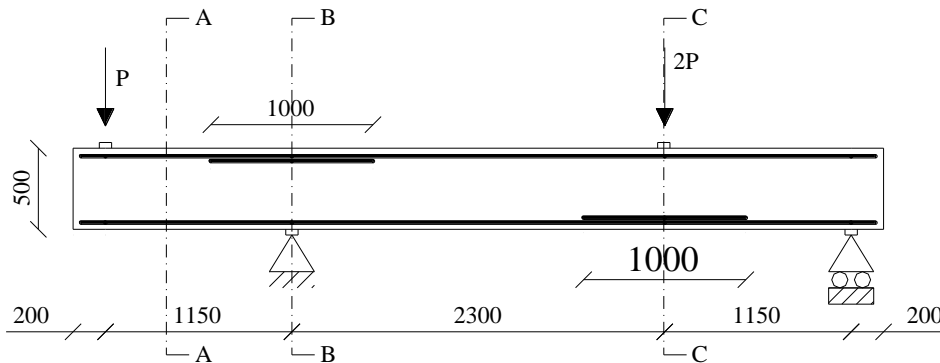


**Figure 3.2-1:** Case RB2. Dimensions (in mm), reinforcements layout and loading, (Hendriks, Belletti et al. 2015)

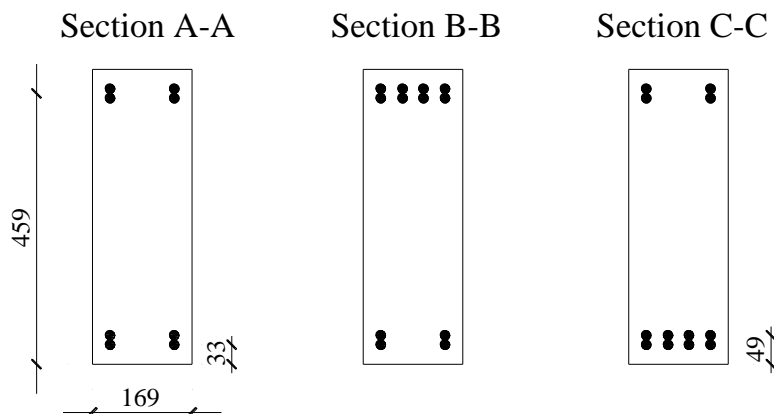


**Figure 3.2-2:** Case RB2. Cross section details (dimensions in mm), (Hendriks, Belletti et al. 2015)

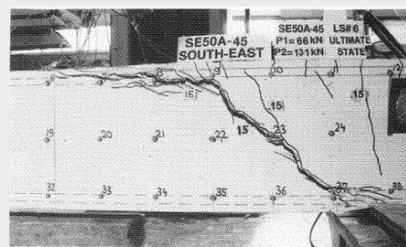
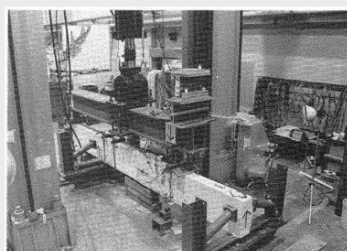
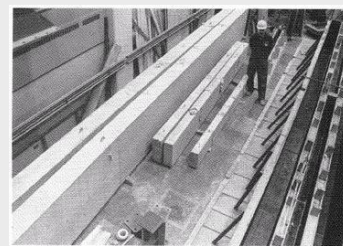
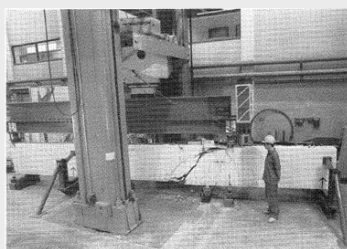
Four #15 bars are placed as tensile and compressive reinforcement along the entire length of the beam. Additional four #15 bars are placed as tensile reinforcement over a length of 1 m in correspondence of Section B-B and Section C-C characterized by the maximum value of applied moment. The beam has no transversal reinforcement.

The experimental set up is shown in Figure 3.2-3. The beam is loaded by two point loads -  $P$  at the top left and  $2P$  at the middle right loading point - as represented in Figure 3.2-1. The beam exhibited a typical brittle diagonal-tension failure mode, shown in Figure 3.2-4. The specimen was tested twice: after the first test, the beam was strengthened and tested with failure in the opposite side. The load-deflection curve is not available the references; the experimental ultimate load values are  $P_{EXP} = 69$  kN for the first test and  $P_{EXP} = 81$  kN for the second test.



**Figure 3.2-3:** Case RB2. Experimental setup, (Collins and Kuchma 1999)

**Beam 8 = SE50A-45, (continued)**



V-ult = 68.6 kN shear

**Figure 3.2-4:** Case RB2. Failure mechanisms observed at ultimate load, (Collins and Kuchma 1999)

### 3.2.2 Finite element model

The characteristics of the model are presented in Figure 3.2-5; the beam was discretized into 36 FEs (approximate length of the beam elements of 0.14 m). The cross section was divided into fibres with approximately 0.01m of width; steel longitudinal filaments were simulated according to their positions in the beam considering the 3 different configurations. There is no shear reinforcement ( $\rho_{sw} = 0$ ). Apart from the concrete cover, all the fibres were considered shear resistant.

Regarding the material properties, the values given in the paper for the concrete and steel mechanical properties were used in the model; the others were considered the same as in DIANA plane stress model (Hendriks, Belletti et al. 2015). The material properties used in the model are listed in Table 3.2-1 for concrete and in Table 3.2-2 for steel.

Loads (P and 2P) were applied as nodal forces, in an incremental form until failure in 77 load steps. Energetic tolerance considered was  $1 \times 10^{-3}$  and updated normal plane switch on in the advanced loading steps. Computation time takes around 3 minutes.

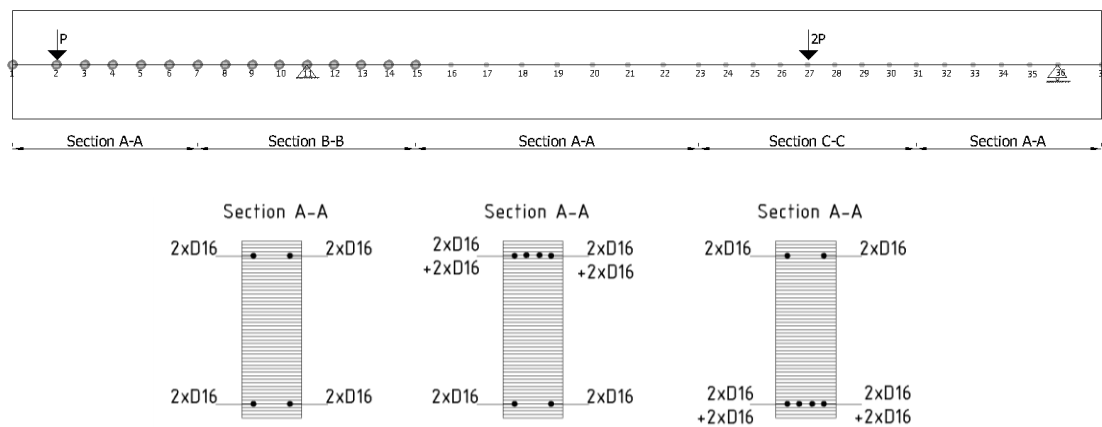


**Figure 3.2-5:** Case RB3. Mesh of the model

**Table 3.2-1:** Case RB2. Constitutive model parameters for concrete

	$f_{cm}$ (N/mm <sup>2</sup> )	$f_{ctm}^*$ (N/mm <sup>2</sup> )	$E_c^*$ (N/mm <sup>2</sup> )	$\epsilon_{cu}^*$
Mean measured values	53.5	3.80	37485	0.0035

\* assumed / determined values (same as DIANA plane stress, Hendriks et al 2014)

**Table 3.2-2:** Case RB2. Reinforcement properties

Bar	$\Phi$ (mm)	$A_s$ (mm <sup>2</sup> )	$E_s$ (N/mm <sup>2</sup> )	$f_{ym}$ (N/mm <sup>2</sup> )	$f_{um}$ (N/mm <sup>2</sup> )	$\epsilon_{su}^*$	$E_{sy}^*$ (N/mm <sup>2</sup> )
#15	16.0	200	200000	400	600	0.0353	6000

\* assumed / determined values (same as DIANA plane stress in Hendriks, Belletti et al. 2015)

### 3.2.3 Nonlinear finite element analysis

#### Load-deflection response

The load – deflection curve is presented in Table 3.2-6 and compared with the DIANA plane stress FE model performed by Hendriks, Belletti et al. (2015). The experimental values of ultimate load are included in the graphic.

In the CONSHEAR model, at first trial, the default softening of concrete in tension was considered (the Cervenka equation for tension stiffening (TS) is considered and the default values in CONSHEAR are  $k_2=0.002$  and  $c=0.5$ ). As the beam has no shear reinforcement and presents a brittle shear failure, this softening curve that represents the ‘energy of fracture’ of concrete is determinant in the failure load. As the peak load was higher than the experimentally observed with the default values for tension softening, another analysis was carried out by diminishing it (with the values  $k_2=0.002$  and  $c=0.3$ ). The two softening curves considered are presented in Figure 3.2-7. With the diminished tension softening the results of CONSHEAR are very similar to the ones computed by DIANA plane stress model, which are also in consistency with the ultimate load observed in the experiment.

The results of the nonlinear analysis for peak load and levels of damage determined by CONSHEAR and the DIANA plane stress model are resumed and compared in Table 3.2-3.

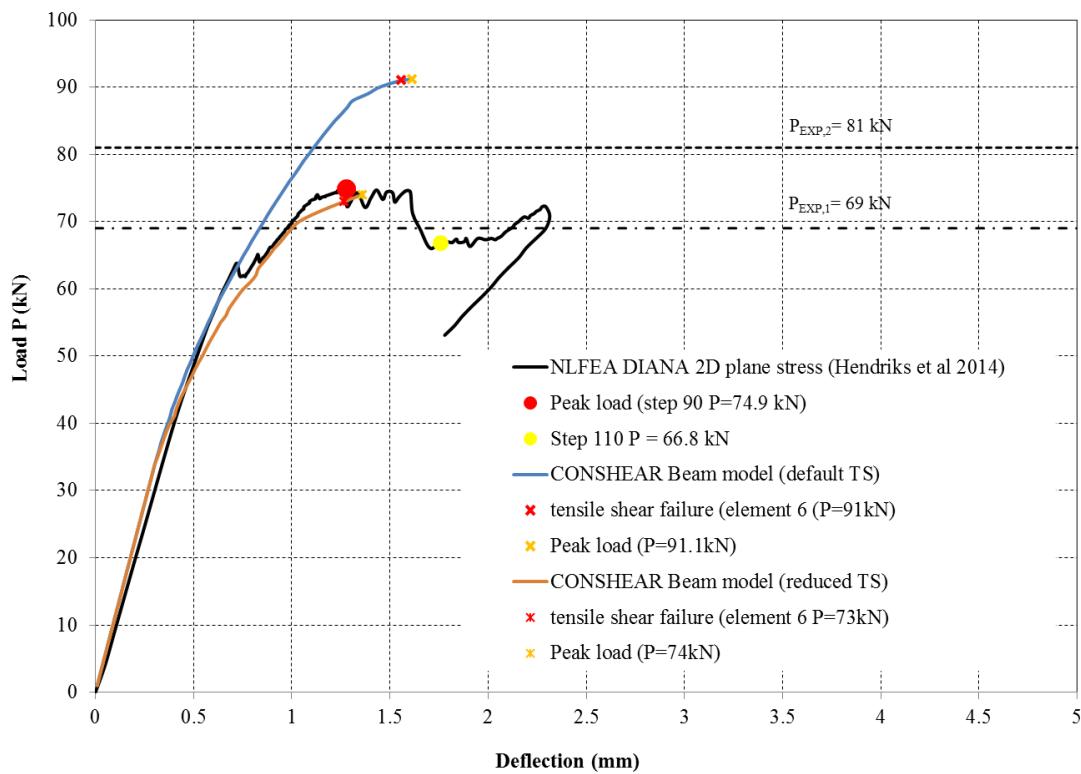


**Figure 3.2-6:** Case RB2. Load-deflection curves and levels of damage

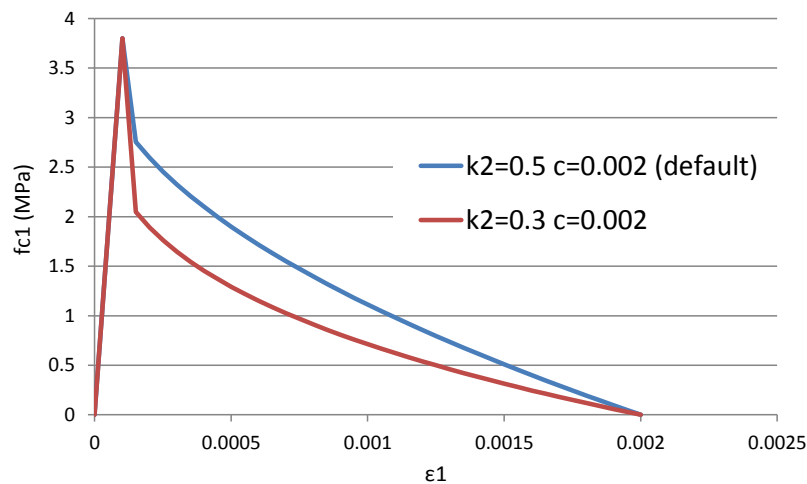


**Figure 3.2-7:** Case RB2. Tension softening of concrete in the model, (Cervenka equation)

**Table 3.2-3:** Case RB2. Results of the nonlinear finite element analysis (kN)

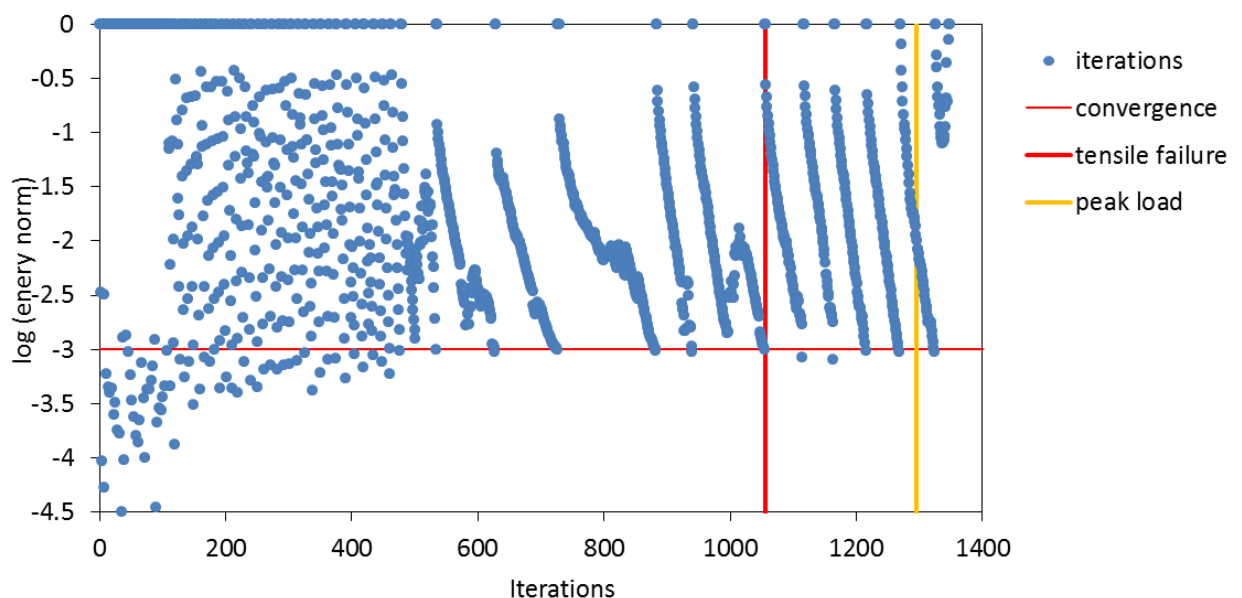
Level of damage	DIANA Plane stress	CONSHEAR Beam element (default TS)	CONSHEAR Beam element (reduced TS)	Comparison	Exp.
Peak load (kN)	74.9	91.1	74.0	≈ reduced TS; > CONSHEAR default TS	75 (average)
Start yielding long. reinf.	No yielding	No yielding	No yielding	Similar	No data
Start yielding stirrups	No stirrups	No stirrups	No stirrups	-	No data
Start crushing of concrete	-	-	-	-	No data
Computation time	2h	3 minutes	3 minutes		

The results of the CONSHEAR model (with reduced TS) are similar to the DIANA plane stress model in terms of ultimate load, failure mechanism and load-displacement curve. There is no experimental data on deflections to compare with the numerical calculations.

Failure was determined in DIANA at load  $P=74.9$  kN by a critical diagonal-tension crack, being sudden and brittle, without ductility in the post-peak regime. In CONSHEAR failure was reached at  $P=74.0$  kN with tensile failure in the web (represented by failure of the virtual stirrups), happening in element 6, located left from the left support (see mesh in Figure 3.2-5). In both models there is no yielding of longitudinal reinforcement. CONSHEAR does not give a clear decay of loading after peak load as happens in the plane stress model.

#### Convergence behaviour

The energy criterion, with a tolerance of  $1 \times 10^{-3}$ , controls the global NR iteration procedure. Figure 3.2-8 represents the energy norm versus the number of iterations throughout the nonlinear analysis until failure; the red line sets the norm for which convergence is achieved and the analysis continues with the next load step. The number of iterations needed for convergence increases near failure load due to the stronger nonlinearities, cracking and overall damage. The key levels of damage identified in the load-displacement curve are marked with vertical lines.

**Figure 3.2-8:** Case RB2. Energy norm vs. global iterations at the NR level

**Strains and stresses**

The strains with increasing load are presented in the following graphics for critical points. The longitudinal reinforcement in the bending critical section remains elastic until failure, as presented in Figure 3.2-9. Axial strains in concrete in the vertical direction in the shear critical area reach high values in failure due to opening of diagonal cracks without existence of transversal reinforcement to absorb the tensile strains (Figure 3.2-10).

Principal stresses in concrete for the shear critical area are presented in Figure 3.2-11 and Figure 3.2-12, showing that maximum tensile stress is attained and cracking occurs in the different heights of the section. In the compressive direction, stresses are not high, being far from crushing. These results represent the predicted failure mechanism: shear-failure by diagonal tension.

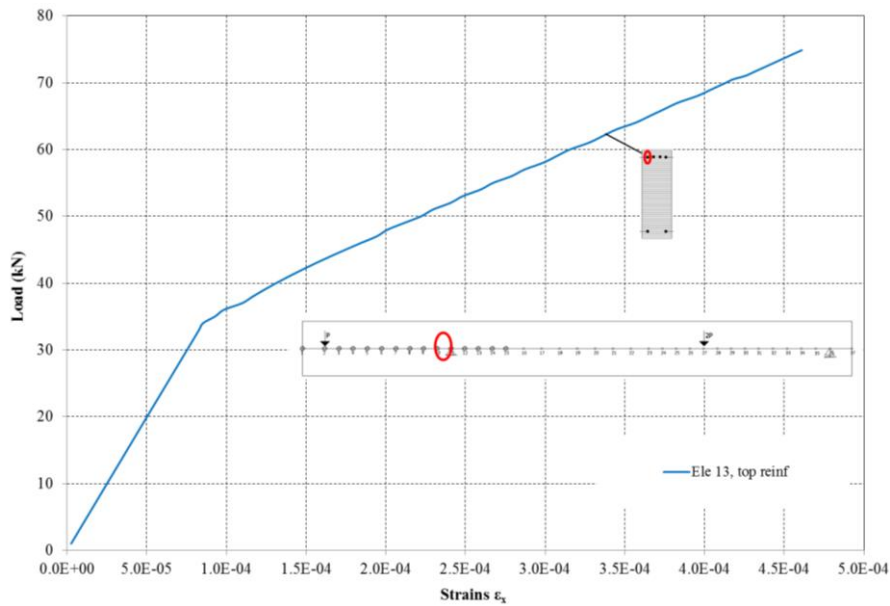


**Figure 3.2-9:** Case RB2. Load vs. axial strains in concrete in the vertical direction

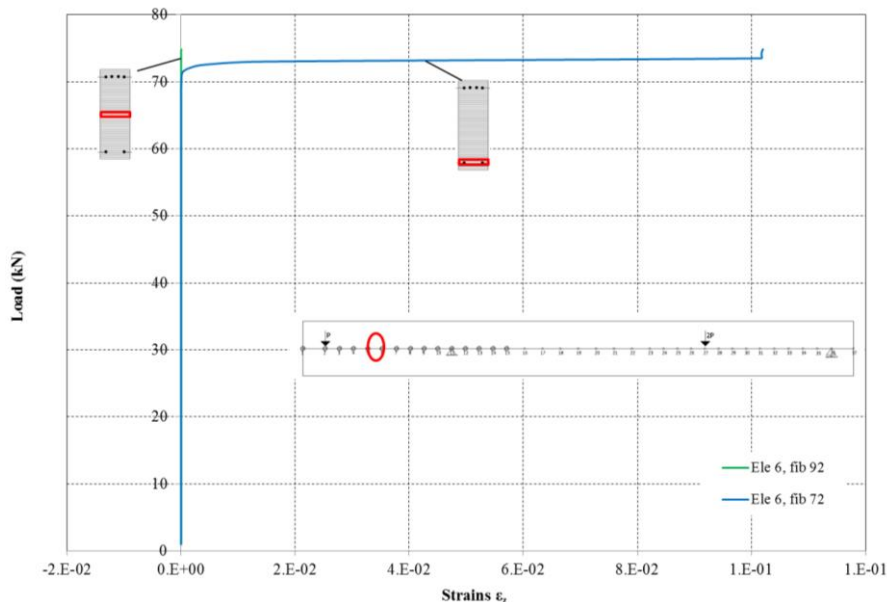


**Figure 3.2-10:** Case RB2. Load vs. longitudinal strains in transversal reinforcement

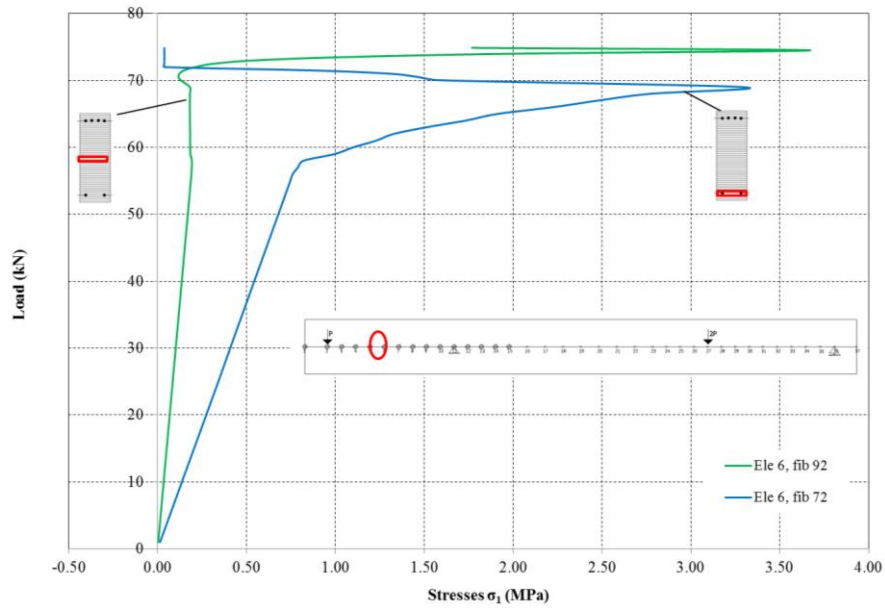


**Figure 3.2-11:** Case RB2. Load vs. principal tensile strain in concrete

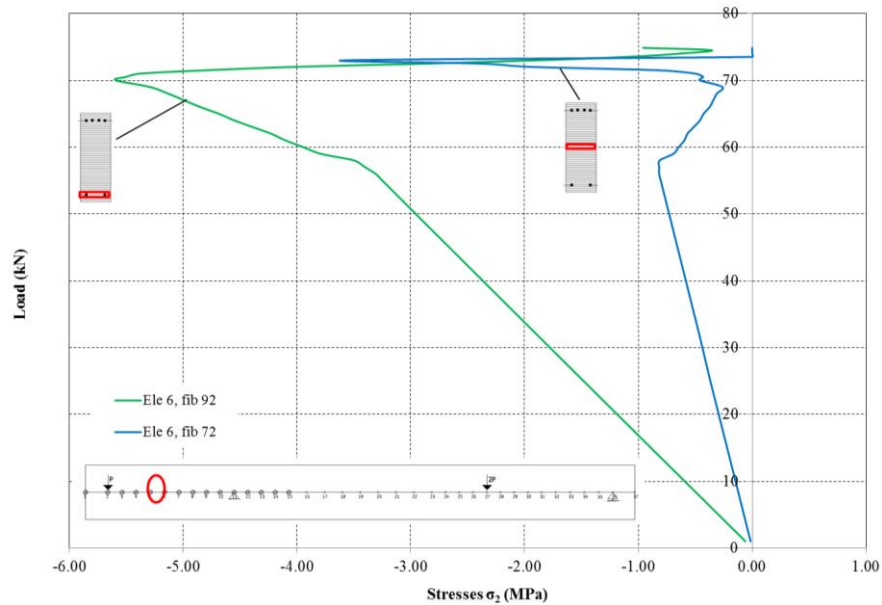


**Figure 3.2-12:** Case RB2. Load vs. principal compressive strain in concrete

**Crack patterns**

The predicted crack patterns are represented in Figure 3.2-13 for the load levels of approximately 50%, 70%, 90% of the failure load and ultimate load. The average crack spacing was determined using the expression of EC2:  $S_m(EC2) = 105 \text{ mm}$ .

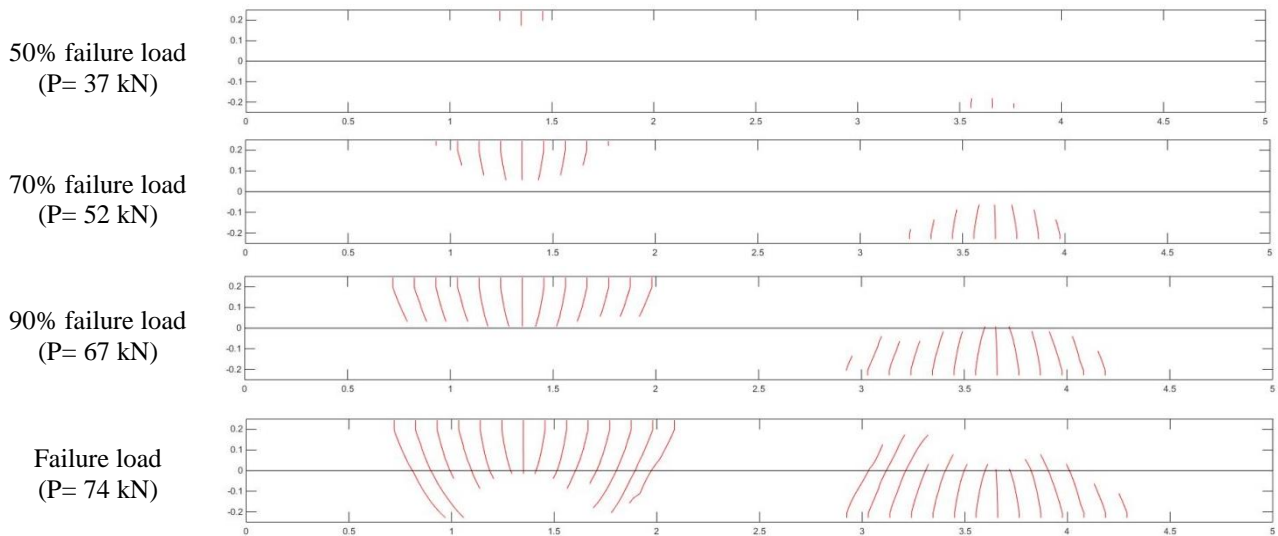


**Figure 3.2-13:** Case RB2. Predicted crack patterns

### 3.2.4 Analysis with beam models in DIANA 9.6

The analyses were performed with DIANA Release 9.6, using the nonlinear beam elements 2D Class III elements.

The mesh is built with 49 FEs with a constant length of 0.10 m and the point load was inserted in nodes 3 and 37 and supports in nodes 14 and 48 as presented in Figure 3.2-14. The cross section was defined according to the geometric properties and the reinforcement was modelled with embedded bar elements in their correspondent positions.



**Figure 3.2-14:** Case RB2. Beam model in DIANA

Regarding the material models in DIANA the following was considered:

#### Concrete

- Total strain crack model
- Rotating crack orientation / fixed crack orientation (default shear retention factor)

Tension: exponential curve

$$F_{ct} = 3.80 \text{e}6 \text{ N/m}^2$$

$$G_f = 0.105 \text{e}3 \text{ N/m (same as use in Hendriks, Belletti et al. 2015)}$$

$$\text{Reducing due to lateral cracking } k_c \text{ (Vecchio and Collins 1993)}$$

Lower bound reduction curve=0.2 (Hendriks, Belletti et al. 2015 used 0.6, maybe is too high)

Poisson ratio reduction: damage based

Compression: parabolic curve

$F_c=53.0\text{e}6\text{N/m}^2$

$G_c=37.29\text{e}3\text{N/m}$

No stress confinement

The mechanical properties for concrete are summarized in Table 3.2-4, similarly to what was considered in CONSHEAR and in DIANA plane stress model by Hendriks, Belletti et al. (2015).

**Table 3.2-4:** Case RB1. Constitutive model parameters for concrete in DIANA beam models

	$f_{cm}$ (N/mm <sup>2</sup> )	$f_{ctm}$ (N/mm <sup>2</sup> )	$E_c$ (N/mm <sup>2</sup> )	$\nu$	$G_F$ (Nmm/mm <sup>2</sup> )	$G_c$ (Nmm/mm <sup>2</sup> )
Mean measured values	53.0	3.80*	37485*	0.2	0.105*	37.29*

\* Not specified in reference; estimated according to MC2010 (fib, 2013) as in Hendriks et al 2014.

### Steel

Class: reinforcement and pile foundations

Material model: Von Mises plasticity

Plastic hardening: yield stress-plastic strain

Curves of steel (see Table 3.2-2, the same curve as considered in CONSHEAR model)

Four analyses were performed considering different integration points along the height of the section (3 and 11 points with Simpson integration scheme), different solution procedures (load control and load control with arc length), and different constitutive models for concrete (rotating and fixed crack approaches). The element type is of Class III 2D in all the analyses and the default integration along the beam's length, which corresponds to 3 points with Simpson integration, was considered in all the analysis. All the convergence checks were considered with their default tolerances. The characteristics of the 4 analyses performed are resumed in Table 3.2-5. The load was applied in approximately 100 steps until failure.

**Table 3.2-5:** Case RB2. Nonlinear analyses performed with beam models available in DIANA 9.6

NLFEA	Class beam element	Integration section height	Concrete crack model	Solution procedure NLA
DIANA Beam #1	III 2D	3 points Simpson*	Rotating	Force control
DIANA Beam #2	III 2D	11 points Simpson	Rotating	Force control
DIANA Beam #3	III 2D	11 points Simpson	Rotating	Force control + Arc length
DIANA Beam #4	III 2D	11 points Simpson	Fixed	Force control + Arc length <sup>±</sup>

\* Default integration scheme in DIANA.

The results of the several nonlinear analyses with beam elements in DIANA are compared in Figure 3.2-15 with the CONSHEAR model, with the plane stress model in DIANA and the experimental results of failure load. The analytical calculation of failure load due to bending, determined in Hendriks, Belletti et al. (2015) is also included in the graphics. A resume of the most relevant results is presented in Table 3.2-6.

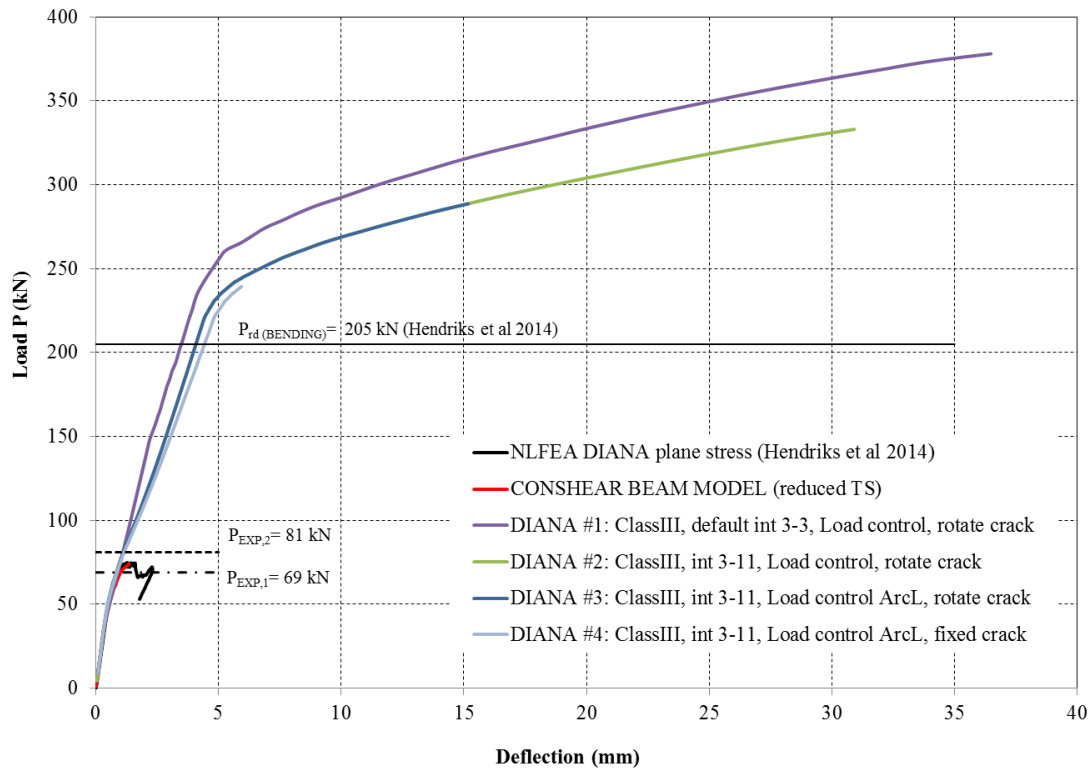


**Figure 3.2-15:** Case RB2. Load-deflection curves

**Table 3.2-6:** Case RB2. Results of the NLFEAs (kN)

Level of damage	DIANA Plane stress	CONSHEAR Beam element	DIANA #2 Beam Class III 3D	Experimental (average)
Peak Load (kN)	74.9	74.0	333.0	75.0
Failure mechanism	Shear	Shear	Bending	Shear
Computation time	2h	3 minutes	<1 minute	

Beam elements in DIANA are pure flexural based, meaning that are not able to capture shear failure. Hence DIANA beam models predicted ductile bending failure at nearly three times the ultimate load measured in the experimental test. This value is consistent with the analytical calculations for the bending capacity of the beam. As this benchmark is shear critical, it exemplifies the fact that flexural beam elements in DIANA are not capable to capture shear failure, giving unsafe predictions of loading capacity.

Analysis #1 with default integration points along the height presented a stiffer response and higher ultimate load than the analysis with increased integration points Analysis #2. Analysis #4 with fixed crack approach, stops convergence. Analysis #3 with activation of arc length reach the maximum load steps without failure, but as the failure is ductile, the results Analysis #2 with load control are enough to demonstrate that the flexural beam model is detached from the experimental response.

### 3.2.5 Concluding remarks

From the analysis of the RB2 test (benchmark failing in shear diagonal-tension) with CONSHEAR, beam elements in DIANA and comparison with DIANA plane stress (Hendriks, Belletti et al. 2015) and experimental observations (Collins & Kuchma 1999) the following conclusions are pointed out:

- CONSHEAR gave similar predictions of the ultimate load, load-deflection curve and failure mechanism in comparison with the DIANA plane stress model;

- The results of ultimate load and shear failure mechanism are consistent with the experimental observations;
- There is no experimental data of load-displacement curves to compare with;
- A good fitting of the results of DIANA plane stress model in terms of load-displacement curve and ultimate load was achieved by CONSHEAR model with reduced tension softening; default tension softening parameters gave an overestimation of failure load;
- As this case presents no shear reinforcement, the softening curve in tension plays a key role on the shear resistance of the beam and consequent ultimate load;
- CONSHEAR presents little decay of loading in post-peak regime; this should be more clearly marked as proof of failure state;
- Flexural beam elements as the ones available in DIANA are not capable of capturing shear failure; the analyses overpass shear failure and continue until ultimate bending capacity is reached resulting in unsafe estimations of the capacity of beams critical in shear.

Some notes in respect to future implementation of CONSHEAR in DIANA are:

- This example represents the relevance of the first objective of the project, which is inserting a shear-sensitive sectional formulation in DIANA and link it to existing beam elements and material models in order to capture shear failures;
- In the present state, CONSHEAR considers that ‘virtual stirrups’ (that are null) reach failure, meaning failure through diagonal cracking. The model can be formulated truly without stirrups in the new implementation;
- Regarding the problems of CONSHEAR in post-peak regime, maybe the SLA can help in tracing post-peak response; or some other work on enhancing the stability of the model in this stage;
- In the present version of CONSHEAR, tension softening of concrete is considered by means of a ‘tension stiffening’ equation, by (Cervenka 1985), that is empirical based and developed for reinforced panels under combination of loading. In the new version in DIANA, perhaps it would be good to link this tension softening to the energy of fracture of concrete in tension. In this case, tension stiffening could be linked to the reinforcement and in this manner would be considered for both longitudinal and transversal reinforcement, and the effective area would be ‘automatically’ found in the model.
- Solving the tension stiffening / tension softening issue in CONSHEAR is especially important for the cases of beams without stirrups and presenting very brittle shear failures.

### 3.3 Case RB3: Grace (2001)

The experimental program of (Grace 2001) studied the effect of strengthening using fiber-reinforced polymer (FRP) strips. The control beam of the category II (group of beams that fail in bending) from this program is used as a case study. The control beam is not strengthened with FRP.

#### 3.3.1 Experimental setup and results

The beam has a total length of 8.230 m, depth of 0.457 m and width of 0.250 m. The geometry, boundary, loading conditions and test setup are represented in Figure 3.3-1. The sectional geometry and reinforcement is represented in Figure 3.3-2. The beam is reinforced with three #8 bars ( $\Phi=25.4$  mm) at the top and bottom. Transversal reinforcement consists in #3 ( $\Phi=9.525$  mm) stirrups spaced of 152 mm. The concrete cover is 51 mm. Both longitudinal and transversal reinforcement are constant through the longitude of the beam. There are some doubts about the construction of the supports, as there is no description in the reference.

The beam exhibited a flexural failure mode, as can be observed in Figure 3.3-3, for an ultimate load of  $P_{EXP} = 141.9$  kN.

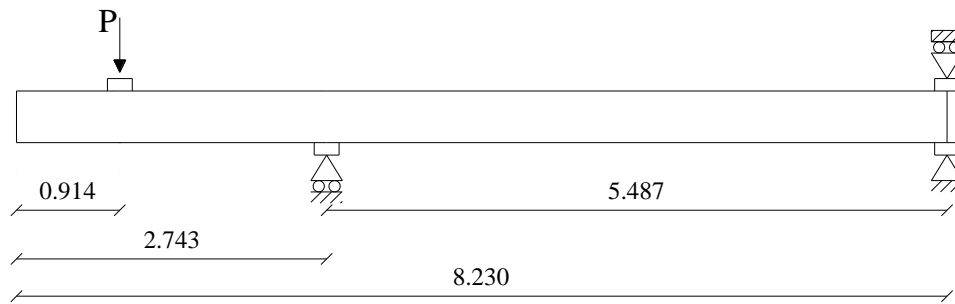


**Figure 3.3-1:** Case RB3. Loading and boundary conditions (dimension in m), (Hendriks et al. 2014)

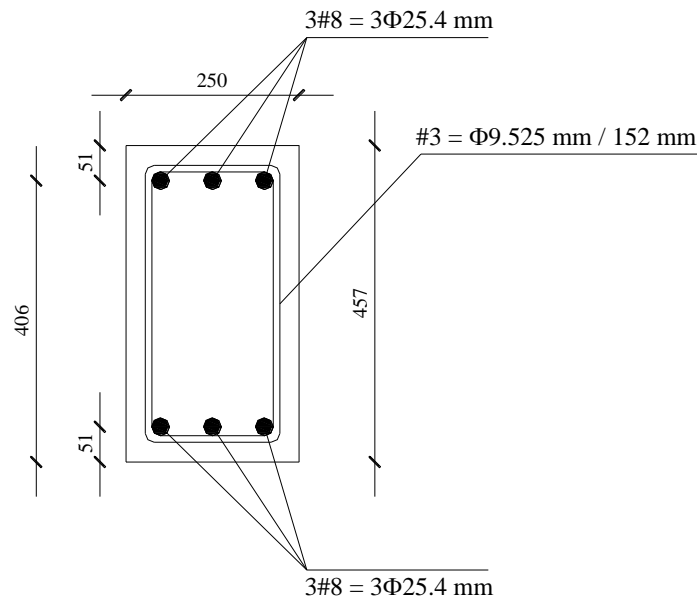


**Figure 3.3-2:** Case RB3. Cross section details (dimensions in mm), (Hendriks et al. 2014)

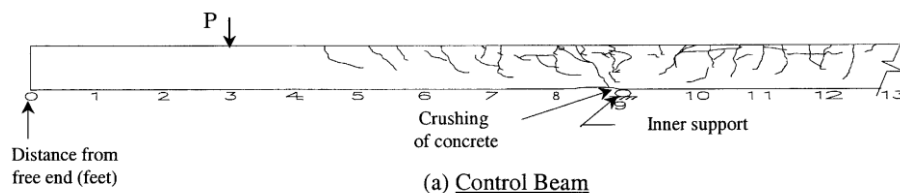


**Figure 3.3-3:** Case RB3. Failure mechanisms observed for ultimate applied load, (Grace 2001)

### 3.3.2 Finite element model

The characteristics of the model are presented in Figure 3.3-4; the beam was discretized into 43 FEs (approximate length of the beam elements of 0.10 m); the cross section was divided into fibres with approximately 0.01m of width; steel longitudinal filaments were simulated according to their positions in the beam, constant along the beam (3+3  $\text{\O}25.4\text{mm}$ ); transversal reinforcement ( $\text{\O}9.2//152\text{mm}$ ) is simulated as smeared in concrete ( $\rho_{sw} = 0.37\%$ ); apart from the concrete cover, all the fibres were considered shear resistant.

Regarding the material properties, the values given in the paper for the concrete and steel mechanical properties were used in the model; the others were considered the same as in DIANA plane stress model (Hendriks, Belletti et al. 2015). The material properties considered are listed in Table 3.3-1 for concrete and in Table 3.3-2 for steel (longitudinal and transversal steel present equal values).

Load P was applied in node 6, in an incremental form until failure in 62 load steps. Energetic tolerance considered was  $1 \times 10^{-3}$  and updated normal plane switch on in the advanced loading steps. Computation time is approximately 2 minutes.

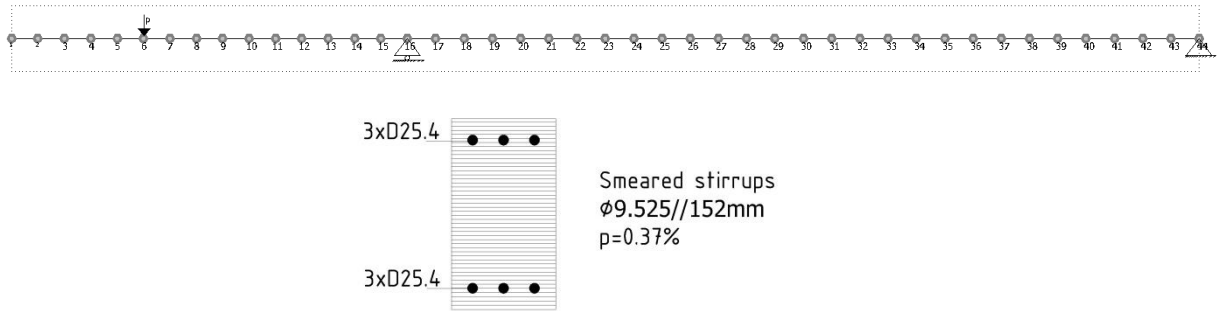


**Figure 3.3-4:** Case RB3. Mesh of the model

**Table 3.3-1:** Case RB3. Constitutive properties for concrete

	$f_{cm}$ (N/mm <sup>2</sup> )	$f_{ctm}^*$ (N/mm <sup>2</sup> )	$E_c^*$ (N/mm <sup>2</sup> )	$\epsilon_{cu}^*$
Mean measured values	31.2	2.44	31297	0.0035

\* assumed / determined values (same as DIANA plane stress, Hendriks, Belletti et al 2014)

**Table 3.3-2:** Case RB3. Reinforcement properties.

Bar	$\Phi$ (mm)	$A_s$ (mm <sup>2</sup> )	$E_s$ (N/mm <sup>2</sup> )	$f_{ym}$ (N/mm <sup>2</sup> )	$f_{um}^*$ (N/mm <sup>2</sup> )	$\epsilon_{su}^*$	$E_{sy}^*$ (N/mm <sup>2</sup> )
#3 (stirrups)	9.5	71	200000	414	500	0.05	1794
#15 (long. reinf.)	25.4	509	200000	414	500	0.05	1794

\* assumed / determined values (same as DIANA plane stress, Hendriks, Belletti et al 2014)

### 3.3.3 Nonlinear finite element analysis

#### Load-deflection response

The load – deflection curve is presented in Figure 3.3-5 and compared with the DIANA plane stress FE model performed by Hendriks, Belletti et al 2014. The experimental failure load is included in the graphic. The results of the nonlinear analysis for the start of the different levels of damage determined by the beam model and the DIANA plane stress model are marked along the curve and resumed in Table 3.3-3.

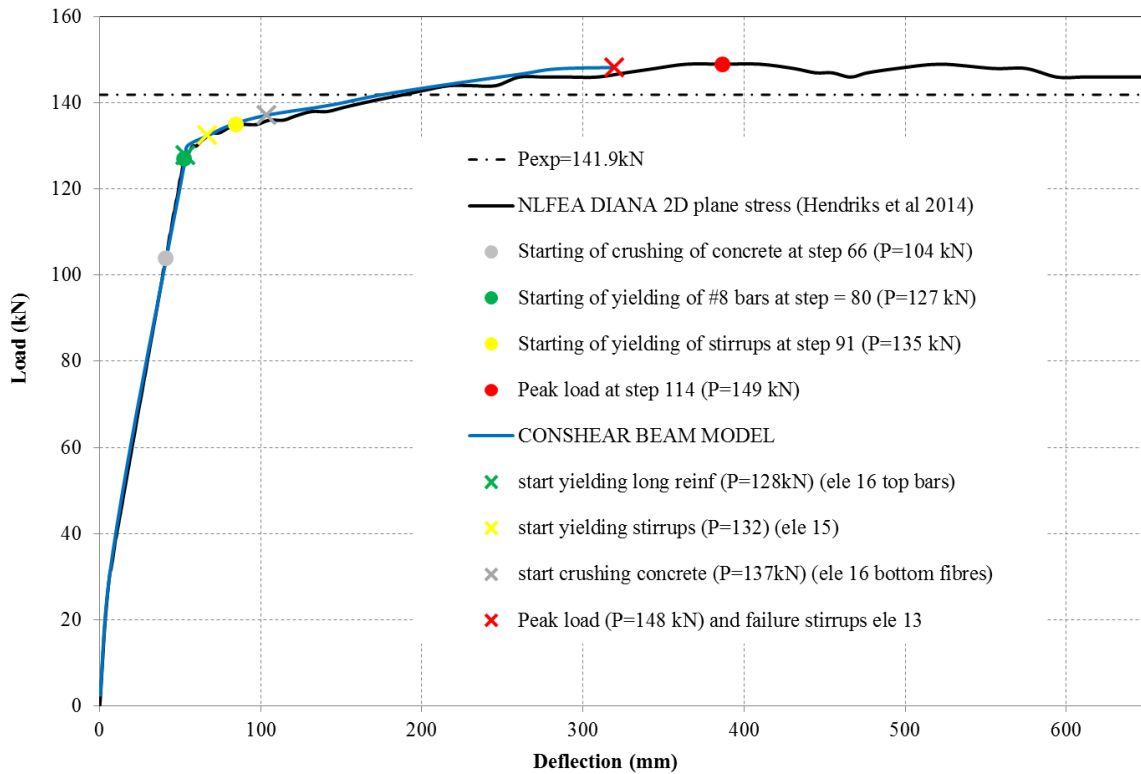


Figure 3.3-5: Case RB3. Load-deflection curves and levels of damage

Table 3.3-3: Case RB3. Results of the NLFEAs (kN)

Level of damage	DIANA Plane stress	CONSHEAR Beam element	Comparison	Experimental
Peak load	149	148	Similar	141.9
Start yielding long. reinf.	127	128	Similar	No data
Start yielding stirrups	135	132	Similar	No data
Start crushing of concrete	104	137	CONSHEAR >>	No data
Computation time	1h	2 minutes		

CONSHEAR determines a bending failure with ductility, with stirrups yielded, longitudinal reinforcement yielded and concrete crush at the bottom fibres near the left support. These results are in correspondence with DIANA calculations and experimental observations.

The results of both models for the load-displacement curve are very similar; however CONSHEAR presents less ductility than DIANA plane stress model. The ultimate load is also very similarly predicted: DIANA P=149kN, CONSHEAR P=148kN.

There is also a good fitting between CONSHEAR and DIANA plane stress model in terms of the development of damage. As presented in Table 3.3-3, similar load levels are observed for the starting of yielding of longitudinal steel (happening in CONSHEAR in element 16 in the top bars, near left support), starting yielding of stirrups (observed in CONSHEAR in element 15, at the left of the left support) (see mesh in Figure 3.3-4). Starting of crushing of concrete is differently predicted by the models: DIANA P=104kN (sooner) vs. CONSHEAR P=137kN (later); the reason for this difference might be that CONSHEAR considers Kupfer strength enhancement factor for the compressive strength of concrete that is not contemplated in DIANA plane stress model.

### Convergence behaviour

The energy criterion, with a tolerance of  $1 \times 10^{-3}$ , controls the global NR iteration procedure. Figure 3.3-6 represents the energy norm versus the number of iterations throughout the nonlinear analysis until failure; the red line sets the norm for which convergence is achieved. The key levels of damage identified in the load-displacement curve are marked with vertical lines.

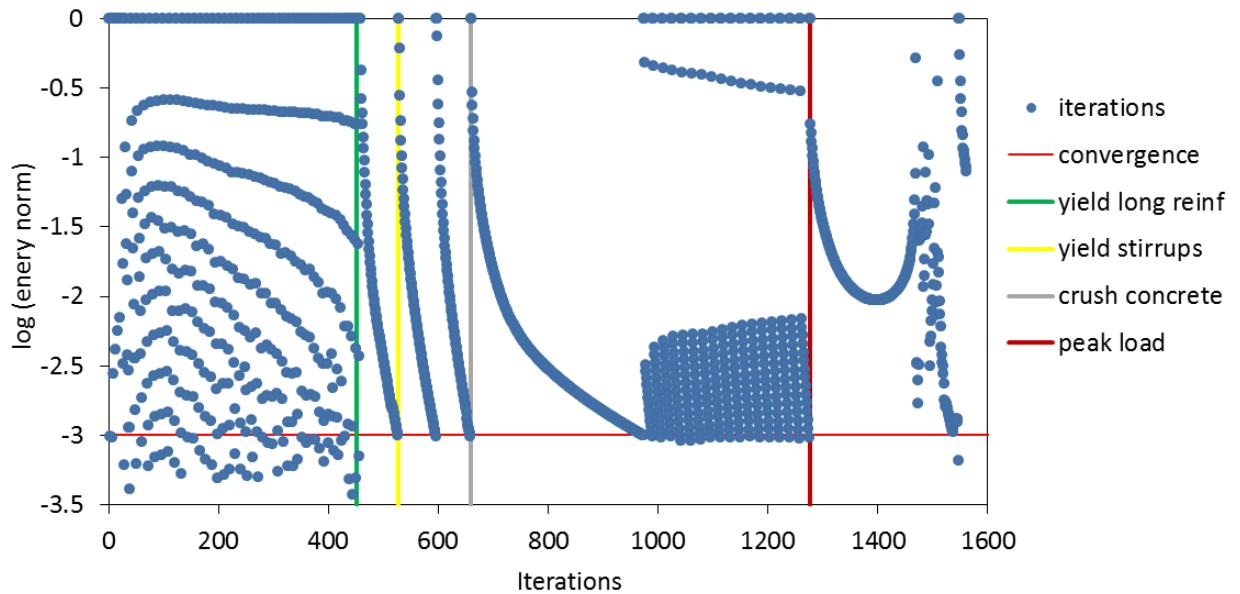


Figure 3.3-6: Case RB3. Energy norm vs. global iterations at the NR level

### Strains

The strains with increasing load are presented in the following graphics for the same points previously marked in the load-deflection curve. The concrete in the bottom fibre of element 16 (area of higher bending moment) reached the maximum strain and crush for ultimate load as presented in Figure 3.3-7. Top longitudinal reinforcement is yielded in this location too (Figure 3.3-8). Stirrups reach yielding in the shear span (Figure 3.3-9).

These results represent the bending failure mechanism predicted by the model.

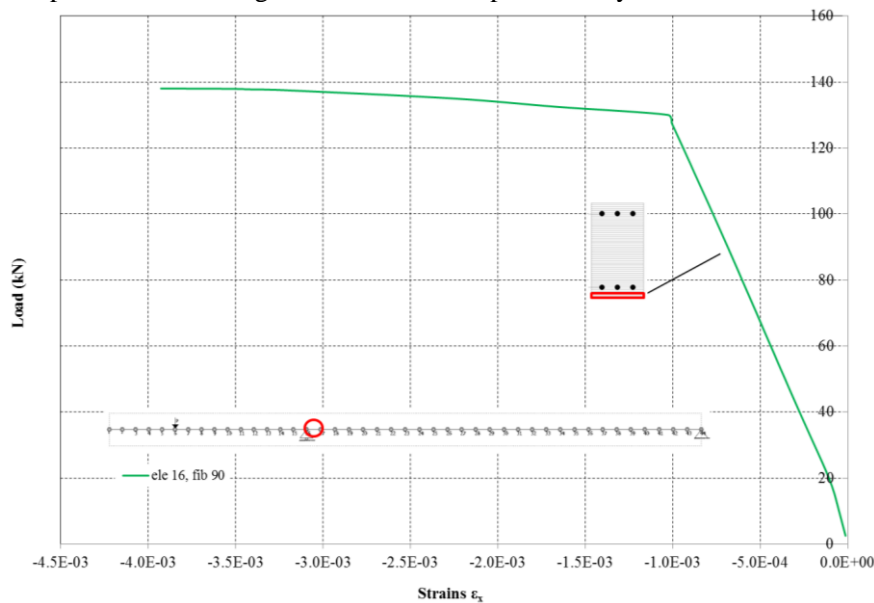
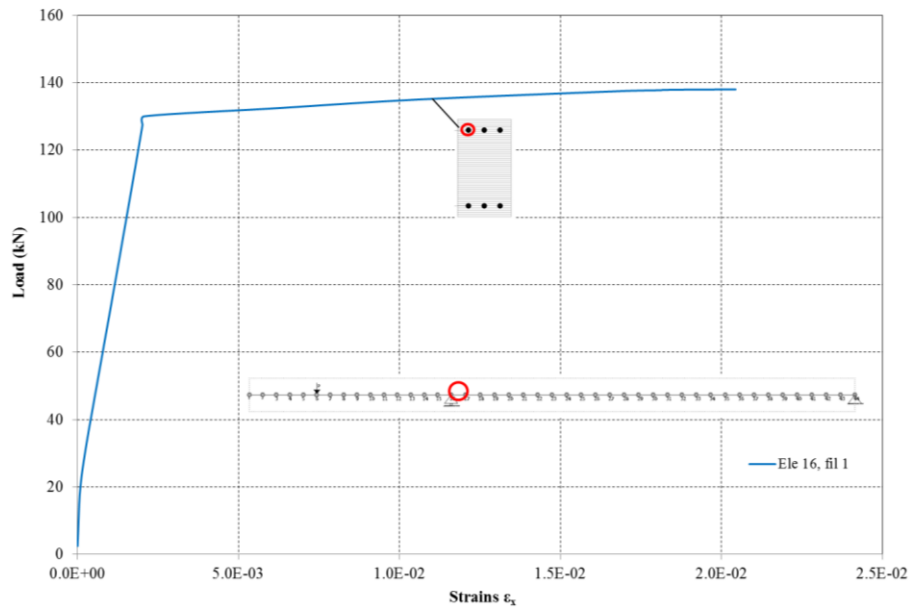
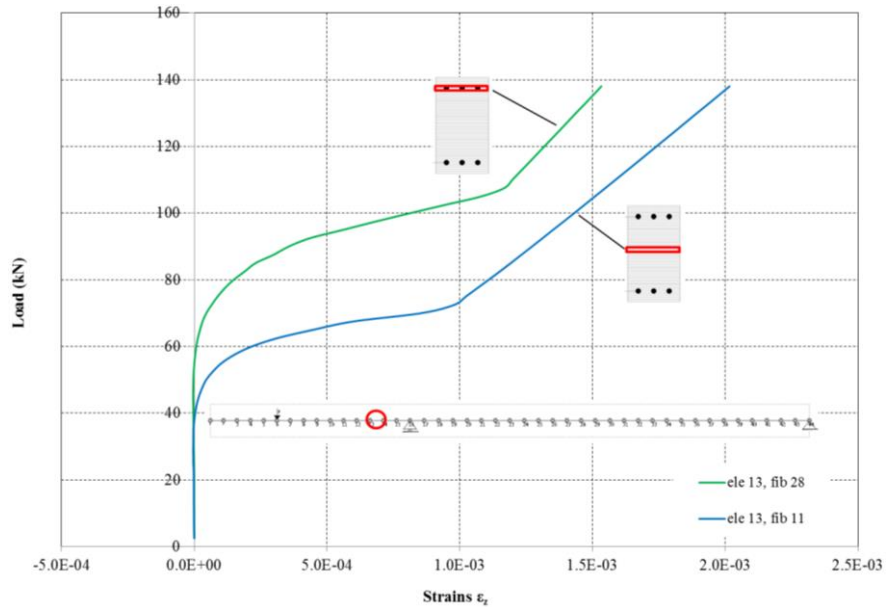


Figure 3.3-7: Case RB3. Load vs. longitudinal strains in concrete



**Figure 3.3-8:** Case RB3. Load vs. longitudinal strains in longitudinal reinforcement



**Figure 3.3-9:** Case RB3. Load vs. longitudinal strains in transversal reinforcement

**Crack patterns**

The predicted crack patterns are represented in Figure 3.3-10 for the load levels of approximately 50%, 70%, 90% of the failure load and ultimate load. The average crack spacing was determined using the expression of EC2:  $S_m(EC2) = 184 \text{ mm}$ .

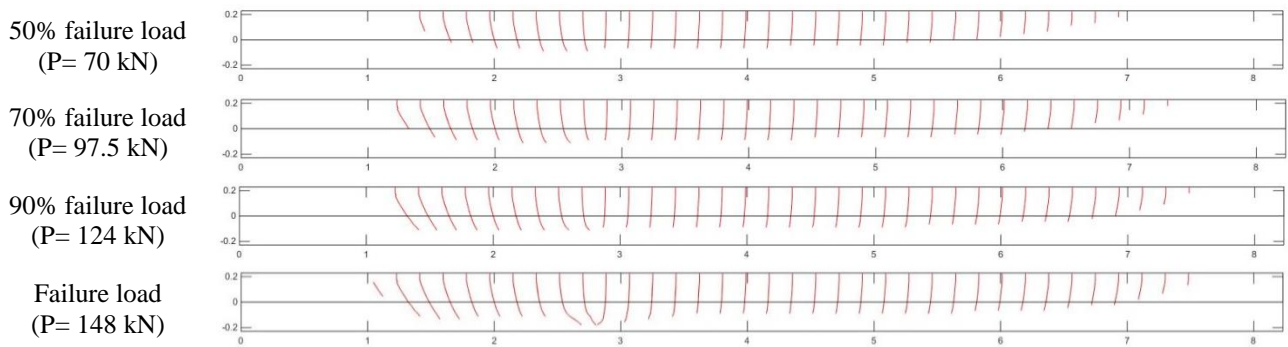


**Figure 3.3-10:** Case RB3. Predicted crack patterns

### 3.3.4 Concluding remarks

From the analysis of the RB3 test (benchmark failing in bending) with CONSHEAR and comparison with DIANA plane stress model (Hendriks, Belletti et al. 2015) and experimental observations (Grace 2001) the following conclusions are pointed out:

- CONSHEAR model gave very similar predictions of the ultimate load, load-deflection curve and failure mechanism in comparison with the DIANA plane stress model;
- The results of ultimate load and failure mechanism are consistent with the experimental observations;
- The start of yielding of reinforcement, both longitudinal and transversal, is similarly predicted by both models;
- The start of crushing of concrete happens for higher load levels in CONSHEAR because it considers the Kupfer strength enhancement factor in compression, that is not accounted in DIANA plane stress model.

## 3.4 Case RB3A: Grace (2001)

The experimental program of (Grace 2001) studied the effect of strengthening using fiber-reinforced polymer (FRP) strips. The control beam of the category I (group of beams that fail in shear) from this program is used as a case study. The control beam is not strengthened with FRP.

### 3.4.1 Experimental setup and results

The only difference between RB3A and RB3 (described in point 3.3) is that the stirrups have a spacing of 0.457 m instead of 0.152 m. All the other dimensions and parameters remain the same.

The beam exhibited a shear failure mode as represented in Figure 3.4-1 for an ultimate load of  $P_{EXP} = 155.7$  kN.

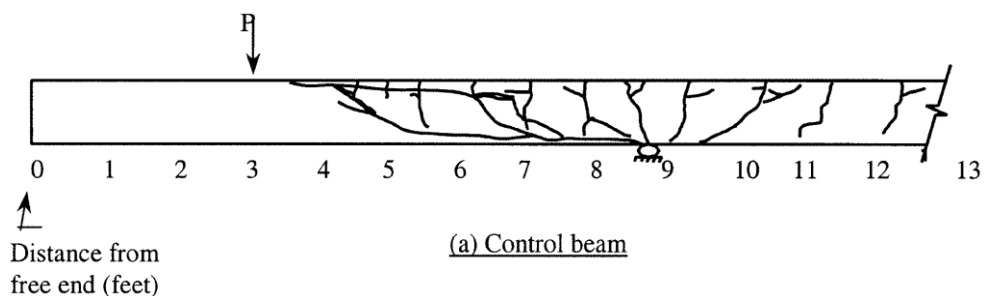


**Figure 3.4-1:** Case RB3A. Failure mechanisms observed at ultimate applied load, (Grace 2001)

### 3.4.2 Finite element model

The model is exactly the same as in case RB3 (presented in Section 3.3, see Figure 3.3-1 and Figure 3.3-2); the only difference is the quantity of stirrups that instead of  $\rho_{sw}=0.37\%$  ( $\text{Ø}9.2//152\text{mm}$ ) in case RB3 is now  $\rho_{sw}=0.12\%$  ( $\text{Ø}9.2//457\text{mm}$ ) for case RB3A. Load is applied in 75 load steps. All the other mesh and material properties are the same.

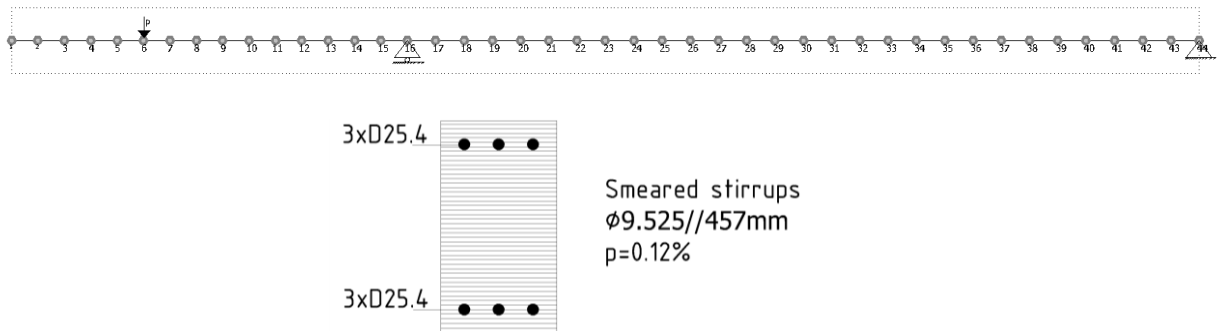


Figure 3.4-2: Case RB3A. Mesh of the model

### 3.4.3 Nonlinear finite element analysis

#### Load – deflection response

The load – deflection curve is presented in Figure 3.4-3 and compared with the DIANA plane stress FE model performed by Hendriks, Belletti et al. (2015). The ultimate load observed experimentally is indicated in the graphic. The results of both nonlinear analyses for the start of different levels of damage are marked along the load-deflection curve and also resumed and compared in Table 3.4-1.

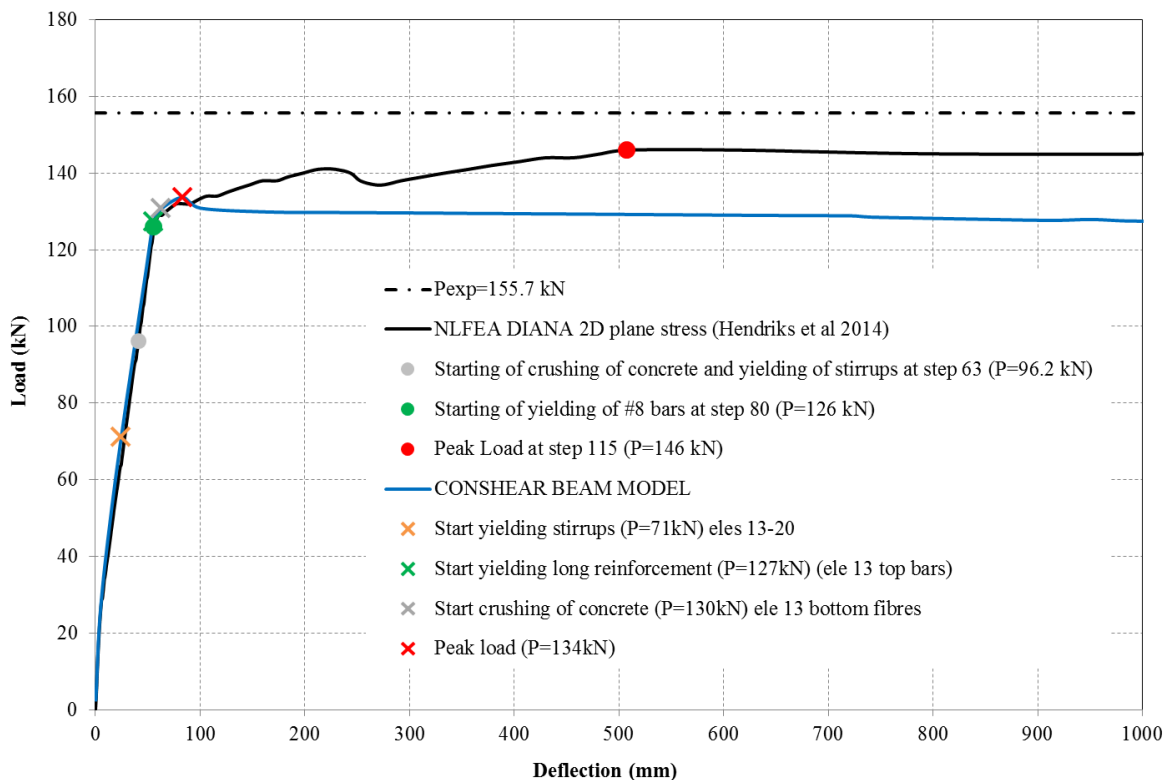


Figure 3.4-3: Case RB3A. Load-deflection curves and levels of damage

**Table 3.4-1:** Case RB3A. Results of the NLFEAs (kN)

Level of damage	DIANA Plane stress	CONSHEAR Beam element	Comparison	Experimental
Peak load	146	134	CONSHEAR <	155.7
Start yielding long. reinf.	126	127	Similar	No data
Start yielding stirrups	96.2	71.1	CONSHEAR <<	No data
Start crushing of concrete	96.2	130	CONSHEAR >>	No data
Computation time	1h	2 minutes		

Failure mechanism is predicted in CONSHEAR to be shear-bending related. CONSHEAR predicted failure of stirrups in the shear span (element 13), yielding of longitudinal reinforcement and crushing of concrete (see mesh in Figure 3.3-4). This damage is consistent with the results of DIANA plane stress model (Hendriks, Belletti et al. 2015). Pertaining to the ultimate load, CONSHEAR predicts a slightly lower value than DIANA: 134kN against 146kN.

The experimental value for ultimate load of case RB3A ( $P=155.7\text{kN}$ ) is higher than for case RB3 ( $P=141.9\text{kN}$ ), which is unexpected has the only difference between the two is that beam RB3A has more stirrups than RB3; this difference must be related with experimental randomness. The numerical models predicted lower ultimate loads for RB3A in comparison with case RB3:  $P=146$  (RB3) against  $149\text{kN}$  (RB3A) for DIANA and  $P=134\text{kN}$  (RB3) against  $P=148\text{kN}$  (RB3A) for CONSHEAR.

The start of yielding of stirrups was predicted for the load level  $P=96\text{ kN}$  in DIANA and  $P=71\text{ kN}$  in CONSHEAR. CONSHEAR predicts sooner yielding of stirrups, starting in elements 13-20, in a large area of the beam. Usually CONSHEAR overestimates strains in transversal reinforcement in the areas of the cross section with relevant damage and cracking; this was observed by comparing computed strains in stirrups with experimental data (Ferreira 2013).

The load level correspondent to the start of yielding of longitudinal reinforcement is very similarly predicted by DIANA ( $P=126\text{ kN}$ ) and CONSHEAR ( $P=127\text{ kN}$ ). In CONSHEAR yielding starts in element 13 (at left of the left support) for the top bars.

The load level for the start of concrete crushing is predicted as  $P=96\text{kN}$  in DIANA and as  $P=130\text{kN}$  in CONSHEAR, representing again a big difference between the two models. The reason for this difference must be the Kupfer compressive strength enhancement factor considered in CONSHEAR that increases the compressive strength of concrete. In CONSHEAR crushing occurs first in element 13 and propagates to several elements at ultimate load level.

### Convergence behaviour

The energy criterion, with a tolerance of  $1 \times 10^{-3}$ , controls the global NR iteration procedure. Figure 3.4-4 represents the energy norm versus the number of iterations throughout the nonlinear analysis until failure; the red line sets the norm for which convergence is achieved. The key levels of damage identified in the load-displacement curve are marked with vertical lines.

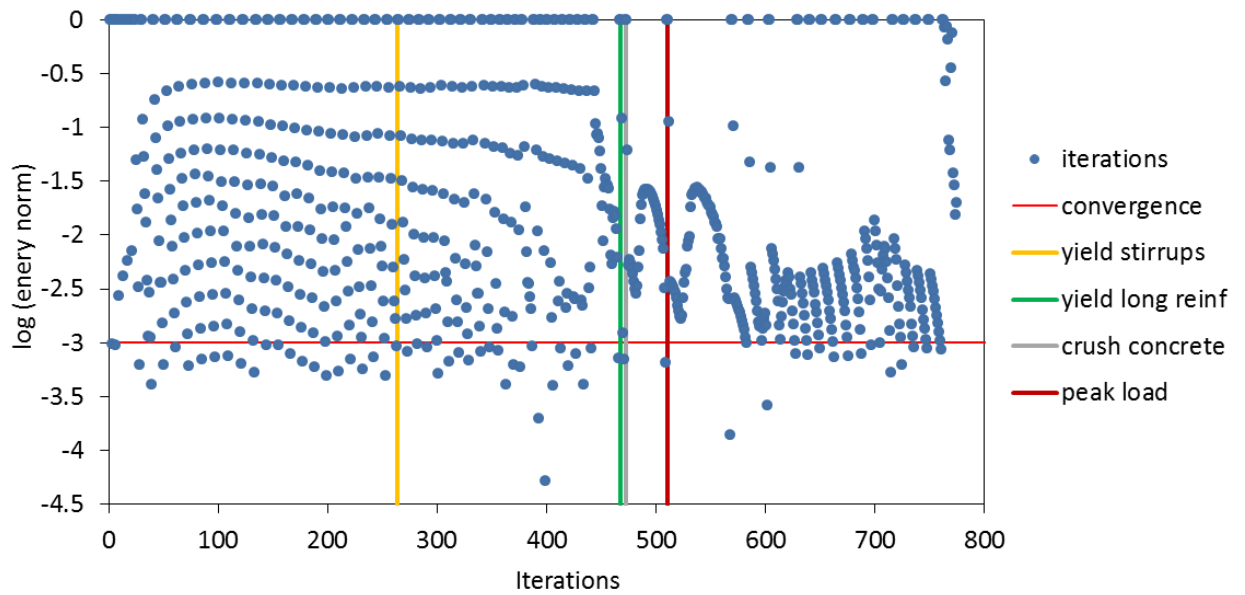


**Figure 3.4-4:** Case RB3A. Energy norm vs. global iterations at the NR level

**Strains**

The strains with increasing load are presented in the following graphics for key points of the beam. Longitudinal reinforcement in the shear span (element 13) and in the area of maximum bending moment (element 16) are presented in Figure 3.4-5; it can be seen that the top longitudinal reinforcement yields in the shear span. Stirrups are also yielded in the shear span as demonstrated in Figure 3.4-6. Concrete in the bottom fibre of element 16 is far from the maximum concrete compressive strain (Figure 3.4-7), however it crushed in the shear span (element 13).

These results represent the shear-bending failure mechanism, with extensive yielding of transversal reinforcement and yielding of longitudinal reinforcement.

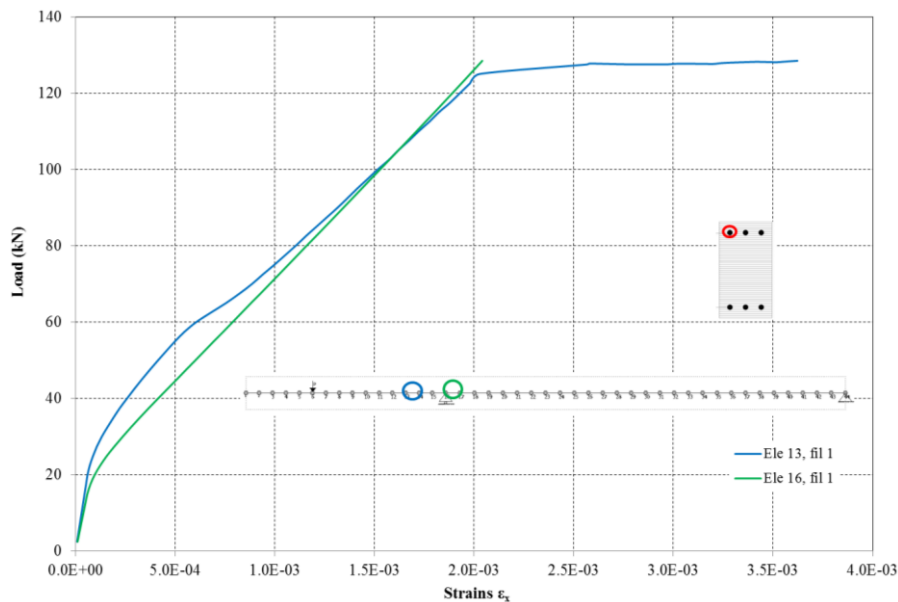


**Figure 3.4-5:** Case RB3. Load vs. longitudinal strains in longitudinal reinforcement

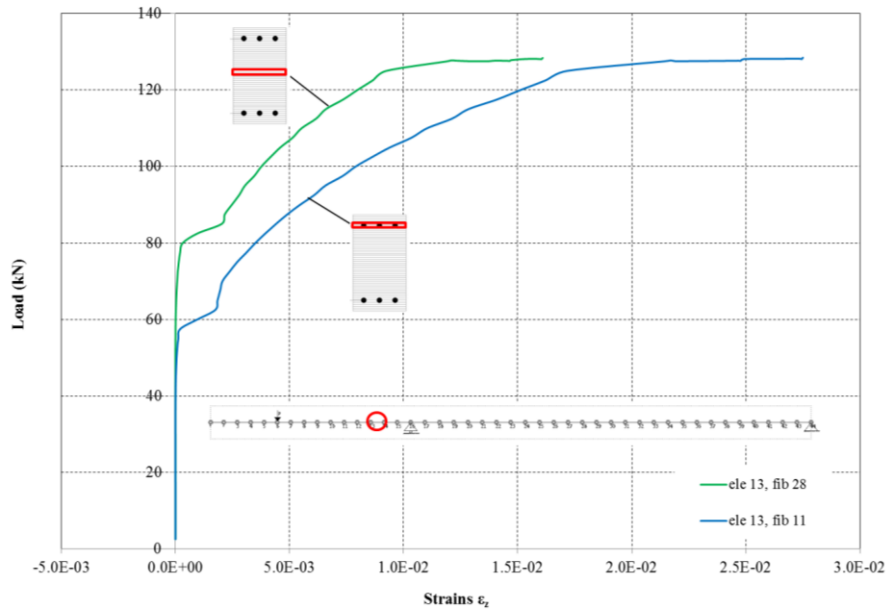


Figure 3.4-6: Case RB3. Load vs. longitudinal strains in transversal reinforcement

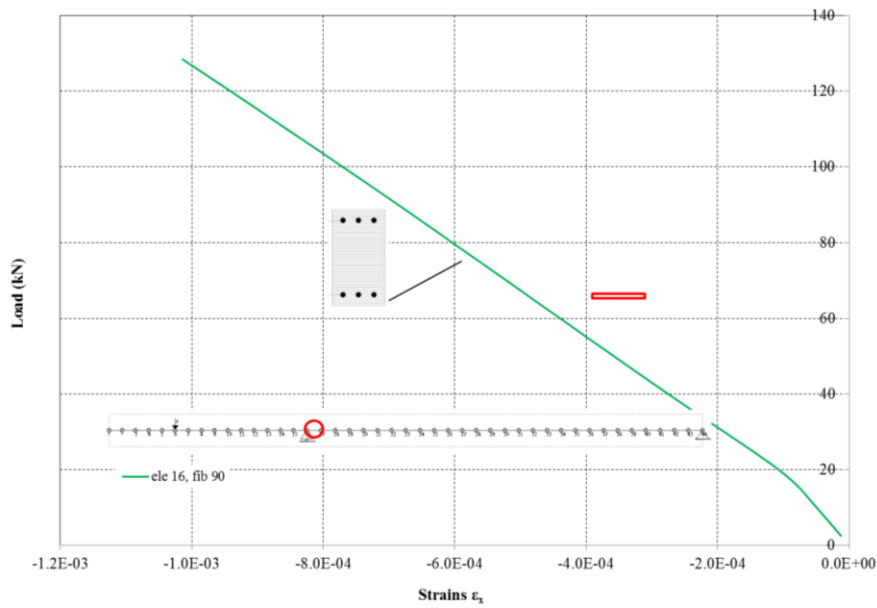
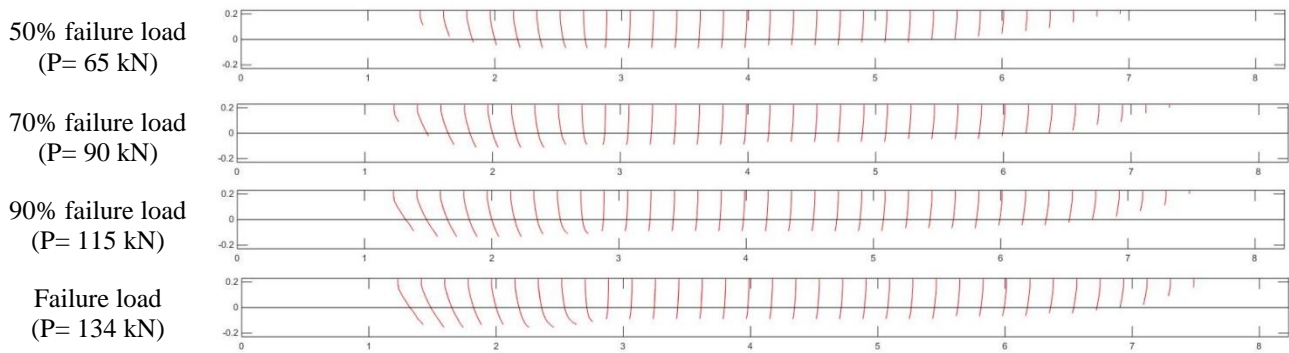


Figure 3.4-7: Case RB3. Load vs. longitudinal strains in concrete

**Crack patterns**

The predicted crack patterns are represented in Figure 3.3-10 for the load levels of approximately 50%, 70%, 90% of the failure load and ultimate load. The average crack spacing was determined using the expression of EC2:  $S_m(EC2) = 184 \text{ mm}$ .



**Figure 3.4-8:** Case RB3. Predicted crack patterns

#### 3.4.4 Concluding remarks

From the analysis of the RB3A test (benchmark failing in shear) with CONSHEAR and comparison with DIANA plane stress model (Hendriks, Belletti et al. 2015) and experimental data (Grace 2001) the following conclusions are pointed out:

- CONSHEAR model gave very similar predictions of the ultimate load, load-deflection curve and failure mechanism in comparison with the DIANA plane stress model;
- Both models slightly underestimated the experimental failure load;
- The start of yielding of longitudinal reinforcement is very similarly predicted by both models;
- CONSHEAR predicts start of yielding of stirrups sooner than DIANA plane stress model;
- The start of crushing of concrete happens for higher load levels in CONSHEAR because it considers the Kupfer strength enhancement factor in compression, that is not accounted in DIANA plane stress model.

Some notes in respect to future implementation of CONSHEAR in DIANA are:

- DIANA beam models do not account for transversal reinforcement. If beam elements in DIANA were used to calculate cases RB3 and RB3A, they would have exactly the same model. With the implementation of CONSHEAR, stirrups will be simulated in beam elements in DIANA.

## 4 RECALCULATION OF PREVIOUS WORKS: PRESTRESSED CONCRETE BEAMS

Three cases of experimental tests available in literature and calculated by Hendriks and Belletti et al. (2014) with plane stress models in DIANA were recalculated with the CONSHEAR model - Cases PB1, PB2 and PB3. These cases embrace different geometries, reinforcement, experimental setups and failure mechanisms.

The NLFEA performed by Hendriks and Belletti et al. (2014) considered for comparison in this work present the following characteristics:

- Model: 2D plane stress;
- FE: 8 node membrane elements for concrete plus embedded truss elements in reinforcement;
- Software: DIANA Release 9.4.4;
- Analysis: nonlinear static,
- Concrete: total strain rotating crack model.
- Solution: NR, norms of force and energy.

In order to attain a direct comparison, the mechanical properties of the materials used in the 2D plane stress DIANA models were, as far as possible, maintained equal in CONSHEAR.

### 4.1 Case PB1: Leonhardt, Koch et al. (1975)

The case PB1 is a prestressed beam tested by (Leonhardt, Koch et al. 1973), in an experimental campaign involving the testing of ten beams. Beam IP1 (original name in the experiments) is selected as case study presenting flexural-compressive failure mechanism.

#### 4.1.1 *Experimental setup and results*

The beam has a total length of 7.0 m, span of 6.5 m and depth of 0.9 m with variable thickness of the web. The geometry, cross-section and reinforcement details and characteristics of the experimental setup are shown in the original draws presented in Figure 4.1-1, Figure 4.1-2 and Figure 4.1-3; and resumed in the scheme of Figure 4.1-4. The beam has longitudinal reinforcement (bars of diameters  $\Phi 8$  and  $\Phi 14$ ) and non-symmetric stirrups of  $\Phi 16$  on the left hand-side and  $\Phi 12$  on the right hand-side distanced of 140mm. The prestressing reinforcement consists of 2 post-tensioned tendons prestressed at both sides and made of 12 $\Phi 12.2$  strands each; the initial stress in each tendon is equal to 635 MPa. The applied prestressing force at each cable corresponded to 995 kN and after the losses the prestressing force measured was of 891 kN in each cable. An assumed cover of 20 mm is considered as in Hendriks, Belletti et al. (2015).

A point load equal of 196 kN was applied at the same time of the prestressing of the tendons. After that the beam was loaded in a 3-point loading scheme until failure. Loading and boundary conditions are represented in Figure 4.1-5 and the global experimental set up in Figure 4.1-6.

The beam exhibited a flexural-compressive failure mode for the maximum load of 1897.5 kN, when the concrete failed. The observed crack pattern near failure ( $P=1765$  kN) is presented in Figure 4.1-7. Crack patterns and deflection with increasing load are the experimental data used for comparison with the numerical results.

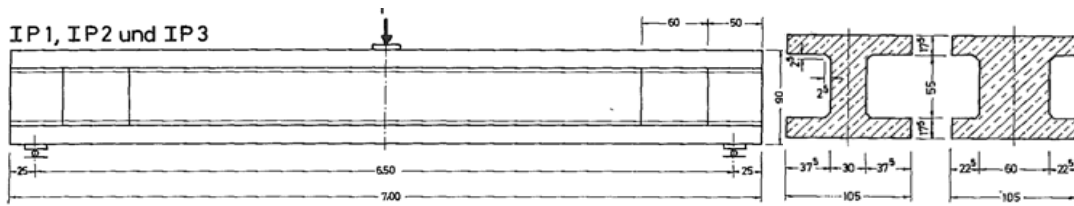


Figure 4.1-1: Case PB1. Elevation and cross-sectional details (in cm) (Leonhardt et al. 1973)

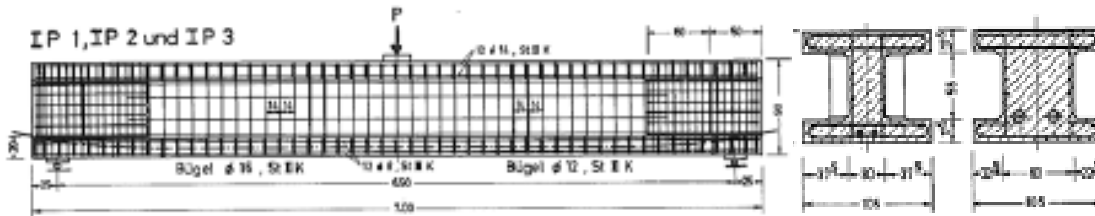


Figure 4.1-2: Case PB1. Reinforcements (in cm) (Leonhardt et al. 1973)

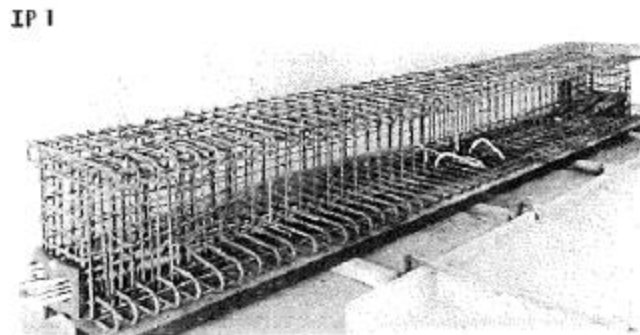


Figure 4.1-3: Case PB1. Reinforcement cage and prestressing cables (Leonhardt et al. 1973)

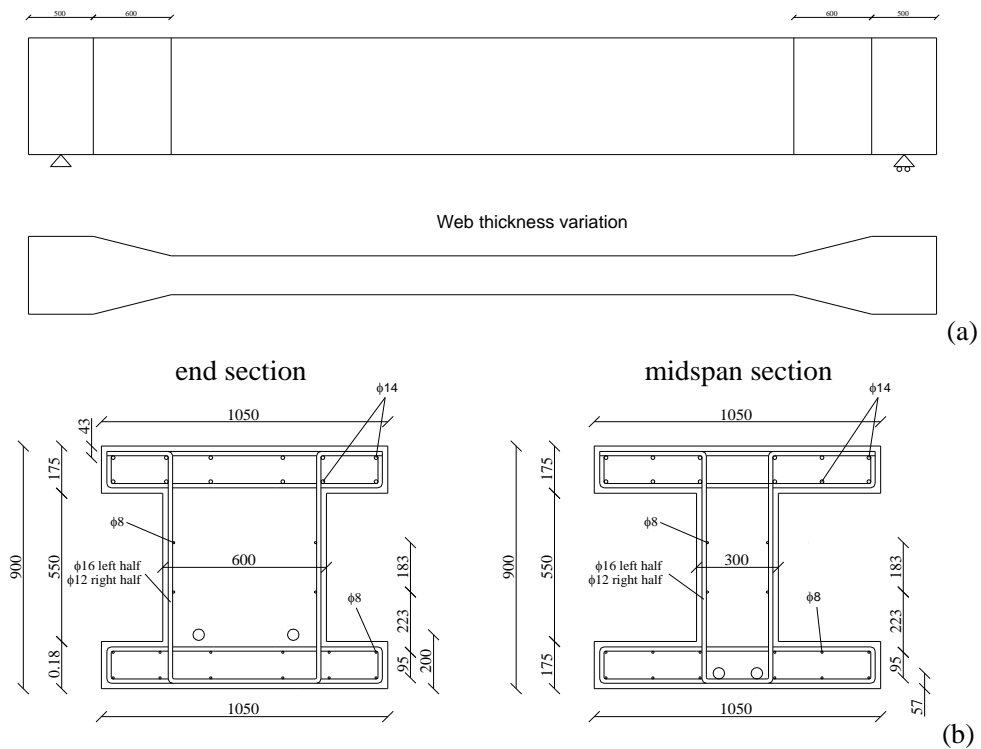
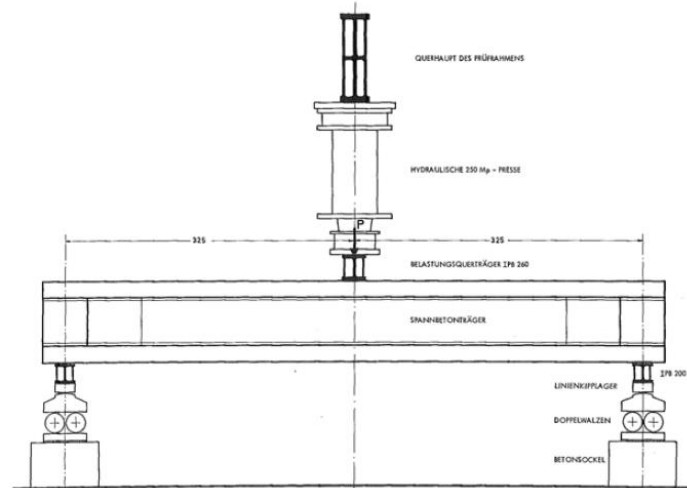
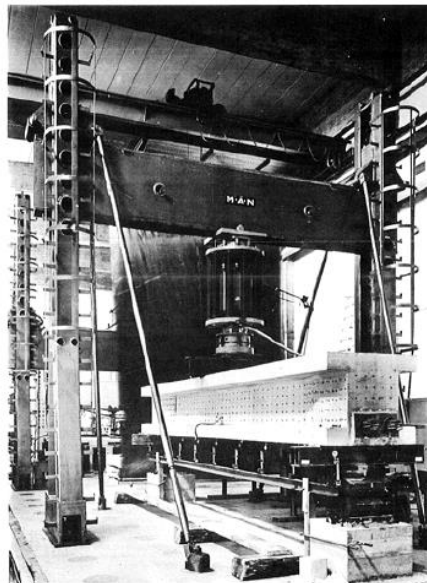


Figure 4.1-4: Case PB1. (a) Variation of the web thickness along the length of the beam (b) transversal cross section (dimensions in mm) (Hendriks & Belletti et al. 2014)



**Figure 4.1-5:** Case PB1. Loading and boundary conditions (Leonhardt et al. 1973)



**Figure 4.1-6:** Case PB1. Experimental setup (Leonhardt et al. 1973)

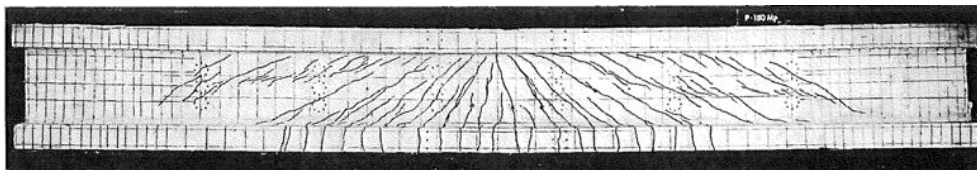


**Figure 4.1-7:** Case PB1. Crack pattern at a load equal to 1765 kN (Leonhardt et al. 1973)

#### 4.1.2 Finite element model

The characteristics of the model are presented in Figure 4.1-8; the beam was discretized into 38 FEs and 39 nodes (length of the beam elements between 0.125 m and 0.2 m). The cross section was divided into fibres with approximately 0.02 m of width. The thickened web zone at the end of the beam was simulated by varying the web width of the various elements in that area; for this 5 different cross sections were considered in the beam. Passive steel longitudinal filaments were simulated according to their positions, using one constant configuration along the beam: 12xØ14 top bars, 4xØ8 web bars and 12xØ8 bottom bars. Transversal reinforcement is considered smeared in the cross-sections, with different quantities in the left and right half parts of the beam: Ø16//140mm in

the left half and  $\text{Ø}12//140\text{mm}$  in the right half. The web of the cross section (discounting the concrete cover) and the top flanges were considered shear resistant.

The 2 prestressing cables were simulated by means of prestressed filaments in CONSHEAR with their respective eccentricity in the cross section, taking into account the slight curvature in both ends.

The beam is simple support, with constraint nodes 3 and 37. The analysis was performed in two phases:

- 1) Dead weight, prestressing force of  $P=891\text{ kN}$  in each cable and application of point load of  $196\text{ kN}$  in the mid-span (node 20);
- 2) Application of incremental load in approximately 100 load steps until failure.

Energetic tolerance considered was  $1 \times 10^{-3}$  and updated normal plane switch on in the advanced loading steps. Computation time takes around 2 minutes.

Regarding the material properties, the values given in the original report for the concrete and steel mechanical properties were used in the model; the others were considered the same as in DIANA plane stress model (Hendriks, Belletti et al. 2015). The material properties used in the model are listed in Table 4.1-1 for concrete and in Table 4.1-2 for steel.

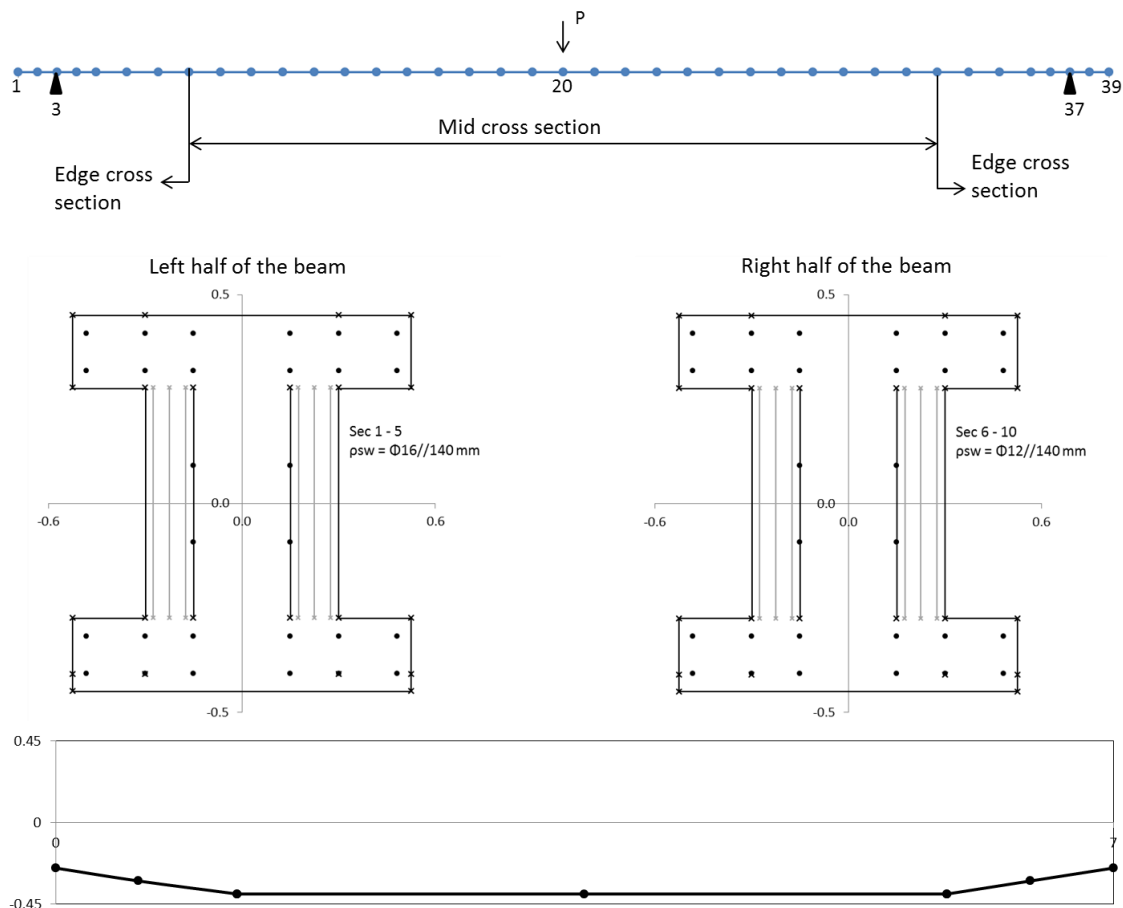


Figure 4.1-8: Case PB1. Mesh of the model

**Table 4.1-1:** Case PB1. Constitutive properties for concrete

	$f_{cm}$ (N/mm <sup>2</sup> )	$f_{ctm}^*$ (N/mm <sup>2</sup> )	$E_c^*$ (N/mm <sup>2</sup> )	$\epsilon_{cu}^*$
Mean measured values	25.3	2.16	26675	0.0035

\* assumed / determined values (when possible, same as DIANA plane stress, Hendriks, Belletti et al 2014)

**Table 4.1-2:** Case PB1. Reinforcement properties

Bar	$\Phi$ (mm)	$A_s$ (mm <sup>2</sup> )	$E_s$ (N/mm <sup>2</sup> )	$f_{ym}$ (N/mm <sup>2</sup> )	$f_{um}$ (N/mm <sup>2</sup> )	$\epsilon_{su}^*$	$E_{sy}^*$ (N/mm <sup>2</sup> )
$\Phi 12$	12.0	113	203000	500	611	0.05	2335
$\Phi 16$	16.0	201	195000	400	512	0.05	2336
$\Phi 8$	8.0	50	197000	460	567	0.05	2245
$\Phi 14$	14.0	154	207000	397	517	0.05	2496
$\Phi 12.2$	12×12.2	12×117	207000	1225	1363	0.02	9799

\* assumed / determined values

### 4.1.3 Nonlinear finite element analysis

#### Nonlinear-deflection response

The load – deflection curve is presented in Figure 4.1-9 and compared with the DIANA plane stress FE model performed by Hendriks, Belletti et al. (2015) and with the experimental curve (Leonhardt, Kock et al. 1973). The results of both nonlinear analyses for the start of different levels of damage are marked along the load-deflection curve and also resumed and compared in Table 4.1-3.

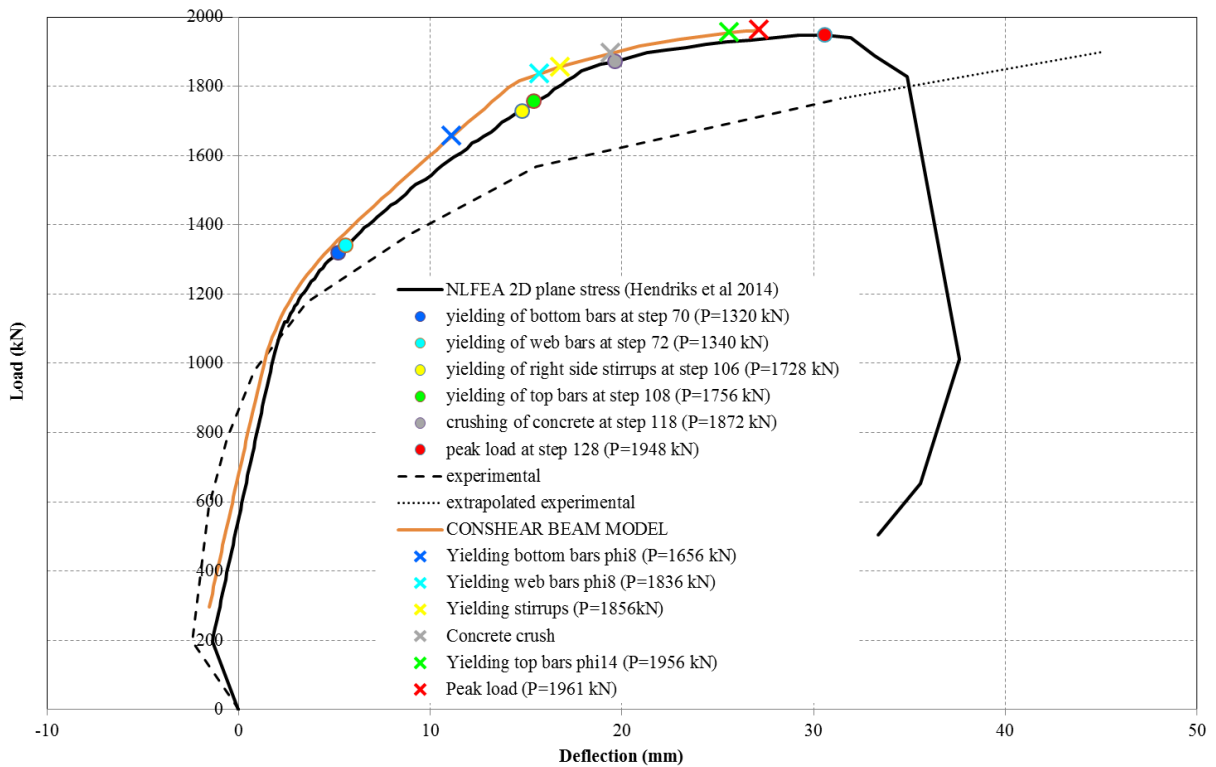


**Figure 4.1-9:** Case PB1. Load-deflection curves and levels of damage

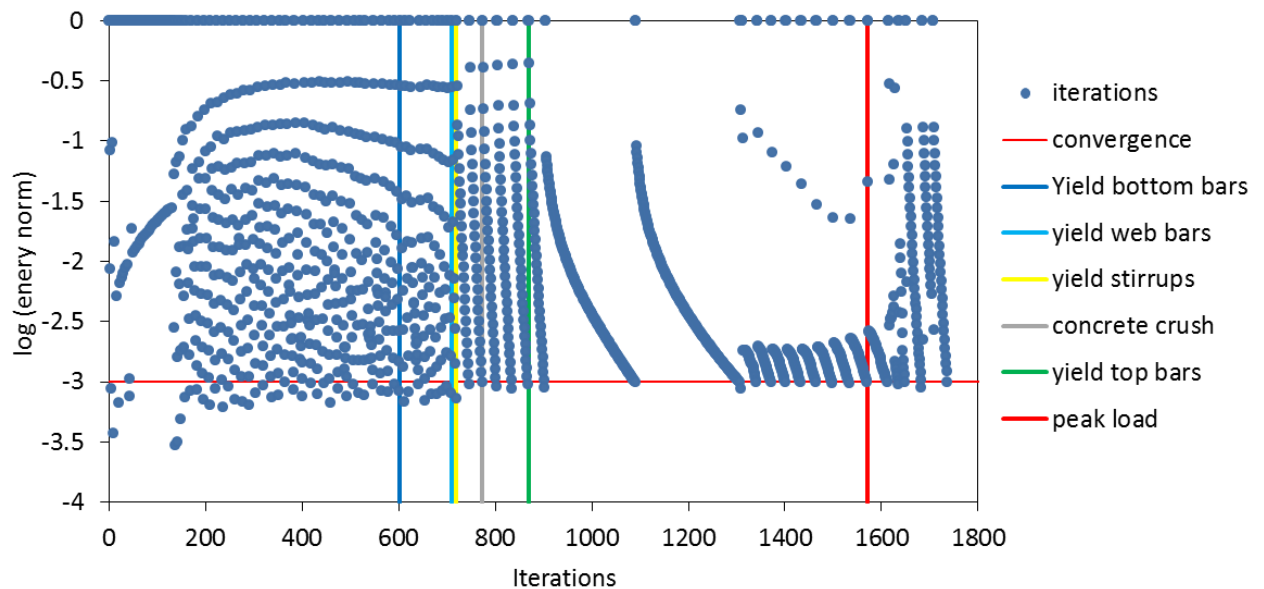
**Table 4.1-3:** Case PB1. Results of the NLFEMs (kN)

Level of damage	DIANA Plane stress	CONSHEAR Beam element	Comparison	Experimental
Start yielding long. reinf. (bottom)	1320	1656	CONSHEAR >>	No data
Start yielding long. reinf. (web)	1340	1836	CONSHEAR >>	No data
Start yielding stirrups	1728	1856	CONSHEAR >	No data
Start yielding long. reinf. (top)	1756	1956	CONSHEAR >>	No data
Crushing of concrete	1872	1896	Similar	No data
Peak load	1948	1961	Similar	1897.5
Computation time	1h30m	2 minutes		

CONSHEAR presented a similar response to DIANA plane stress model, which also agrees with the experimental results. Similar values for ultimate load were predicted and for the same failure mechanism related to bending, with yielding of reinforcement (transversal and longitudinal) and crushing of concrete. The sequence of the development of damage is similarly predicted by CONSHEAR and DIANA plane stress model; however CONSHEAR presents later yielding of longitudinal and also transversal reinforcement. Crushing of concrete appears for similar load levels. Both models are stiffer than the experimental response for advanced loading. Both models predicted well the failure mechanism and peak load.

### Convergence behaviour

The energy criterion, with a tolerance of  $1 \times 10^{-3}$ , controls the global NR iteration procedure. Figure XX represents the energy norm versus the number of iterations throughout the nonlinear analysis until failure; the red line sets the norm for which convergence is achieved. The key levels of damage identified in the load-displacement curve are marked with vertical lines.

**Figure 4.1-10:** Case PB1. Energy norm vs. global iterations at the NR level

### Strains

The strains with increasing load are presented in the following graphics for key points of damage in the beam.

Strains in longitudinal reinforcement are presented in Figure 4.1-11 for the two spans (element 23 and element 13, that have different area of stirrups) and in Figure 4.1-12 for the position of higher bending moment (element 20). There is little difference in the strains in the two spans. Extensive yielding is attained in the bottom and web filaments in element 20.

Prestressing steel in element 20 is yielded but did not reach ultimate strength (Figure 4.1-13).

Strains in transversal reinforcement are represented in Figure 4.1-14 for two positions of fibres and for both spans (left span has  $\Phi 16$ mm stirrups and right span has  $\Phi 12$ mm). Strains in stirrups are higher in the right span in comparison with the left span for the same load level. Stirrups reach yielding in the right span for load levels near failure. Concrete is crushed in compression in the top fibre at mid span as presented in Figure 4.1-15.

These results represent the bending failure mechanism predicted by the model.

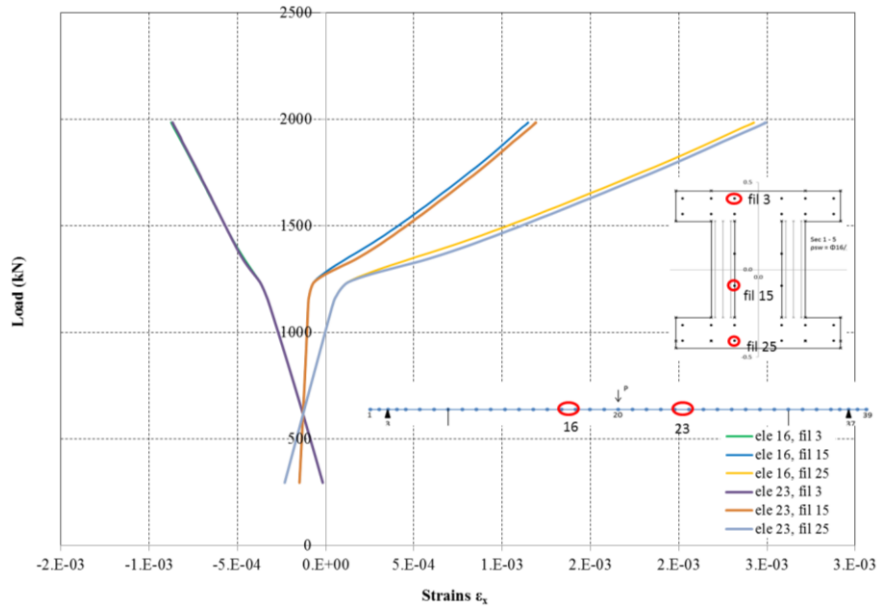


Figure 4.1-11: Case PB1. Load vs. longitudinal strains in longitudinal reinforcement at shear spans

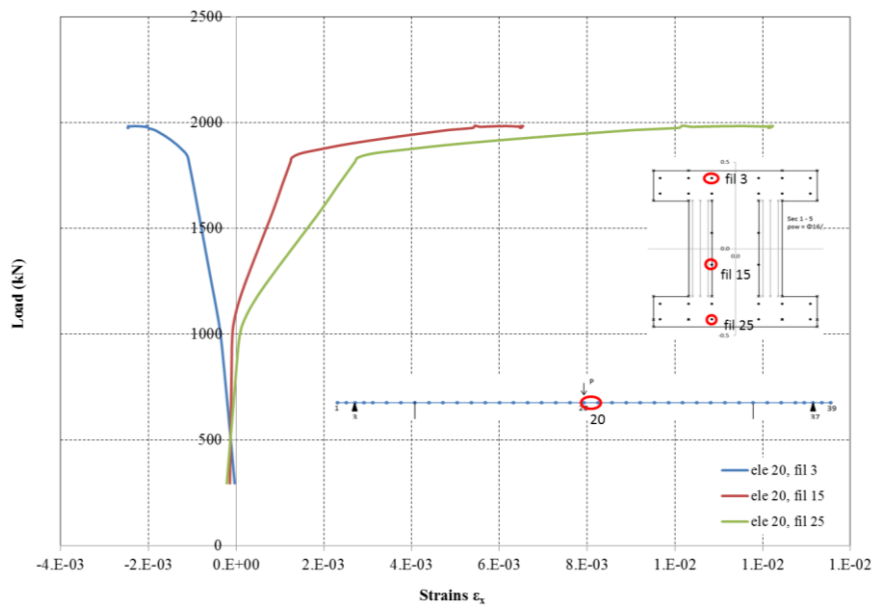


Figure 4.1-12: Case PB1. Load vs. longitudinal strains in longitudinal reinforcement at mid span

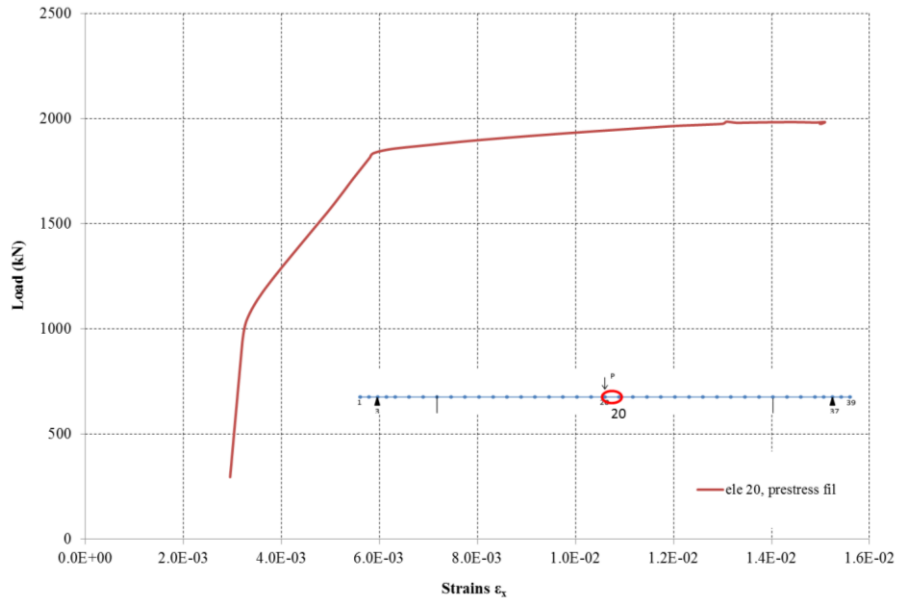


Figure 4.1-13: Case PB1. Load vs. longitudinal strains in prestressed tendon at mid span

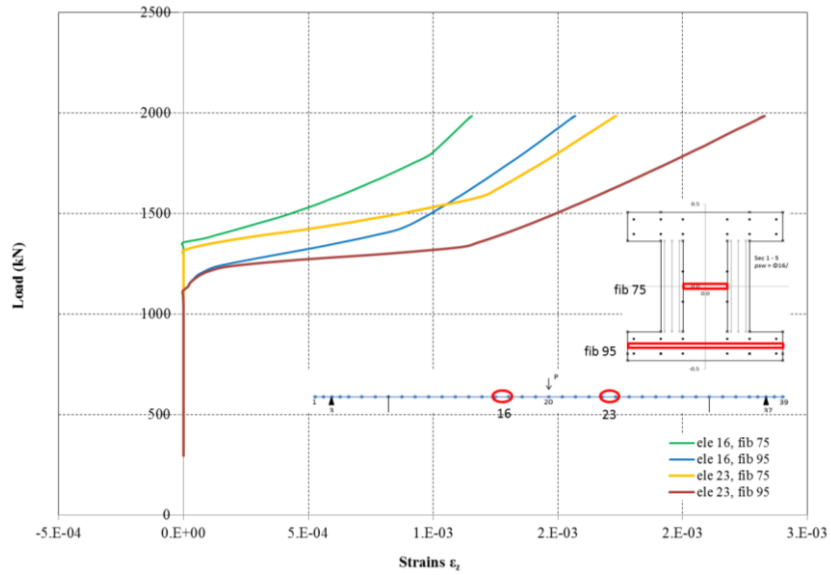
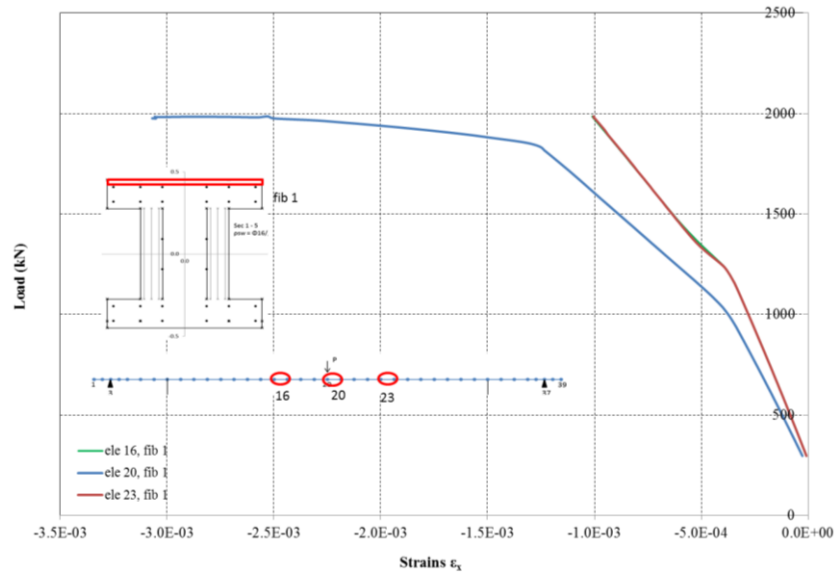


Figure 4.1-14: Case PB1. Load vs. longitudinal strains in transversal reinforcement



**Figure 4.1-15:** Case PB1. Load vs. longitudinal strains in concrete

### Crack patterns

The predicted crack patterns are represented in Figure 4.1-16 for the load levels of approximately 50%, 70%, 90% of the failure load and ultimate load. The average crack spacing was determined using the expression of EC2:  $S_m(EC2) = 208 \text{ mm}$ .

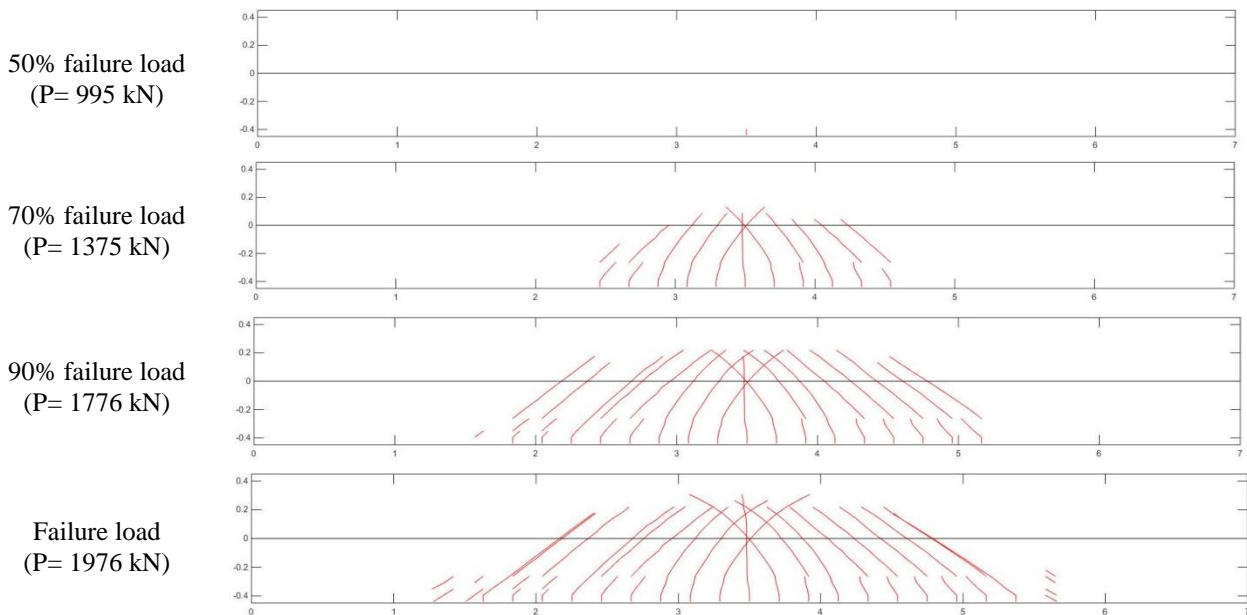


**Figure 4.1-16:** Case PB1. Predicted crack patterns

#### 4.1.4 Concluding remarks

From the analysis of the PB1 test (benchmark failing in shear) with CONSHEAR and comparison with DIANA plane stress model (Hendriks, Belletti et al. 2015) and experimental data (Leonhardt et al. 1973) the following conclusions are pointed out:

- CONSHEAR and DIANA plane stress model presented quite similar results in terms of load-deflection curve, maximum load and bending failure mechanism;
- The results were consistent with the experimental measurements.

### 4.2 Case PB2/NSEL: Sun and Kuchma (2007)

The work of (Sun and Kuchma 2007) consisted in a large experimental campaign to study the shear behaviour and resistant mechanism of high strength concrete prestressed girders of large dimensions. The high strength concrete prestressed girders were designed according to AASHTO LRFD Bridge Design Specifications and tested at the Newmark Structural Laboratory. From this experimental campaign, Girder 3 is selected as case study presenting shear - compressive failure mechanism.

#### 4.2.1 Experimental setup and results

The beam has a T-shape cross section, total length of 15.85 m and depth of 1.6 m; a concrete deck is casted on top of the girder. The cross-section, geometry and reinforcement details are shown in the original draws of Figure 4.2-1; and also resumed in **Figure 4.2-2**.

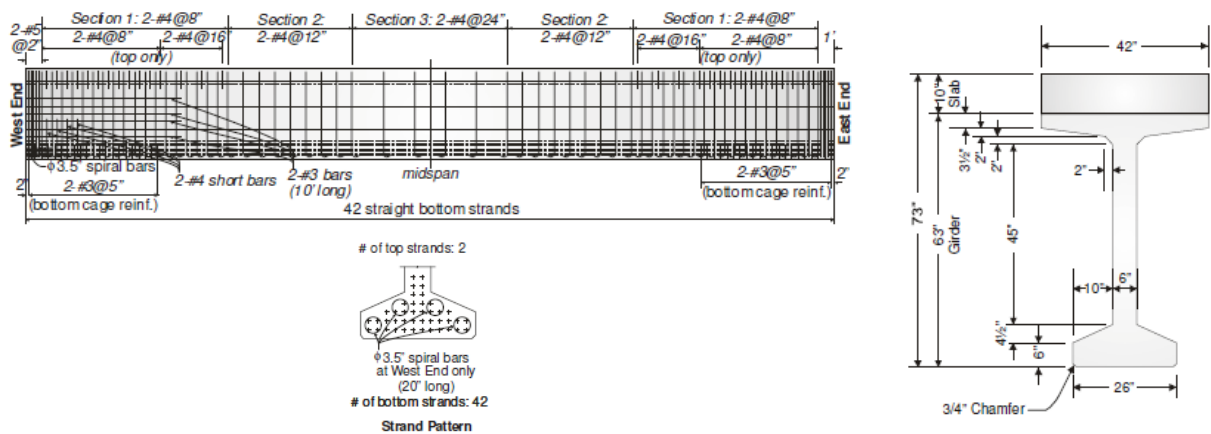


**Figure 4.2-1:** Case PB2. Cross section details (dimensions in inch) (Sun and Kuchma 2007)

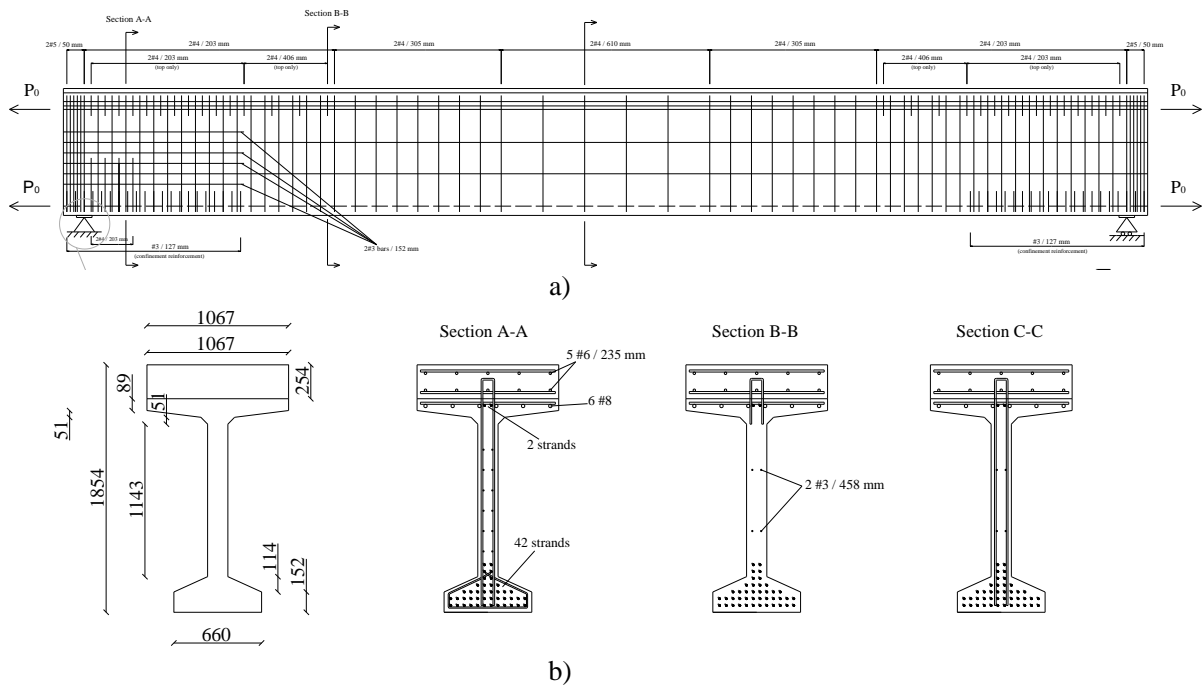


**Figure 4.2-2:** Case PB2. (a) dimensions of the beam and loading scheme, (b) reinforcement and cross section (dimensions in mm) (Hendriks, Belletti et al 2014)

Main transversal reinforcement consists of #4 double legged deformed bars with different spacings - 203 / 305 / 610 mm. In both ends this shear reinforcement is increased in #5 double legged bars at 50

mm spacing in a length of 500 mm from each ends. The passive longitudinal reinforcement consisted in two pairs of #3 longitudinal bars in the web (spaced at 458 mm) and one layer of 6x#8 bars in the top flange. The East end was designed to satisfy LRFD requirements while the West end region contained addition reinforcement: distributed horizontal, vertical and confinement reinforcement. In this region, passive longitudinal reinforcement in the web was increased to 6 pairs of #3 bars (spaced at 152.4mm), in a length of 3.408m. The concrete deck has two layers of 5#6 bars.

Pertaining to prestressing steel, 44 seven-wire low-relaxation straight strands (with diameter of  $\Phi 15.2$  mm each) were used: 42 strands in the bottom bulb and 2 strands in the top flange. The effective initial stress in the prestressing steel, measured before testing and after immediate losses, was  $1068 \text{ N/mm}^2$ .

The test consists in a simple supported configuration with distributed load in a length of 13.41 m as represented in Figure 4.2-3. The beam exhibited a shear-compression failure mechanism with crushing of concrete at web-bulb interface, as represented in Figure 4.2-4. The beam was tested twice: after the East end failed, this side was repaired by adding reinforcement and concrete and vertical post-tensioning; the beam was then reloaded in the same loading and support conditions until failure of the West end. This case study relates to the first test only: failure was achieved for a load level of 6984 kN at a deflection of 76.2mm.

Experimental data available in the reference consists on deflections, crack patterns, strains in concrete and reinforcement.

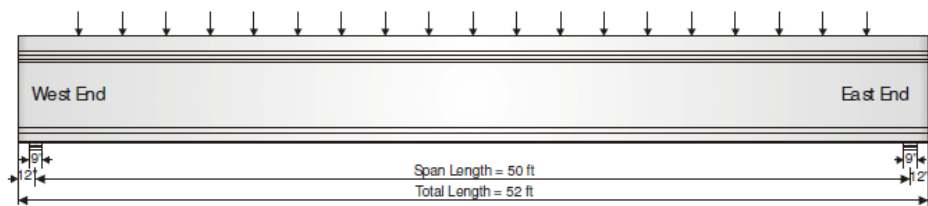


**Figure 4.2-3:** Case PB2. Loading, boundary conditions and dimension (in ft) (Sun and Kuchma 2007)

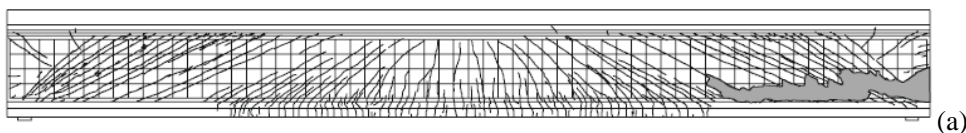


**Figure 4.2-4:** Case PB2. Failure mechanisms at ultimate load of East end (Sun and Kuchma 2007)

#### 4.2.2 Finite element model

The characteristics of the model are presented in Figure 4.2-5; the beam was discretized into 52 FEs and 53 nodes (length of the beam elements approximately of 0.3 m). The cross section was divided into fibres with approximately 0.02 m of width. Passive steel longitudinal filaments were simulated according to their positions in the beam using 2 different configurations in the girder as represented in Figure 4.2-5:  $A_{s11}$  - 6#8 top bars, 6x2#3 web bars;  $A_{s12}$  - 6#8 top bars, 2x2#3 web bars. The deck part has two layers of 5#6 bars.

Transversal reinforcement is considered smeared in the cross-sections, with different quantities along the beam as also presented in Figure 4.2-5:  $A_{sw1}$  - 2#4//203mm,  $A_{sw2}$  - 2#4//305mm,  $A_{sw3}$  - 2#4//610mm. The web of the girder and the top flanges were considered shear resistant; the fibres of the deck and the fibres of the bottom flange are non-shear resistant. This choice is consistent with what was observed and considered in the work of Sun and Kuchma (Figure 4.2-6).

The 44 prestressing cables were assembled into 8 groups of bars with the same eccentricity. These 8 groups of bars were simulated by means of prestressed filaments in CONSHEAR with their respective eccentricity in the cross section and the area correspondent to the numbers of cables of each group.

The beam is simple support, with constraint nodes 2 and 52. The analysis was performed in two phases:

- 1) Dead weight and prestressing force of  $P=149.52$  kN per cable;
- 2) Application of incremental distributed load (between nodes 5 to 49) in approximately 100 load steps until failure.

Energetic tolerance considered was  $1 \times 10^{-3}$  and updated normal plane switch on in the advanced loading steps. Computation time takes around 30 minutes (very difficult and slow to converge in the last load steps, near failure).

Regarding the material properties, the values given in the report for the concrete and steel mechanical properties were used in the model; the others were considered the same as in DIANA plane stress model (Hendriks, Belletti et al. 2015). The material properties used in the model are listed in Table 4.2-1 for concrete and in Table 4.2-2 for steel. For the tension stiffening curve, the default parameters were not used; instead the values of  $k_2=0.8$  and  $c=0.004$  were considered (see Figure 4.2-7).

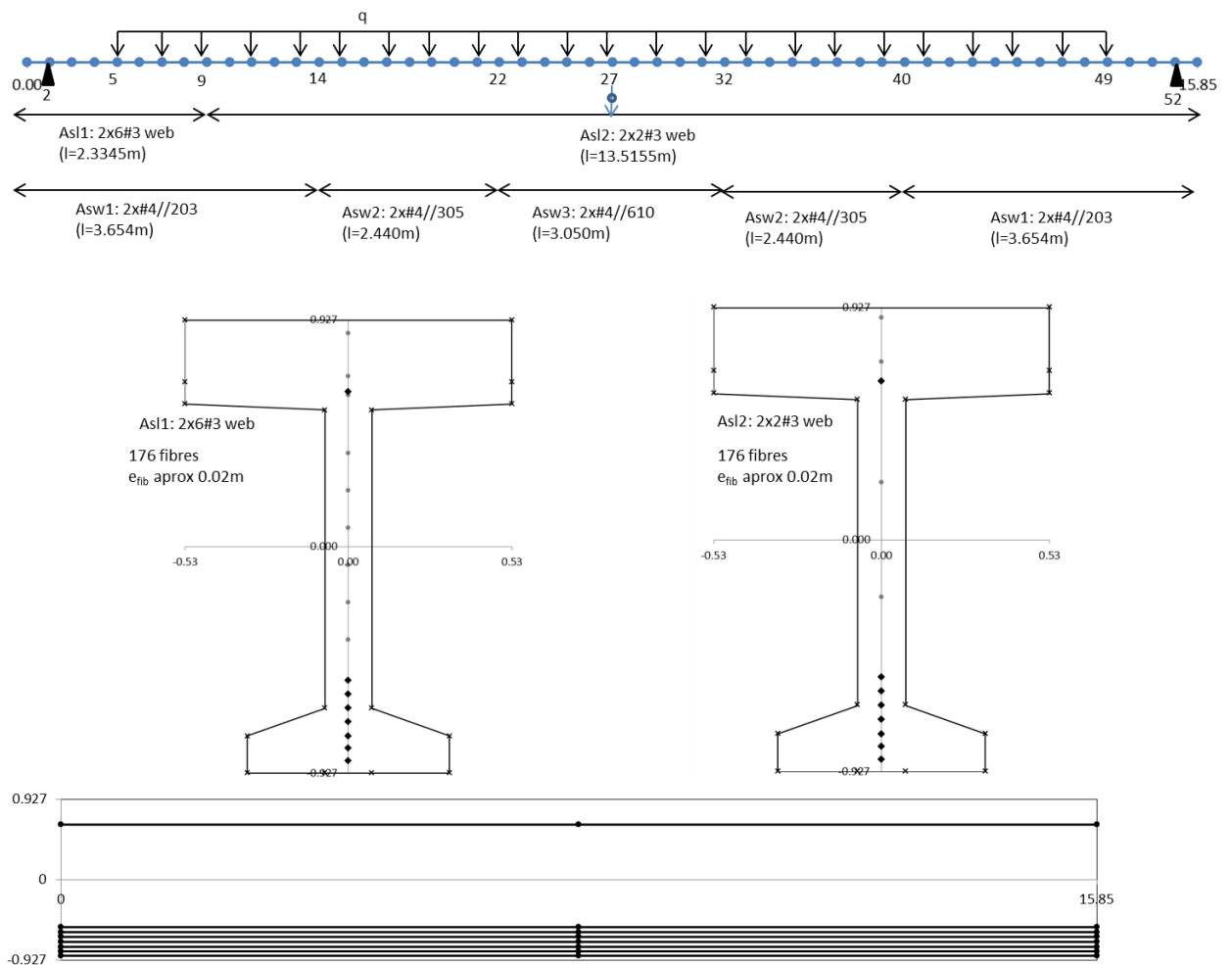
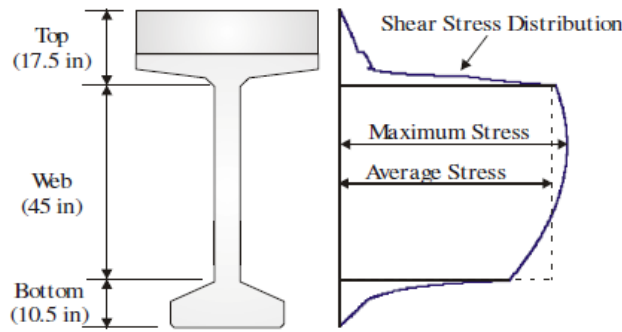


Figure 4.2-5: Case PB2. Mesh of the model



**Figure 4.2-6:** Case PB2. Shear stress distribution in the girder section (Sun and Kuchma 2007)

**Table 4.2-1:** Case PB2. Constitutive properties for concrete

	$f_{cm}$ (N/mm <sup>2</sup> )	$f_{ctm}^*$ (N/mm <sup>2</sup> )	$E_c^*$ (N/mm <sup>2</sup> )	$\epsilon_{cu}^*$
Girder: Mean measured values	109.63	5.28	52710	0.0026
Deck: Mean measured values	24.82	2.65	25076	0.0035

\* assumed / determined values (when possible, same as DIANA plane stress, Hendriks, Belletti et al 2014)

**Table 4.2-2:** Case PB2. Reinforcement properties.

Bar	$\Phi$ (mm)	$A_s$ (mm <sup>2</sup> )	$E_s$ (N/mm <sup>2</sup> )	$f_{ym}$ (N/mm <sup>2</sup> )	$f_{um}$ (N/mm <sup>2</sup> )	$\epsilon_{su}^*$	$E_{sy}^*$ (N/mm <sup>2</sup> )
#3	9.5	71	200000	413.7	620.5	0.05	4315
#4	12.7	129	200000	467.5	731.5	0.05	5539
#6	19.1	284	200000	413.7	620.5	0.05	4315
#8	25.4	510	200000	413.7	620.5	0.05	4315
strands,7wire	15.24	140	196500	1675	1862	0.02	16295

\* assumed / determined values

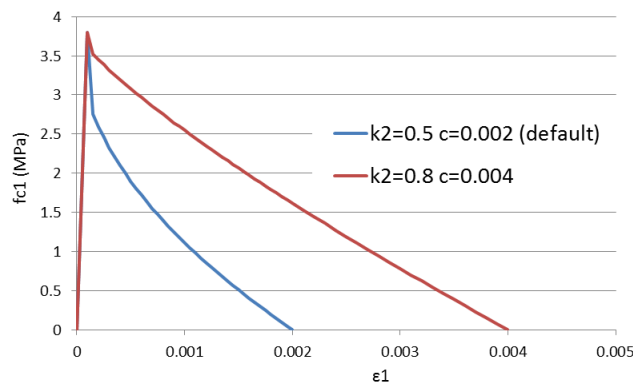


**Figure 4.2-7:** Case PB2. Softening of concrete in tension considered in the model CONSHEAR (Tension stiffening equation of Cervenka)

### 4.2.3 Nonlinear finite element analysis

#### Load – deflection response

The load – deflection curve is presented in Figure 4.2-8 and compared with the DIANA plane stress FE model performed by Hendriks, Belletti et al. (2015) and with the experimental curve (Sun and

Kuchma 2007). The results of both nonlinear analyses for the start of different levels of damage are marked along the load-deflection curve and also resumed and compared in Table 4.2-3. The numerical deflections were corrected from the initial results related to the dead weight and application of prestressing forces.

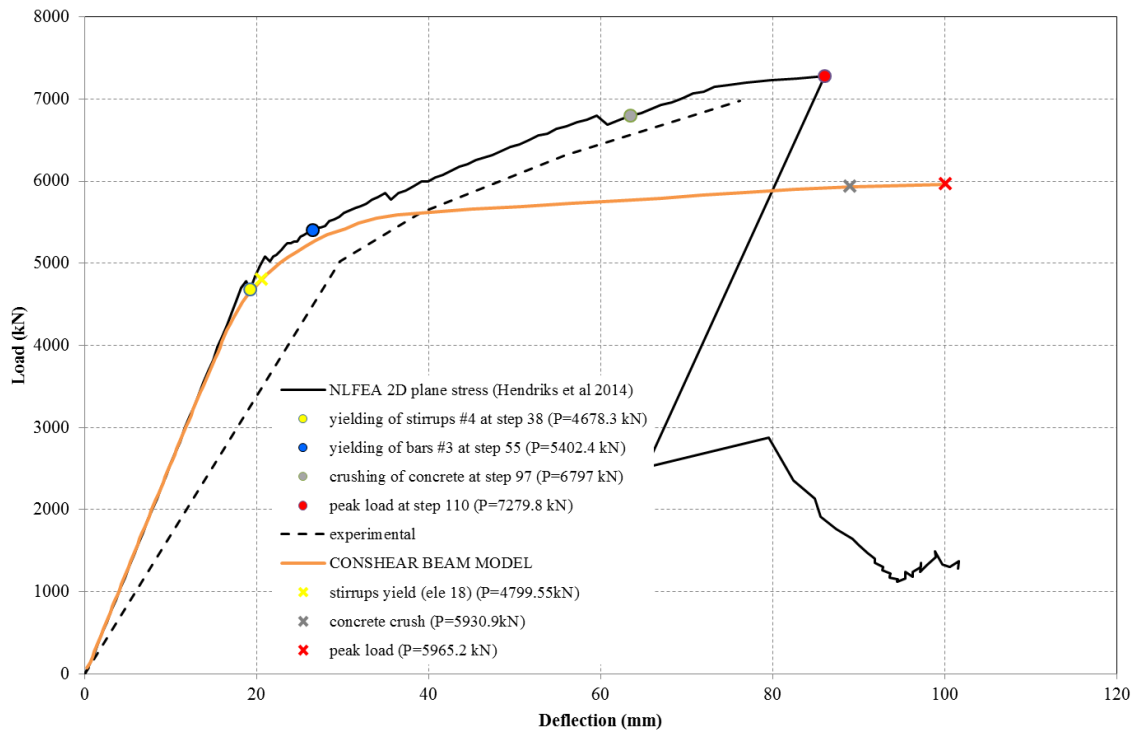


Figure 4.2-8: Case PB2. Load-deflection curves and levels of damage

Table 4.2-3: Case PB2. Results of the NLFEAs and experimental data (kN)

Level of damage	DIANA Plane stress	CONSHEAR Beam element	Comparison	Experimental
Start yielding stirrups #4	4678.3	4799.55	Similar	No data
Start yielding long. reinf. #3 (web)	5402.4	-	Different	No data
Crushing of concrete	6797	5930.87	CONSHEAR <	No data
Peak load	7279.8	5965.15	CONSHEAR <	6984
Failure mechanism	Shear-compression	Shear	Similar	Shear-compression
Computation time	5h	30 minutes		

The initial elastic response predicted by CONSHEAR fits the results of the DIANA plane stress model; which are stiffer than the experimental behaviour. This must be due to uncertainties of the real elasticity modulus of concrete. After cracking, CONSHEAR presents much more deflections, with less stiffness than experimental and DIANA results. The load level for the start of yielding of stirrups is similar between the two models. CONSHEAR predicts sooner crushing of concrete than DIANA plane stress model. In CONSHEAR model, longitudinal reinforcement (passive and prestressing) remains elastic until failure; in contrast, DIANA plane stress model predicts yielding of longitudinal reinforcement. Shear failure in CONSHEAR is due to concrete crushing for a lower failure load (P=5965 kN) in comparison with the experimental value (P=6984kN); DIANA plane stress model predicted an higher maximum load (P=7279.8kN) for a shear-compression failure mechanism involving crushing of concrete in the web.

**Convergence behaviour**

The energy criterion, with a tolerance of  $1 \times 10^{-3}$ , controls the global NR iteration procedure. Figure 4.2-9 represents the energy norm versus the number of iterations throughout the nonlinear analysis until failure; the red line sets the norm for which convergence is achieved. The key levels of damage identified in the load-displacement curve are marked with vertical lines.

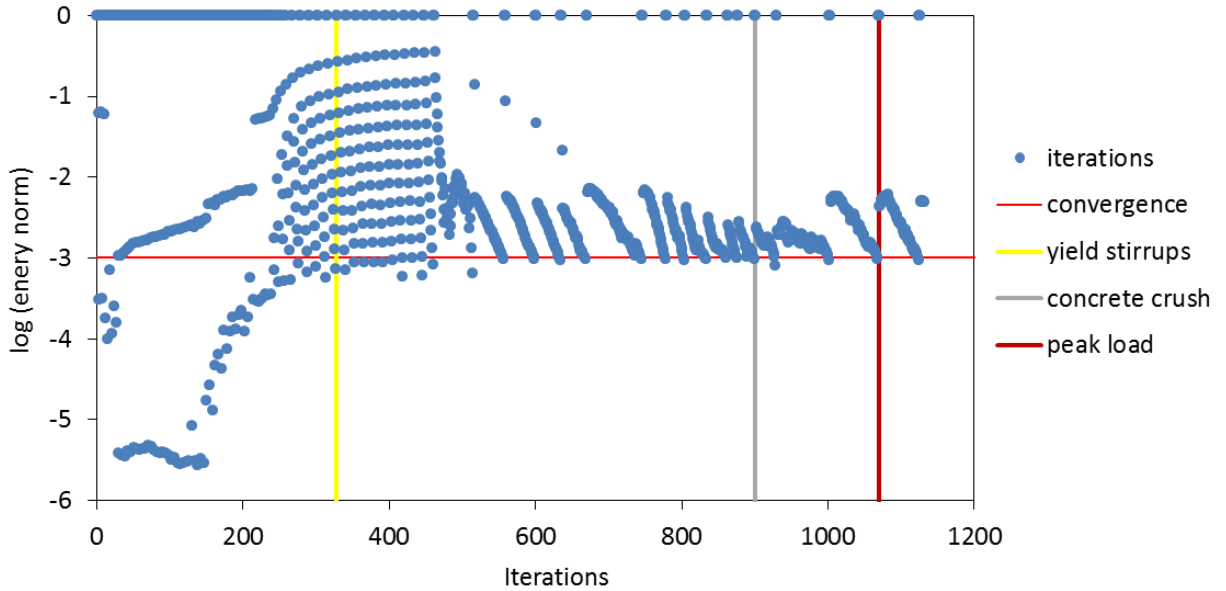


**Figure 4.2-9:** Case PB2. Energy norm vs. global iterations at the NR level

**Strains and stresses**

Strains in longitudinal reinforcement in the mid span (passive in Figure 4.2-10 and active in Figure 4.2-11) remain elastic until ultimate load. Concrete does not reach crushing in the bending zone as represented in Figure 4.2-12. Stirrups are only activated for advanced load levels, but reach failure suddenly at ultimate load (Figure 4.2-13).

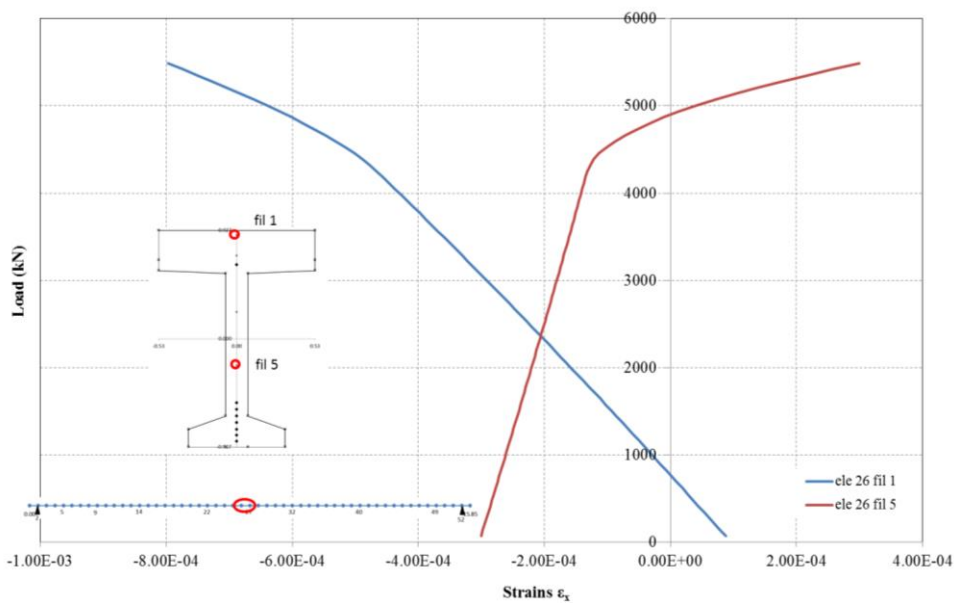


**Figure 4.2-10:** Case PB1. Load vs. longitudinal strains in longitudinal reinforcement

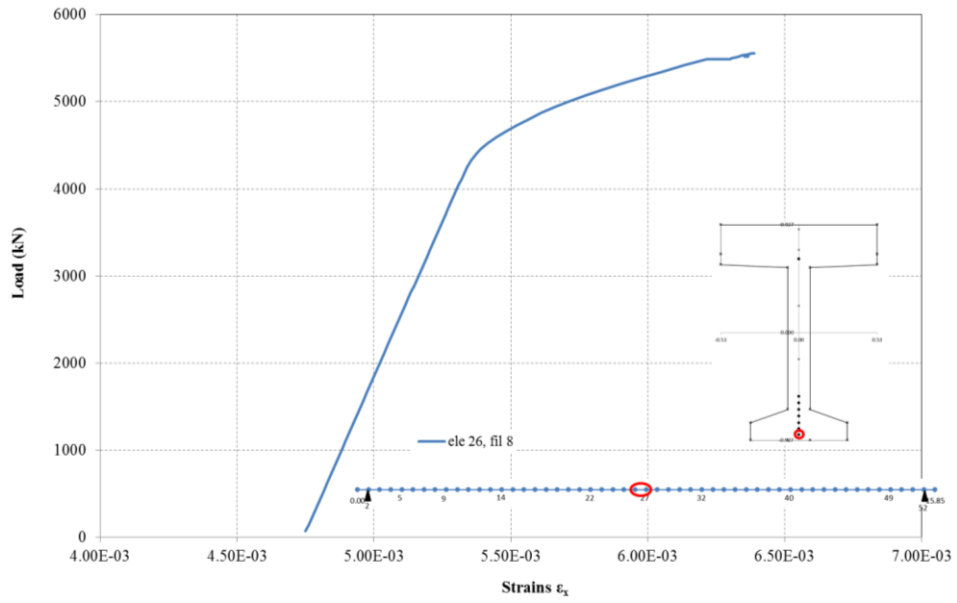


Figure 4.2-11: Case PB1. Load vs. longitudinal strains in prestressed reinforcement

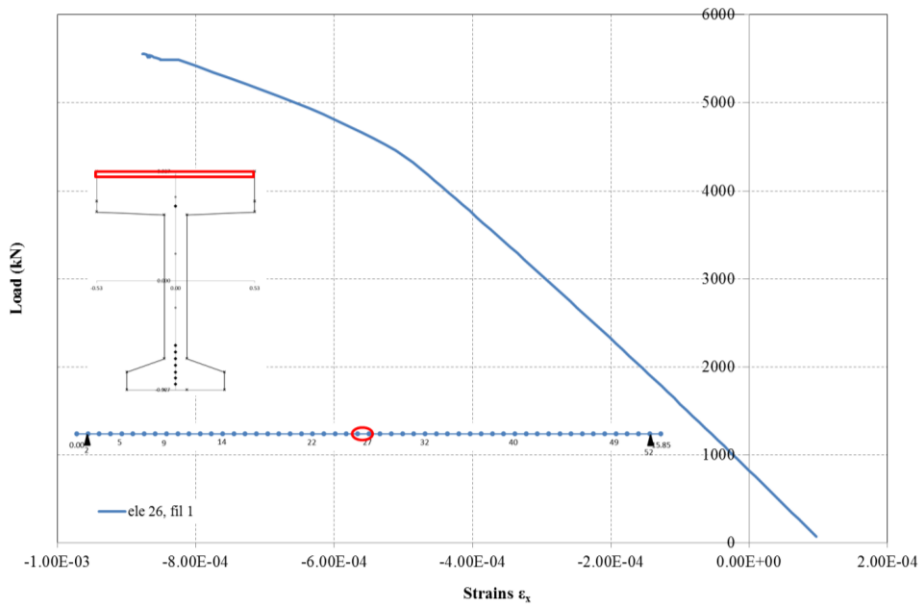
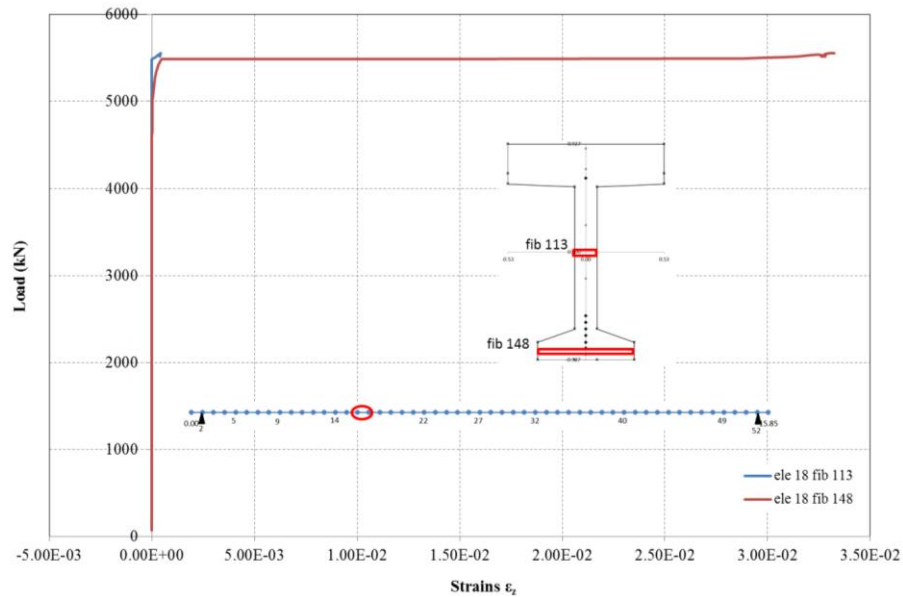


Figure 4.2-12: Case PB1. Load vs. longitudinal strains in concrete



**Figure 4.2-13:** Case PB1. Load vs. longitudinal strains in transversal reinforcement

### Crack patterns

The predicted crack patterns are represented in Figure 4.2-14 for the load levels of approximately 50%, 70%, 90% of the failure load and ultimate load. The average crack spacing was considered as 0.4m (because EC2 gave a very high crack spacing (1.3m), that is not coherent with the experimental observations).

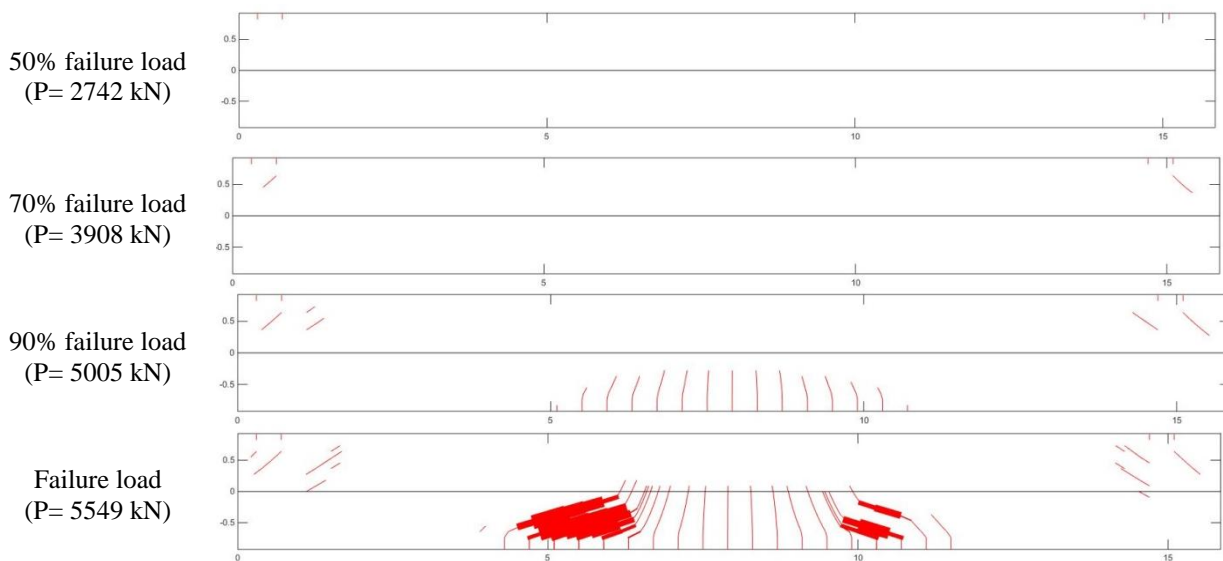


**Figure 4.2-14:** Case PB2. Predicted crack patterns

### 4.2.4 Concluding remarks

From the analysis of the PB2 test (benchmark failing in shear-compression) with CONSHEAR and comparison with DIANA plane stress model (Hendriks, Belletti et al. 2015) and experimental data (Sun and Kuchma 2007) the following conclusions are pointed out:

- In general, CONSHEAR is consistent with DIANA and with experimental observations in terms of failure mechanism and overall response;

- CONSHEAR presents softer response for advanced loading stages in comparison with experimental data and with the results of the DIANA plane stress model;

### 4.3 Case PB3/MnDOT: Runzell et al. (2007)

Case PB3 is a prestressed beam from the experiments of (Runzell, Shield et al. 2007), in which two ends of a 26.822 m girder removed from a bridge (Mn/DOT Bridge No. 73023) were tested. The dismantled bridge was around 20 years old; meaning that the girder was designed according to either the 1983 Standard or 1979 Interim specifications. The experimental tests were carried out in the University of Minnesota Structures Laboratory. The specimens were tested without and with the deck, referred in the report as Specimens I and II, respectively. PB3 relates to Specimen I (without the deck).

#### 4.3.1 Experimental setup and results

The original length of the girder was 26.82 m. The specimens cut from the girder were 9.29 m as represented in Figure 4.3-1. The experimental test was designed in order to fulfill the laboratory characteristics and capacities in terms of maximum length and maximum load possible to be applied and also to meet the objective of studying the shear behavior and resistance of the girders. The experiment was designed in order to present a shear span-to-depth ratio of 2.7. The specimen was modified by increasing its length from 9.29 m to approximately 12.116 m by adding a cast-in-place beam extension onto the original prestressed beam as presented in Figure 4.3-2 and Figure 4.3-3. This cast-in-place beam extension was designed to resist the maximum bending moment and shear force possible to be applied in the lab.

Details on the decisions of the design of the experiments can be found in Runzell et al. (2007) and in Hendriks, Belletti et al (2014).

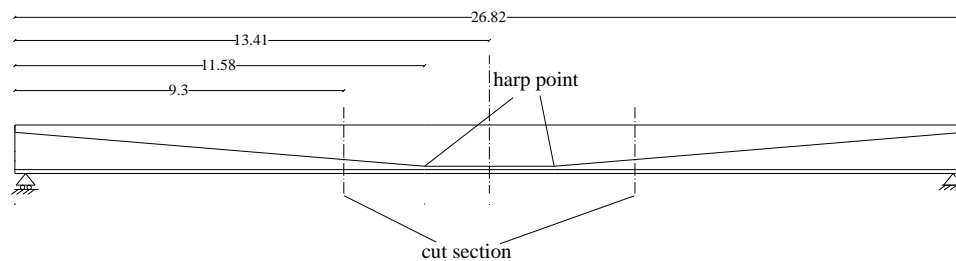


**Figure 4.3-1:** Case PB3. Girder of Mn/DOT Bridge No. 73023 (dimensions in m) (Hendriks, Belletti et al 2014)

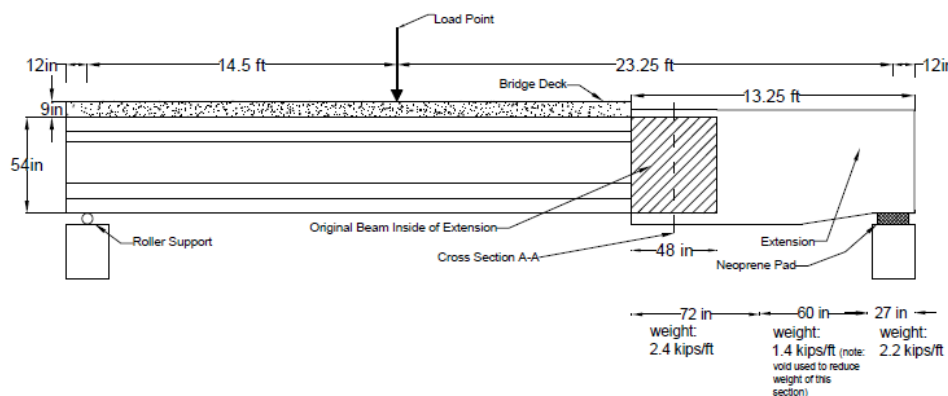


**Figure 4.3-2:** Case PB3. Modified specimen (Runzell et al. 2007)



**Figure 4.3-3:** Extension construction (a) before casting, (b) after casting (Runzell et al. 2007)

The geometry of the I-shape cross section is presented in Figure 4.3-4. The girder has 10 inclined and 33 straight strands of 13 mm diameter each. Prestressing stress was measured in laboratory, presenting a value after all losses of 864 N/mm<sup>2</sup>. Details on the prestressing geometry, in terms of longitudinal and sectional configuration are presented in Figure 4.3-5 and Figure 4.3-6, respectively. The girder has no longitudinal passive reinforcement. In terms of transversal reinforcement there are double led stirrups of 13mm of diameter spaced of 531mm throughout the beam, with closer spacing at the left end of the girder, corresponding to the anchorage zone. The bridge deck presents two layers of 13mm longitudinal bars, spaced of 457mm (at the top) and 229mm (at the bottom), as presented in Figure 4.3-4b. The cross section geometry and reinforcement of the extension beam is presented in Figure 4.3-7.

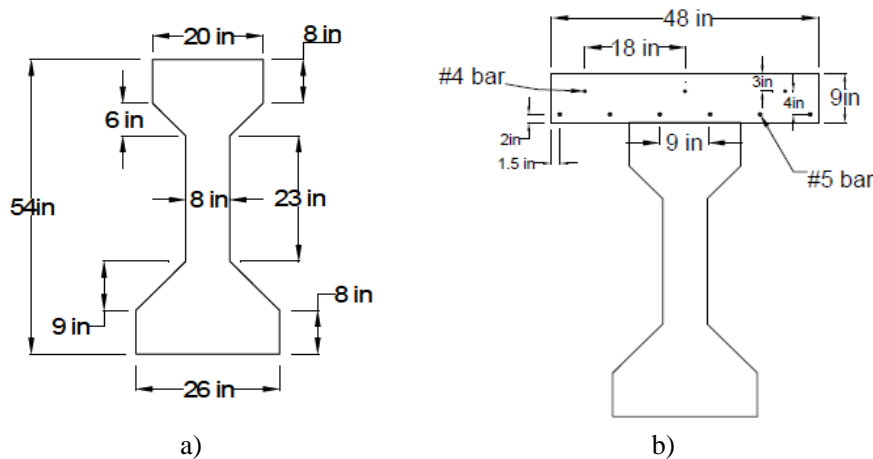


**Figure 4.3-4:** Cross-sectional details (measures in ft and in) of (a) specimen I (without the deck), (b) specimen II (with the deck) (Runzell et al. 2007)

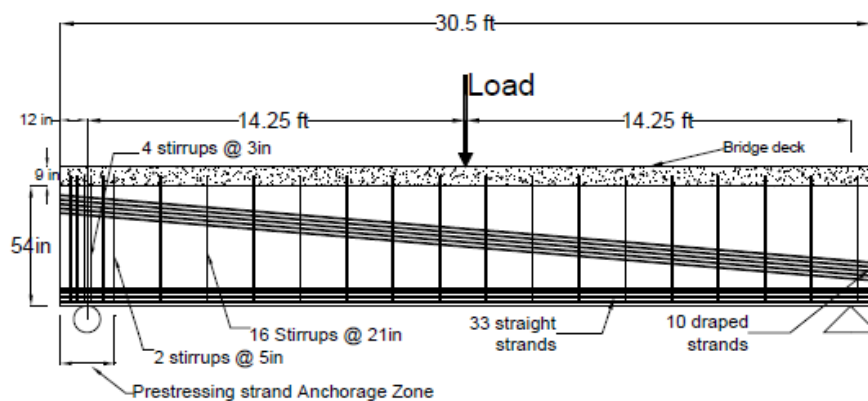


**Figure 4.3-5:** Case PB3. Reinforcement details (Runzell et al. 2007).

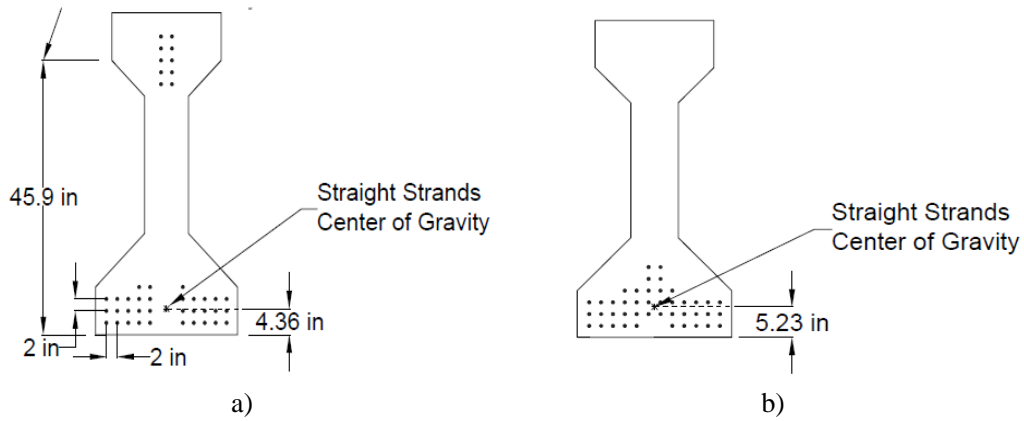


**Figure 4.3-6:** Case PB3. (a) Prestressing Strand Pattern at Girder End, (b) Prestressing Strand Pattern at harp point (Runzell et al. 2007)

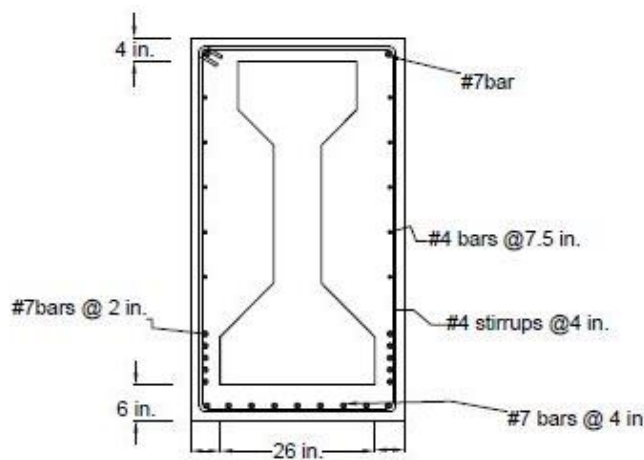


**Figure 4.3-7:** Case PB3. Geometry and reinforcement of the extension beam (dimensions in inches) (Runzell et al. 2007)

The loading and boundary conditions of the experimental setup are shown in Figure 4.3-8. The beam was submitted to a three-point loading scheme, with increasing load until failure. A diagonal tension failure mechanism was observed in the experimental test, involving crushing of concrete at web-bulb interface with spalling of concrete in the web, as can be seen in Figure 4.3-9. The first cracks were due to bending in bottom flange below the point of load application. Several large web cracks were formed for higher load levels.

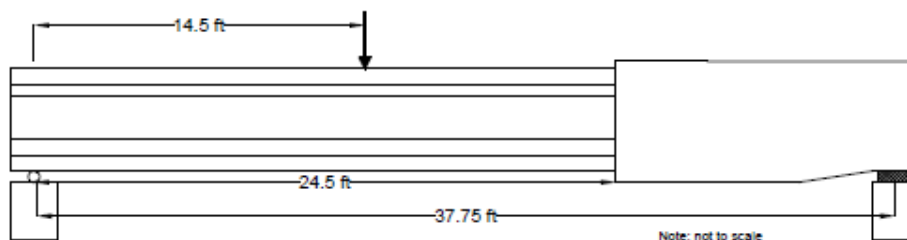


**Figure 4.3-8:** Case PB3. Loading, boundary conditions and dimension (dimension in ft) (Runzell et al. 2007)

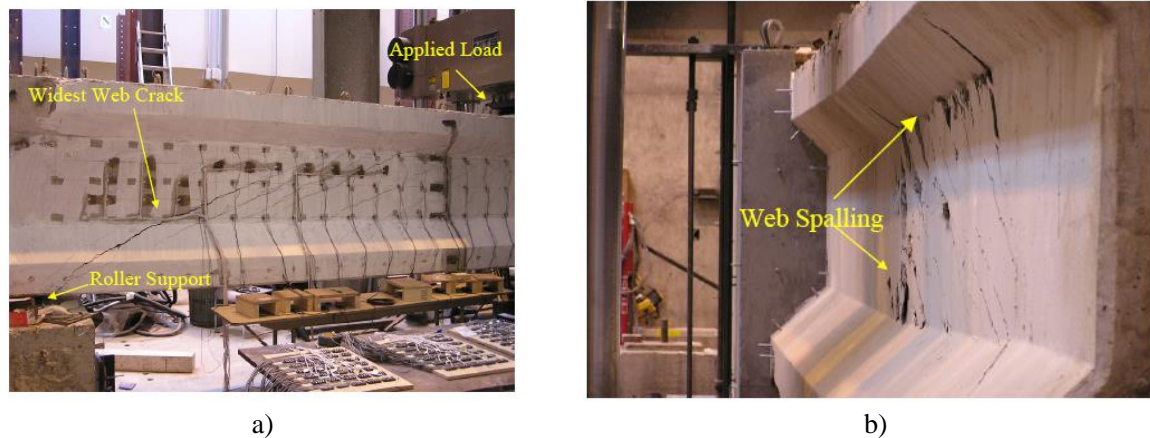


**Figure 4.3-9:** Case PB3. Failure mechanisms at peak load of Specimen I, (a) cracking, (b) web crushing (Runzell et al. 2007)

#### 4.3.2 Finite element model

The characteristics of the model are presented in Figure 4.3-10; the beam was discretized into 48 FEs and 49 nodes (length of the beam of 0.25-0.3 m). The cross section was divided into fibres with approximately 0.02 m of width. Two types of concrete cross section were considered; one for the I-shaped girder and other for the rectangular extension beam. No passive steel reinforcement was considered. Specimen I, without the top deck, was simulated. Transversal reinforcement is considered smeared in the cross-sections, with a constant quantity along the beam of  $2\Phi 13/531\text{mm}$ . The web of the girder and the top flanges were considered shear resistant; the fibres of the bottom flange are non-shear resistant.

The 43 prestressing cables were assembled into 2 groups of bars with the same eccentricity, one linear and one with inclined configuration. These 2 bars were simulated by means of prestressed filaments in CONSHEAR with their respective eccentricity in the cross section and the area correspondent to the numbers of cables of each group. A prestressing force of  $P=85.337\text{kN}$  / cable was considered, referring to the reported stress in the cable at the time of testing (864MPa).

The beam is simple support, with constraint nodes 2 and 48. The analysis was performed in two phases:

- 1) Dead weight and prestressing force of  $P=85.337 \times 10 = 853.37\text{kN}$  for the group 1 with 10 cables and  $P=85.337 \times 33 = 2816.13\text{kN}$  for group 2 with 33 cables;
- 2) Application of incremental point load in node 20 in approximately 100 load steps until failure.

Energetic tolerance considered was  $1 \times 10^{-3}$  and updated normal plane switch on in the advanced loading steps. Computation time takes around 15 minutes (very slow in the last load steps near failure, of difficult convergence).

Regarding the material properties, the values given in the report for the concrete and steel mechanical properties were used in the model; the others were considered the same as in DIANA plane stress model (Hendriks, Belletti et al. 2015). The material properties used in the model are listed in Table 4.3-1 for concrete and in Table 4.3-2 for steel. Regarding the tension stiffening curve, the default parameters were used;  $k_2=0.5$  and  $c=0.002$ . At lack of more information, the same concrete material properties were used for the girder and for the extension beam (DIANA 2D simulations considered elastic concrete material in the extension part of the beam)

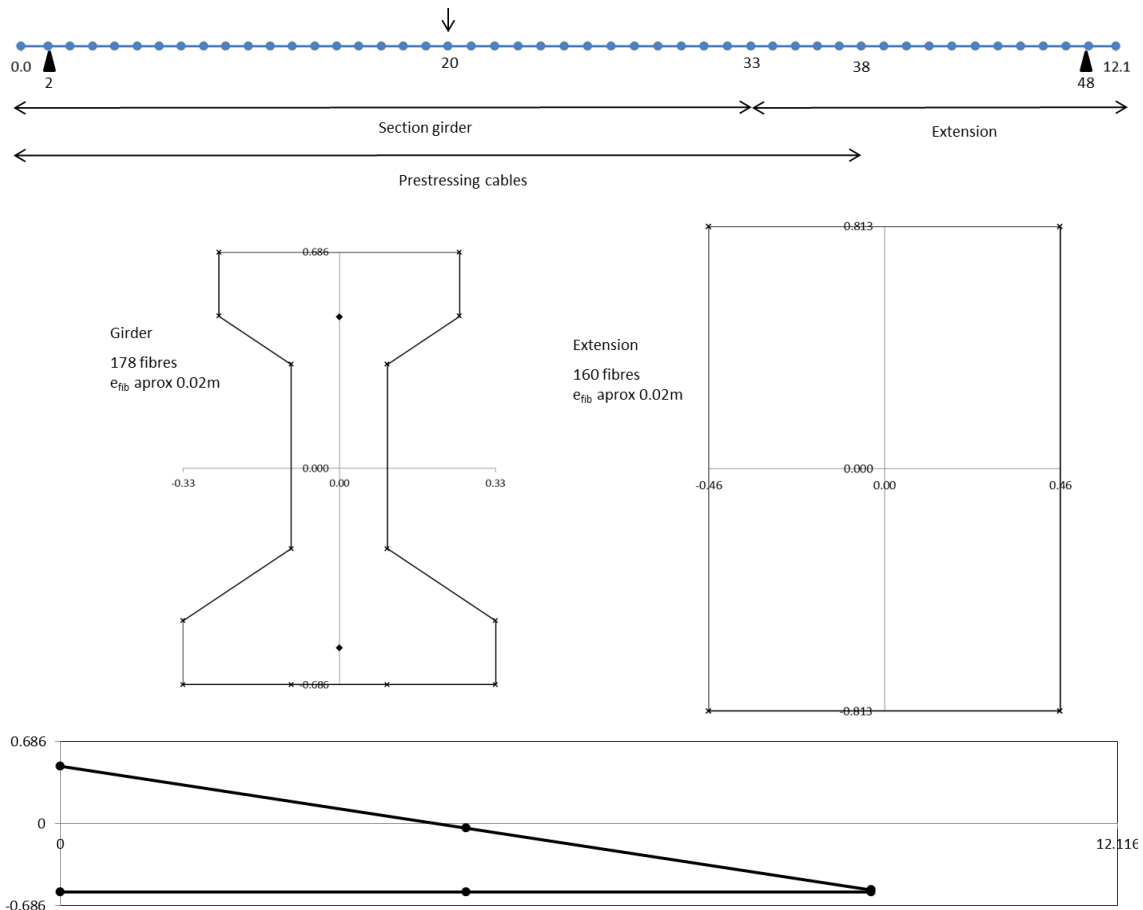


Figure 4.3-10: Case PB3. Mesh of the model

Table 4.3-1: Case PB3. Constitutive properties for concrete

	$f_{cm}$ (N/mm <sup>2</sup> )	$f_{ctm}^*$ (N/mm <sup>2</sup> )	$E_c^*$ (N/mm <sup>2</sup> )	$\epsilon_{cu}^*$
Mean measured values	69.84	4.54	34819	0.0031

\* assumed / determined values (when possible, same as DIANA plane stress, Hendriks, Belletti et al 2014)

Table 4.3-2: Case PB3. Reinforcement properties.

Bar	$\Phi$ (mm)	$A_s$ (mm <sup>2</sup> )	$E_s$ (N/mm <sup>2</sup> )	$f_{ym}$ (N/mm <sup>2</sup> )	$f_{um}$ (N/mm <sup>2</sup> )	$\epsilon_{su}^*$	$E_{sy}^*$ (N/mm <sup>2</sup> )
strands $\Phi 11.2$	43x11.2	43x98.77	196500	1675	1862	0.05	

\* assumed / determined values

### 4.3.3 Nonlinear finite element analysis

#### Load – deflection curve

The load – deflection curve is presented in Figure 4.3-11 and compared with the DIANA plane stress FE model performed by Hendriks, Belletti et al. (2015) and with the experimental curve (Runzell et al. 2007). The results of both nonlinear analyses for the start of different levels of damage are marked along the load-deflection curve and also resumed and compared in Table 4.3-3. Initial displacements due to dead weight and prestressing were discounted from the presented results.

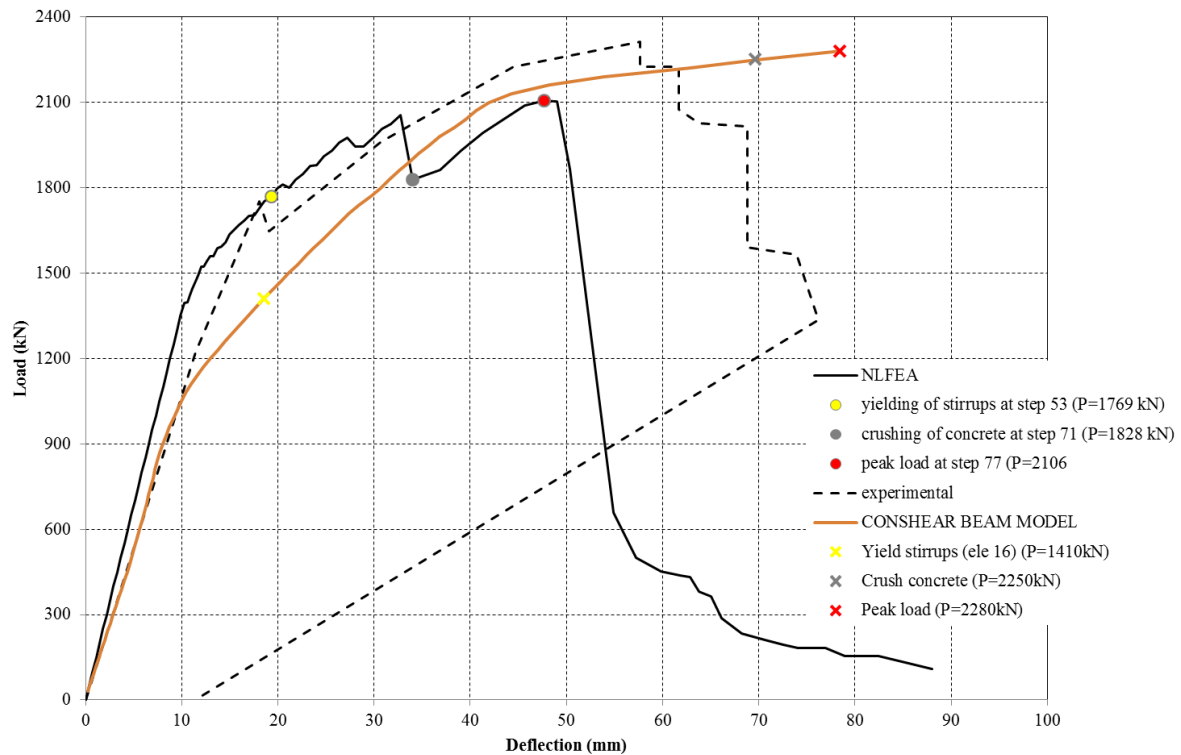


**Figure 4.3-11:** Case PB3. Load-deflection curves and levels of damage

**Table 4.3-3:** Case PB3. Results of the NLFEAs and experimental data (kN)

Level of damage	DIANA Plane stress	CONSHEAR Beam element	Comparison	Experimental
Start yielding stirrups	1769	1410	CONSHEAR <	No data
Crushing of concrete	1828	2280	CONSHEAR >	No data
Peak load	2106	2280	CONSHEAR >	2313
Failure mechanism	Shear: diagonal-tension	Shear	Similar	Shear: diagonal - tension
Computation time	1h	15 minutes		

CONSHEAR and DIANA plane stress models present very similar initial stiffness in the elastic behavior, which is also consistent with the experimental results. Cracking appears sooner in the CONSHEAR model, presenting softer response than DIANA and experimental results for advanced loading. This sooner decrease of the stiffness of the beam might be due to uncertainties about the value of the concrete tensile strength of the girder and the extension beam. Also, no longitudinal reinforcement was considered in the extension beam, that might also justify this difference. In DIANA plane stress model the extension was simulated as elastic concrete and the reinforcement of the part of the beam that penetrated in the extension is considered. The ultimate load and failure mechanism is consistent with both experimental values and predictions of the plane stress model. CONSHEAR reached failure by crushing of concrete and yielding of stirrups, while longitudinal prestressing remained elastic, representing a shear mechanism.

Regarding the development of damage, the start of yielding of the transversal reinforcement appeared for a lower load level in CONSHEAR ( $P=1410\text{kN}$ ) than in DIANA ( $P=1769\text{kN}$ ); and crushing of concrete happened later in CONSHEAR ( $P=2280\text{kN}$ ) in comparison with DIANA ( $P=1828\text{kN}$ ). This is consistent with the observations made in the previous cases. Peak load was predicted in CONSHEAR to be  $P=2280\text{kN}$ , which is similar to the experimental value of  $P=2313\text{kN}$  and a little lower than DIANA prediction of  $P=2106\text{kN}$ .

**Convergence behaviour**

The energy criterion, with a tolerance of  $1 \times 10^{-3}$ , controls the global NR iteration procedure. Figure 4.3-12 represents the energy norm versus the number of iterations throughout the nonlinear analysis until failure; the red line sets the norm for which convergence is achieved. The key levels of damage identified in the load-displacement curve are marked with vertical lines.

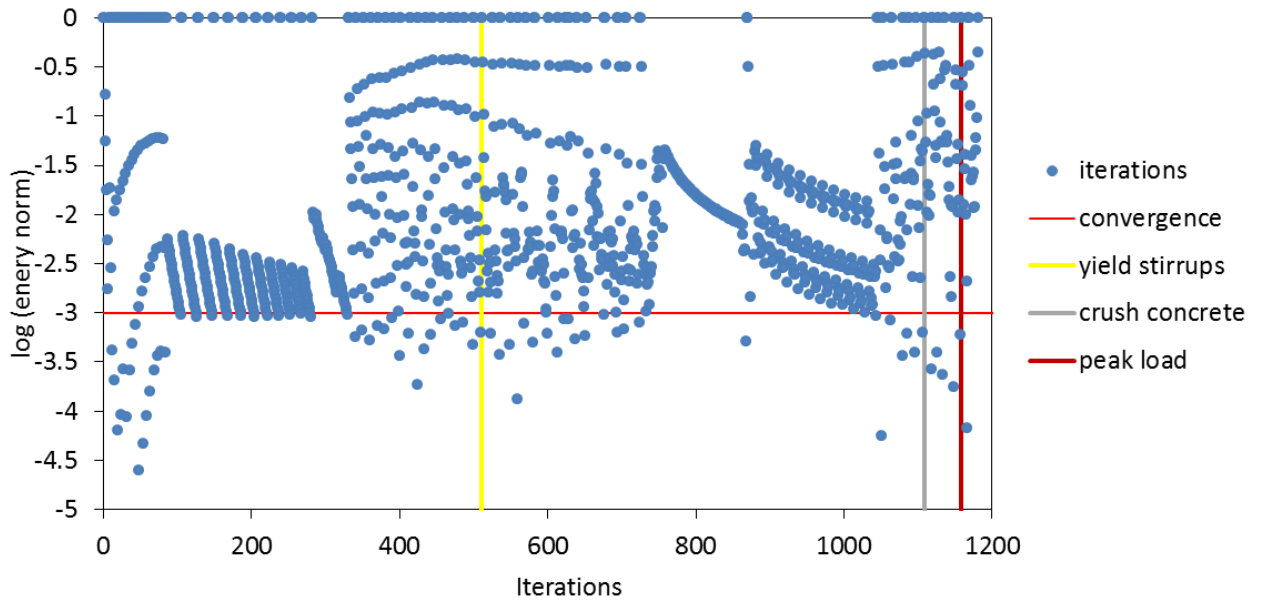


**Figure 4.3-12:** Case PB3. Energy norm vs. global iterations at the NR level

**Strains**

The strains with increasing load are presented in the following graphics for key points of damage. The longitudinal prestressed reinforcement remains elastic until failure, as can be seen in Figure 4.3-13, for the position near application of the load. Figure 4.3-14 shows that the concrete is not crushed in the top fibres of the bending zone. Figure 4.3-15 shows the yielding of the stirrups at shear span for the bottom fibre, demonstrating the shear failure.

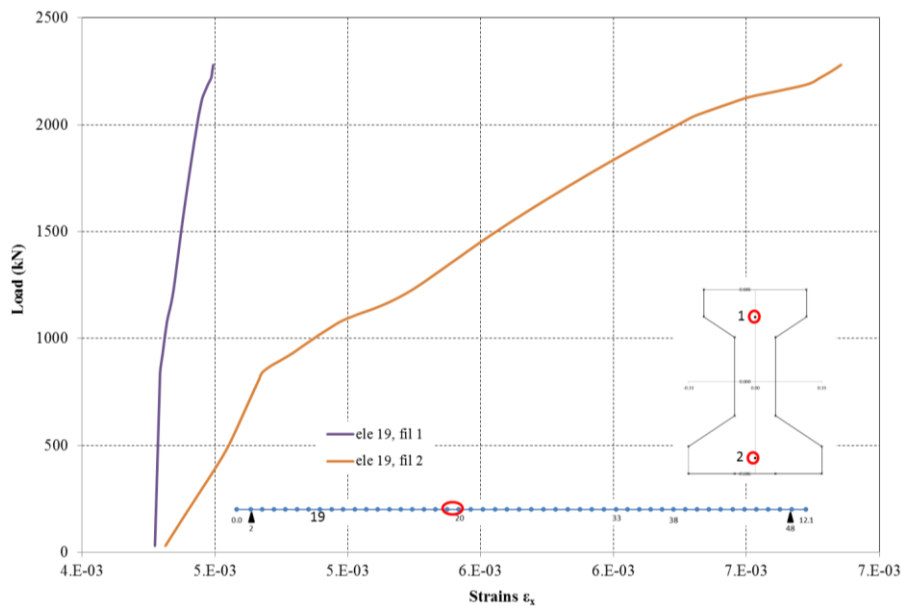


**Figure 4.3-13:** Case PB3. Load vs. longitudinal strains in prestressed reinforcement

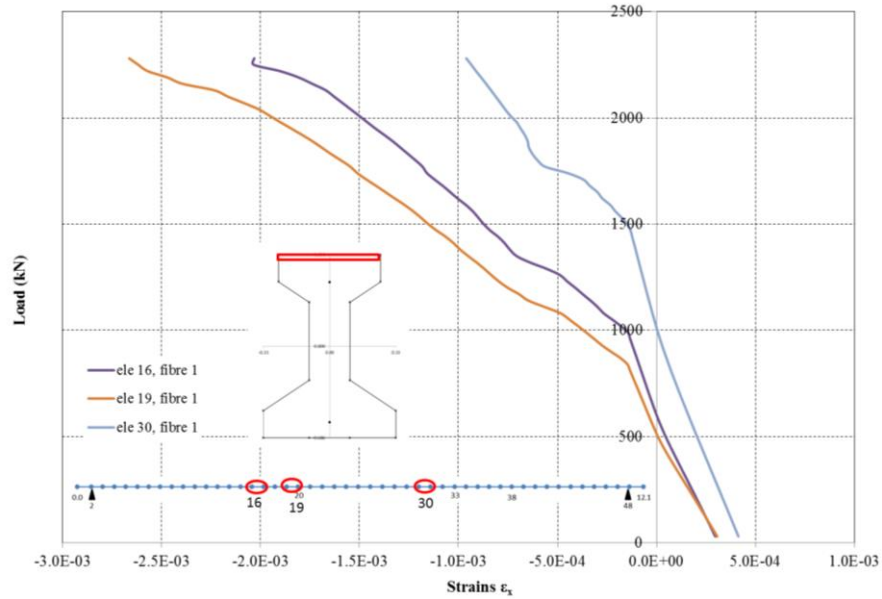


**Figure 4.3-14:** Case PB3. Load vs. longitudinal strains in concrete

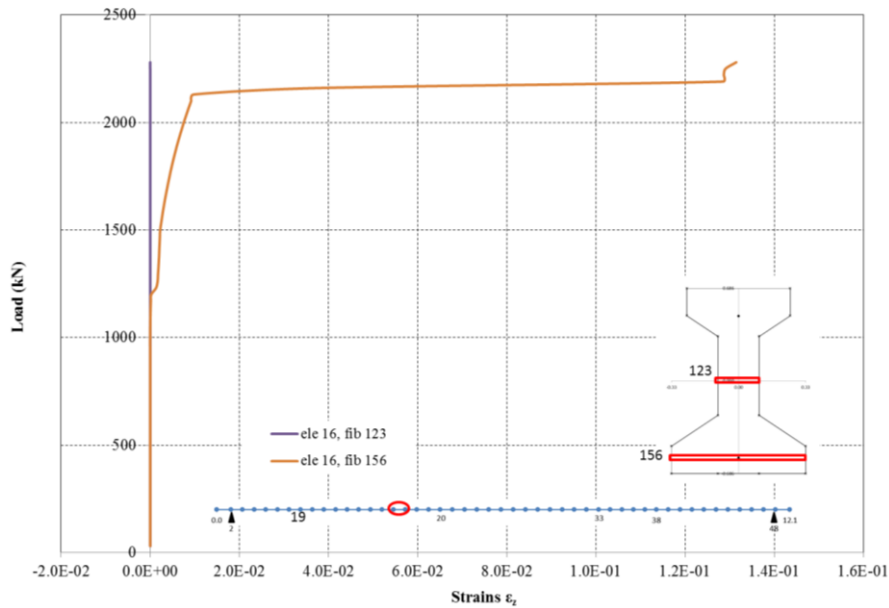


**Figure 4.3-15:** Case PB3. Load vs. longitudinal strains in transversal reinforcement

**Crack patterns**

The predicted crack patterns are represented in Figure 4.3-16 for the load levels of approximately 50%, 70%, 90% of the failure load and ultimate load. The average crack spacing was determined using the expression of EC2:  $S_m(EC2) = 656 \text{ mm}$ .

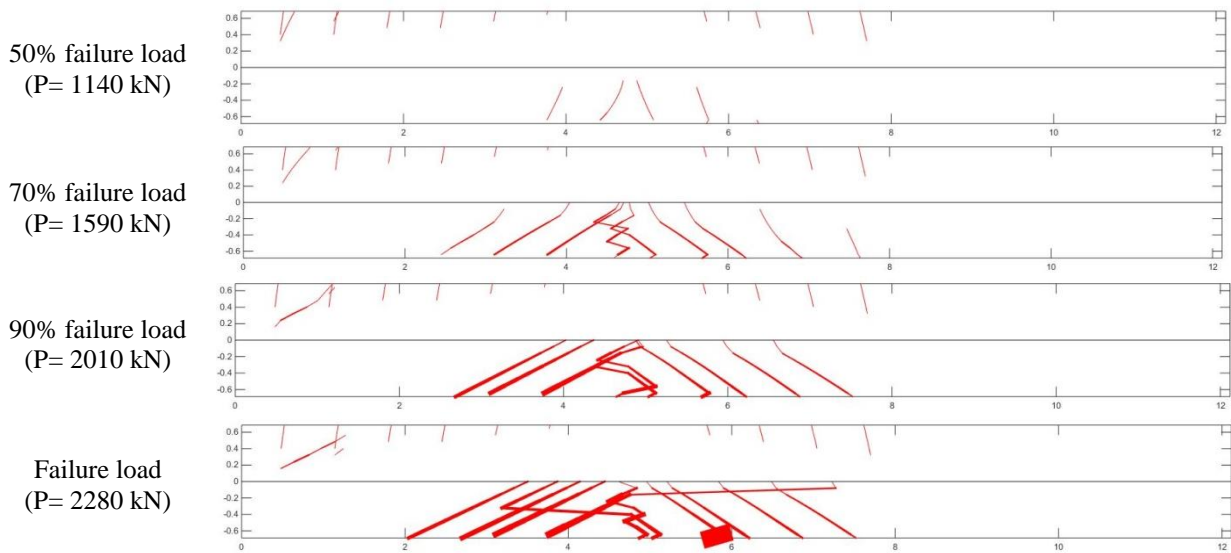


**Figure 4.3-16:** Case PB3. Predicted crack patterns

#### 4.3.4 Concluding remarks

From the analysis of the PB3 test (benchmark failing in shear) with CONSHEAR and comparison with DIANA plane stress model (Hendriks, Belletti et al. 2015) and experimental data (Runzell et al. 2007) the following conclusions are pointed out:

- Failure mechanism and peak load predicted by CONSHEAR is consistent with experimental observations and computations performed by the DIANA plane stress model;
- CONSHEAR presented a softer response and sooner cracking when compared with the experimental behaviour and also with the predictions of the higher order model.

## 5 NEW CASE STUDIES

Three cases studies are analysed: one large T-shaped prestressed concrete girder, and two reinforced concrete beams without transversal reinforcement and failing by brittle shear mechanism. The simulations in this section were only performed with the CONSHEAR beam model and compared with experimental data.

### 5.1 Cases of the DIANA User's Contest: large T-shaped prestressed concrete girders tested at TU Delft (Tests A – original load position)

A prediction contest for the results of T-shaped prestressed girders tested in the Stevin Laboratory of TU Delft was organized by TU Delft, Rijkswaterstaat and University of Parma. The blind predictions were submitted by the participants until August 2014, the experimental tests were carried out during autumn 2014 and the Workshop was held in Parma in November 5 2014.

This section relates to the blind prediction carried out with the model CONSHEAR and submitted as blind prediction to the contest.

Experimental results, when published, will be used for comparison with the numerical predictions.

#### 5.1.1 Experimental test, contest and results

The experimental campaign consisted of 4 T-shaped girders, 2 mid beams ( $b_f=750\text{mm}$ ) and 2 edge beams ( $b_f=875\text{mm}$ ), casted in May 2012 (Figure 5.1-1). The width of the top flange is the only difference between the two types of girders. The girders have a total length of 12.0 m and a depth of 1.3 m. The geometry and general reinforcement of the girders are represented in Figure 5.1-2 and Figure 5.1-3.

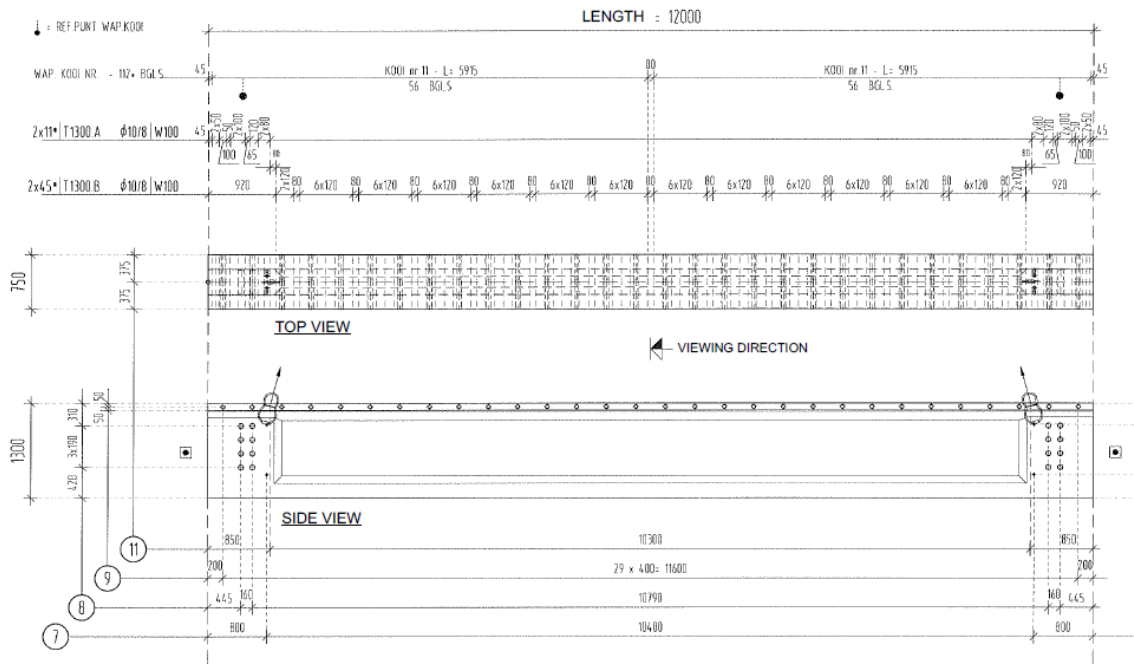
Each girder is pre-tensioned with 24 strands of  $\Phi 15.7\text{mm}$  ( $150\text{ mm}^2$  per strand) of steel type FeP1860. Concrete is of type C53/65. The measured prestressing force per strand before casting was of 214kN; and the mean cubic concrete compressive strength at time of prestressing was 54 MPa.

Passive reinforcement consisted of stirrups  $\Phi 10\text{ mm}$  distanced of 120 and 80 mm and  $10 \times \Phi 8\text{ mm}$  longitudinal bars. The type of steel is B500A for the longitudinal passive reinforcement and B500B for the stirrups.

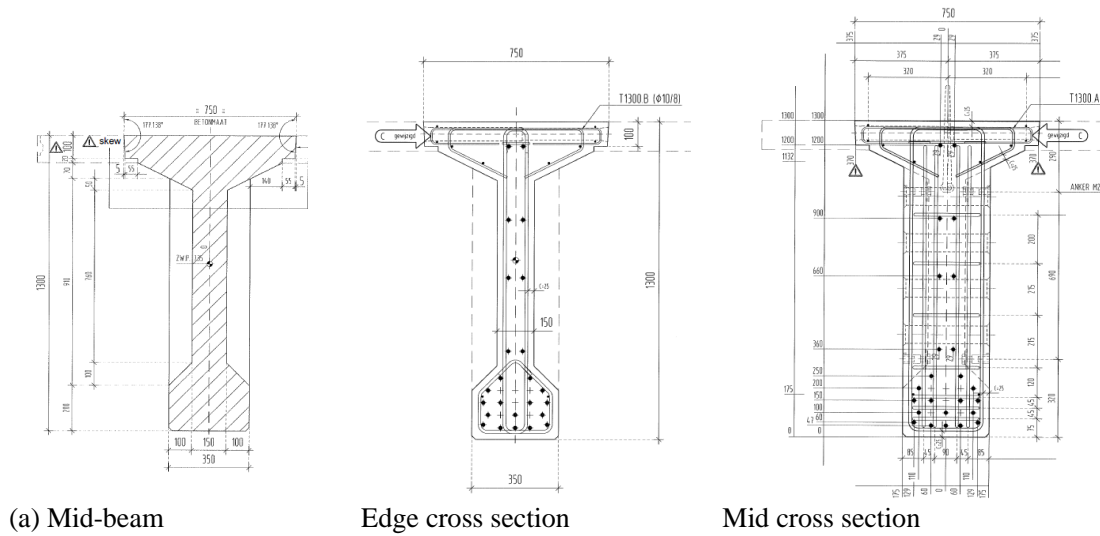
The test setup is represented in Figure 5.1-4: the loading jack is located at 2.950 m from the centre of the support. Data on the geometry, reinforcement, materials, support and loading systems were provided to the participants and available in [www.dianausers.nl](http://www.dianausers.nl).

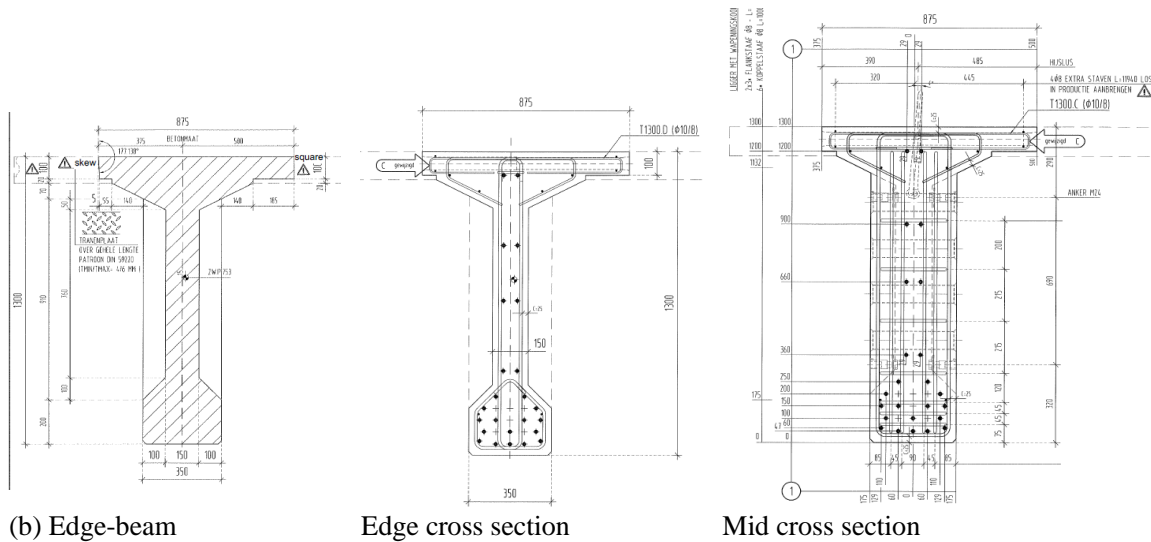


**Figure 5.1-1:** Case of DIANA User’s Contest. T-shaped prestressed girders tested in the Stevin Laboratory at TU Delft (picture given in the contest, [www.dianausers.nl](http://www.dianausers.nl))



**Figure 5.1-2:** Case of DIANA User’s Contest. Dimensions of the girders (draws given in the contest, [www.dianausers.nl](http://www.dianausers.nl))





(b) Edge-beam

Edge cross section

Mid cross section

**Figure 5.1-3:** Case of DIANA User's Contest. Dimensions and reinforcement of the girders (draws given in the contest, [www.dianausers.nl](http://www.dianausers.nl))



**Figure 5.1-4:** Case of DIANA User's Contest. Experimental test setup

The questions of the contest were:

- Maximum (and) minimum load at failure;
- Failure mechanism;
- Cracking pattern at 75% and 100% of the failure load;
- Crack width at 75% of failure load;
- Load – displacement diagram at position of the load.

The failure mechanism was localized around the point of load application by crushing in compression of the empty ducts localized in the top flanges of the girders (see in Figure 5.1-1). These empty ducts acted as a weak spot that triggered the failure mechanism. The experimental results in terms of ultimate load, ultimate displacement and crack width are resumed in Table 5.1-1 (according to what was divulgated in the Workshop in Parma, [www.dianausers.nl](http://www.dianausers.nl)). In the edge-beams it was observed a twist of the cross section that resulted in lower ultimate loads in comparison with the mid-beams.

**Table 5.1-1:** Case of DIANA User's Contest. Experimental results divulgated in Parma, November 5

	Mid-beam 1 (bf=750mm)	Mid-beam 2 (bf=750mm)	Edge-beam 1 (bf= 875)	Edge-beam 2 (bf= 875)
Ultimate load (kN)	2696	2540	2378	2575
Ultimate displacement (mm)	≈ 42	≈ 60	≈ 37	≈ 43
Failure mechanism	Bending local*	Bending local*	Bending local*	Bending local*
$w_{cr}$ (mm) (at 75% $P_u$ )	0.10	-	-	-

\* Crushing compression flange, localized zone in the empty ducts (weak spot)

### 5.1.2 Finite element model

The characteristics of the model are presented in Figure 5.1-5: the beam was discretized into 55 FEs (length of the beam elements of 0.15 - 0.25 m) and the cross section was divided into fibres with approximately 0.02 m of width. The thickened web zone at the end of the beam was simulated by varying the web width of the various elements in that area. The beam is simple supported with the vertical support stiffness considered as  $K_z = 3069 \text{ kN/mm}$ , that corresponds to the average compressive stiffness provided in the contest data.

All the fibres in the flange were considered shear resistant, because the effective  $b_{ef}$  (Zararis, Karaveziroglou et al. 2006) = 3030 mm >  $b_f$ . The transversal empty ducts in the flanges of the beams were disregarded in the numerical model. The passive reinforcement was accounted as constant along the entire beam: longitudinal reinforcement as 10xØ8filaments and transversal reinforcement as Ø10//114.3mm (average of sequence 6Ø10//120 + 2Ø10// 80, corresponding to a quantity of  $\rho_{sw} = 0.92\%$ ). The 24 prestressing strands were simulated by means of prestressed filaments in CONSHEAR with their respective eccentricity in the cross section.

A prestressing force of  $P=214 \text{ kN}$  was applied in the model as the program includes elastic deformation and losses with time. The age of application of prestressing was considered 2.8 days, being estimated through EC2 expression for development of compressive strength with time and using the value of  $f_{cm,cube}$  given at time of prestressing application (54 MPa). As the girders have bonded prestressing the basic anchorage length  $l_{bp}$ , was determined through MC2010 expression (using the given value for  $f_{ct,exp,m}$  at 9 months - 6.3 Mpa). The anchorage length was considered in the model by reducing the prestressing tendon area  $A_{sp}$  in each element (located at coordinate  $x < L_{bp}$ ) through the expression:  $A_{sp}(x)=A_{sp} x/L_{bp} \leq A_{sp}$ .

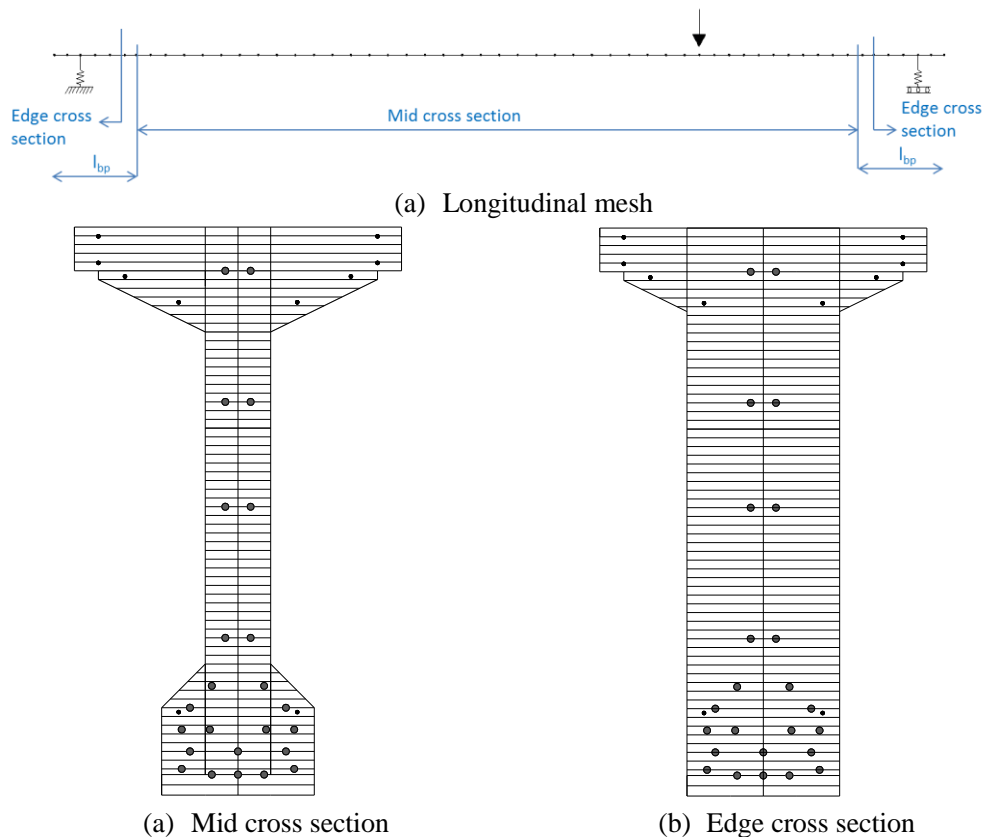


**Figure 5.1-5:** Case of DIANA User’s Contest. Mesh of the CONSHEAR model

A phased analysis was performed considering the following phases in the model:

Phase 1: t = 3 days

- Dead weight
  - Prestressing:  $F_p=241$  kN, both sides ( $\epsilon_p=7.32$ mm/m)
  - ...- Supports: simple supported beam
- $$k_z = \infty$$

Phase 2: t = 3-850 days

- 10 time steps
  - Creep (HR=60%) and shrinkage
  - Development of mechanical properties of concrete
  - Supports: simple supported beam
- $$k_z = \infty$$

Phase 3: t = 850 days

- Load applied incrementally until failure
  - Arc-length: automatic load steps
  - Default load step = 40 kN (start)  
4kN near failure
  - Energetic convergence, toler=0.001
  - Supports: simple supported beam
- $$k_z = 3069 \text{ kN/mm at loading test (determined as an average of the data provided)}$$

The computation time is approximately 3 minutes.

Regarding the concrete properties, the average experimental properties provided for the contest are listed in Table 5.1-2. The model considers the development of concrete properties  $f_{ct}$ ,  $f_c$ ,  $E_{cm}$  according to the EHE08 Spanish Code (CPH 2008); each parameter has its own curve of development. The inputs of the model refer to the values at 28 days of age, that were determined in order to match the given properties at 9 months.

Table 5.1-3 resumes the input values in the model for 28 days, the correspondent calculated by the development curves in CONSHEAR for 9 months and for the age of testing (considered as 850 days). These values correspond to the average material properties for concrete. A cement of fast cure was considered for the parameters of the development curves.

In order to calculate an estimation of minimum ultimate load the same model was performed but with the characteristic values for the materials instead of the average properties. In Table 5.1-4 are listed the formulas and the determined characteristic values for concrete.

**Table 5.1-2:** Case of DIANA User's Contest. Experimental mechanical properties of concrete provided in the contest

<b>Experimental properties</b>	<b>t = 28 days</b>	<b>t = 273 days (9 months)</b>
$f_{cm,cube}$ (MPa)	83	89.83
$f_{cm,cylinder}^*$ ( $f_{c,cube}-15$ ) (MPa)	68	<b>74.83</b>
$f_{ck,cube}$ (MPa)	77	-
$f_{ck,cylinder}^*$ ( $f_{c,cube}-15$ ) (MPa)	62	-
$f_{ctm,sp}$ (MPa)	-	<b>6.3</b>

**Table 5.1-3:** Case of DIANA User's Contest. Average mechanical properties of concrete considered in the model

Properties in the model Average values	Input	Calculated, f(t) EHE08 (Spanish Code)	
	t = 28 days	t = 273 days (9 months)	t = 850 days (testing age)
$f_{cm,cylinder}$ (MPa)	65.32	<b>74.83</b>	76.94
$f_{ctm,sp}$ (MPa)	5.9	<b>6.3</b>	6.4
$E_{cm}$ (GPa) (EC2 f( $f_{cm}$ ))	38.62	44.25	45.51
$f_{cm,cube}$ ( $f_{cm,c}+15$ ) (MPa)	80.32		91.94
$\epsilon_{cu}$ (EC2, f( $f_{cm}$ ))	0.0026		

**Table 5.1-4:** Case of DIANA User's Contest. Characteristic mechanical properties of concrete considered in the model

Properties in the model Characteristic values	Input t = 28 days
$f_{ck}$ ( $f_{cm}=f_{ck}+8$ ) (MPa)	57.32
$f_{ctk}$ ( $0.7 \times f_{ctm}$ ) (MPa)	4.13
$E_{ck}$ (GPa) (EC2 f( $f_{ck}$ ))	37.15
$\epsilon_{cu}$ (EC2, f( $f_{cm}$ ))	0.0026

For the steel properties the only information given was the class of the materials (B500B for passive reinforcement and FeP1860 for active reinforcement); there was no experimental data available. The mechanical properties considered in the model are listed in Table 5.1-5 for passive reinforcement and in Table 5.1-6 for active reinforcement. The average values were considered as 1.1 x characteristic values.

**Table 5.1-5:** Case of DIANA User's Contest. Mechanical properties of steel considered in the model (passive reinforcement ( $\varnothing 8$ ,  $\varnothing 10$ ) - B500B)

Properties in the model	Characteristic values	Average values (1.1f <sub>s,m</sub> )
$f_{sy}$ (MPa)	500	550
$f_{su}$ (MPa) (1.08f <sub>y</sub> )	540	594
$E_s$ (GPa)	200	200
$\epsilon_{su}$	0.05	0.05

**Table 5.1-6:** Case of DIANA User's Contest. Mechanical properties of steel considered in the model (active reinforcement ( $\varnothing 15.7$ , 150mm<sup>2</sup>) – FeP1860)

Properties in the model	Characteristic values	Average values (1.1f <sub>p,m</sub> )
$f_{yp}$ (MPa)	1640	1804
$f_{up}$ (MPa)	1860	2046
$E_s$ (GPa)	195	195
$\epsilon_{up}$	0.025	0.025

### 5.1.3 Nonlinear finite element analysis

The predicted load-displacement curve at position of the load is presented in Figure 5.1-6 for both girders. The results include support displacements; the initial displacements due to prestressing and dead weight were discounted. The results relate to both simulations: with average and characteristic values of material mechanical properties. The experimental values for ultimate load level are included in the graphics.

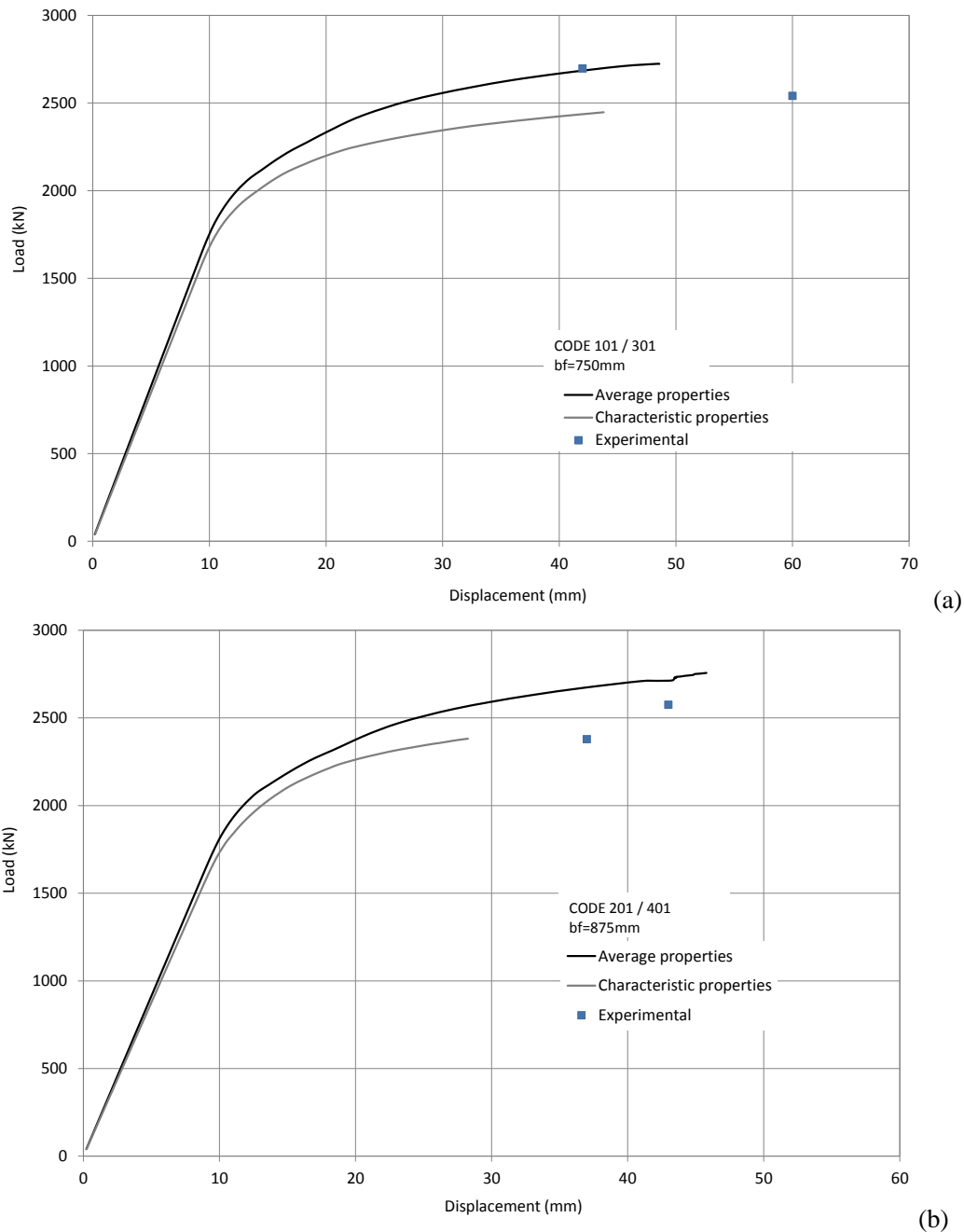


**Figure 5.1-6:** Case of DIANA User's Contest. Load-deflection curves: (a) girder bf=750mm and (b) girder bf=875mm

The numerical predictions present some consistency with the available experimental data on the ultimate failure stage.

Experimental results for comparison are expected to be available in the summer of 2015

The blind predicted results of failure load (maximum and minimum) are resumed in Table 5.1-7 for the two types of girders, where the average of the experimental results is included.

CONSHEAR predicted a flexural-shear failure mechanism including yielding of bottom longitudinal prestressed reinforcement (strands) near the area of load application, concrete crush in the web at shear span, yielding of stirrups in the web at shear span, severe diagonal cracking, and failure of the stirrups in the last non-convergent load step.

CONSHEAR predicted higher ultimate load than the experimental measured value, with an average overestimation of 1.08 (relating to the analysis with average material properties). This is because the experimental failure mode was localized in the weak spots of the empty ducts and neither the flexural nor shear resistant capacities were fully developed. CONSHEAR model is not able to simulate this localized failure mechanisms.

CONSHEAR predicted higher ultimate load for girders 101/301 than for girders 201/401. The opposite was observed in the experiments: the symmetric girders resisted more load than the no symmetric girders with larger width of the top flange. The mechanism of twisting of the cross section in the no symmetric girders was not captured by the model.

**Table 5.1-7:** Case of DIANA User’s Contest. Ultimate load

Girders	$P_{u,max}$ (kN)*	$P_{u,min}$ (kN) <sup>+</sup>	$P_{u,exp}$ (kN) (average)
Code101 / 301 (bf=750mm)	2740.41	2447.16	2617
Code 201 / 401 (bf=875mm)	2756.76	2381.37	2477
Computation time	3 minutes	3 minutes	

\*Average material mechanical properties

<sup>+</sup>Characteristic material mechanical properties

The predicted crack patterns are represented in Figure 5.1-7 for the load levels of 75% of the failure load and ultimate load and for both girders. These results relate to the simulation with average values of material mechanical properties. The crack spacing is an input parameter of this post-processing algorithm of drawing of the cracking pattern and was determined using the expression of EC2:  $S_{m0}$  (EC2) = 116.5 mm. The mechanical properties of concrete ( $E_c$ ,  $f_{ct}$ ) are also needed as inputs of this post-processing algorithm and were considered as the average mechanical properties at t=850 days (assumed testing day).

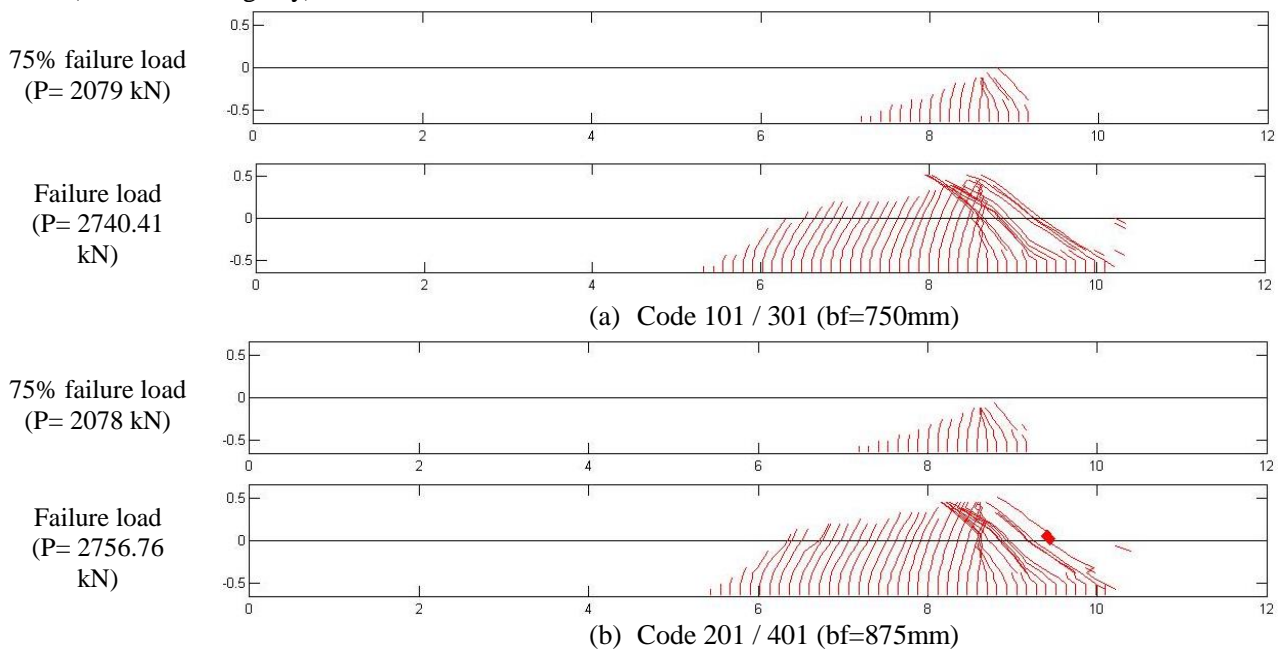


**Figure 5.1-7:** Case of DIANA User’s Contest. Predicted crack patterns at SLS and ULS

The predicted crack widths at SLS, correspondent to 75% of the failure load are presented in Table 5.1-8 for both types of girders. The results relate to the simulation with average values of material mechanical properties and are determined by multiplying the crack spacing with the principal tensile strain in the cracked fibres.

An experimental value of 0.10 mm of crack width for girder 101/301 was provided in the workshop. CONSHEAR predicts higher crack width, but this is not directly comparable as it refers to a higher load level.

**Table 5.1-8:** Case of DIANA User's Contest. Cracking width

Girders	$w_{cr,max}$ (mm) <sup>*</sup>	$w_{cr,m}$ (mm) <sup>+</sup>
Code 101 / 301 (bf=750mm) 75% failure load: P= 2079 kN	0.1975	0.0550
Code 201 / 401 (bf=875mm) 75% failure load: P= 2078 kN	0.1336	0.0514

\*Maximum crack width along the entire girder

<sup>+</sup>Average crack width along the entire girder

#### 5.1.4 Concluding remarks

From the analyses of the T-shaped prestressed girders and comparison with the experimental data provided in the Workshop, the following conclusions are drawn:

- Experimental failure mechanism was localized around the point of load application by crushing of the empty ducts
- The empty ducts were not accounted in the model; the fibre beam model is not able to capture localized failure modes; for that it is needed to go to 2D and 3D analyses;
- Considering the models of the other participants presented in the Workshop, the results of CONSHEAR were quite similar to some models performed with 2D and 3D NLFE simulations;
- CONSHEAR overestimated the experimental failure load in an average of 1.08, for a failure mechanism involving shear and flexural damage;
- The guidelines are difficult to apply to fibre beam elements as they are mainly thought to be used with 2D and 3D finite element simulations.

## 5.2 Cases of the DIANA User's Contest: large T-shaped prestressed concrete girders tested at TU Delft (Tests B – new load position)

In the original load configuration (2.95m from point load to the support), the beams presented local failure mechanism with crushing of the empty ducts localized in the top flanges to the girders. In an attempt to reach shear failure, in a second phase of the experimental campaign, the position of the load was changed to 2.35m from the support.

A new calculation was performed with this configuration using the exact same beam model, by only changing the position of the load. The girder with  $b_f=750$ mm was analysed. The analysis relate to average mechanical properties. The result of load vs. displacement under load is presented in

The predicted ultimate load is 3132.6 kN. Failure mechanism is still predicted as bending-shear related, with yielding of transversal reinforcement and crushing of concrete in the shear span. Stirrups are near yielding limit in the last converged load step. Computation time is around 1 minute.

Experimental results, when published, will used for comparison with the numerical predictions.

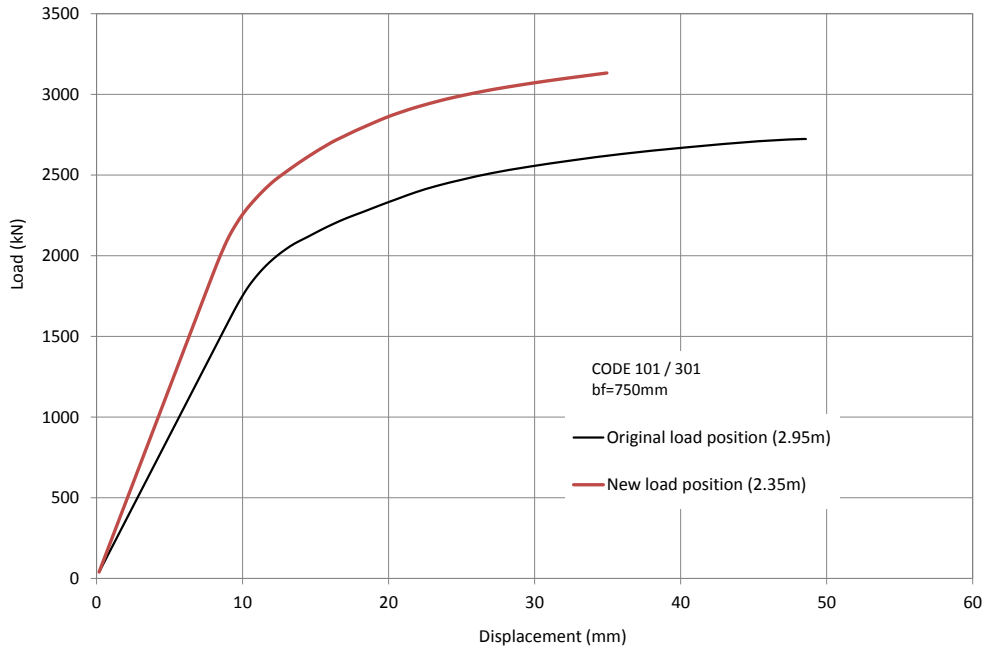


**Figure 5.2-1:** Case of DIANA User’s Contest. Load-deflection curves girder bf=750mm and (b) girder bf=875mm

### 5.3 Case OA1: Vecchio & Shim (2004)

The series of beams tested by (Vecchio and Shim 2004) in Toronto were a reproduction of the experiments by (Bresler and Scordelis 1963), as already mentioned in Point 3.1. Specimen OA1 is selected because it presents a shear brittle failure.

#### 5.3.1 Experimental setup and results

The beam has a total length of 4.1 m (span of 3.660 m), depth of 0.552 m and width of 0.305 m. The characteristics of the beam in terms of geometry, reinforcement, loading, boundary conditions and experimental setup are presented in Figure 5.3-1. The bottom longitudinal reinforcement is extended outside the beam and welded to thick plates.

The beam exhibited a diagonal-tension shear failure mode (Figure 5.3-2) with a clear maximum in the load-deflection response. The experimental ultimate value of applied load was equal to  $P_{EXP} = 331$  kN at a deflection of 9.1 mm.

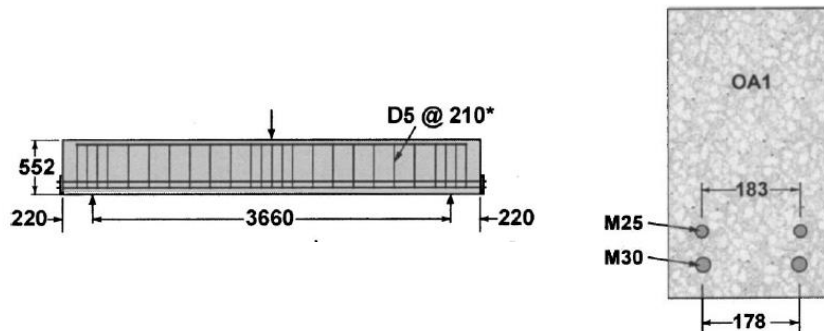


**Figure 5.3-1:** Case OA1. Dimensions, cross section and experimental setup (dimensions in mm) (Vecchio & Shim 2004)

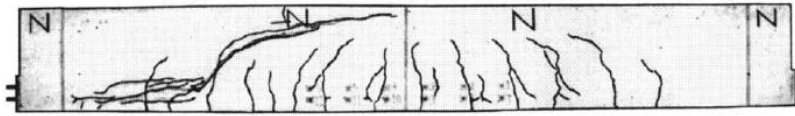


**Figure 5.3-2:** Case OA1. Failure mechanisms observed at ultimate applied load (Vecchio & Shim 2004)

### 5.3.2 Finite element model

The characteristics of the model are presented in

Figure 5.3-3; the beam was discretized into 20 FEs and 21 nodes (constant length of the beam elements of 0.183 m). The cross section was divided into fibres with 0.013 – 0.016 m of width; steel filaments were simulated according to their positions in the beam (2xM25 and 2xM30) and shear reinforcement is null ( $\rho_{sw}=0.0\%$ ). Apart from the concrete cover, all the fibres were considered shear resistant.

Regarding the material properties, the values given in the paper for the concrete and steel mechanical properties were used in the model as resumed in Table 5.3-1 for concrete and in Table 5.3-2 for steel.

Load (P) was applied as a nodal force, in an incremental form until failure in approximately 90 load steps. Energetic tolerance considered was  $1 \times 10^{-3}$  and updated normal plane switch on in the advanced loading steps. Computation time takes around 1 minute.

As the beam has no shear reinforcement and is shear critical presenting a brittle failure, the choice of the tension softening curve will be an important factor in the results. Hence two curves were considered in the simulations, as presented in Figure 5.3-4, representing top and bottom levels for the softening curve in tension.

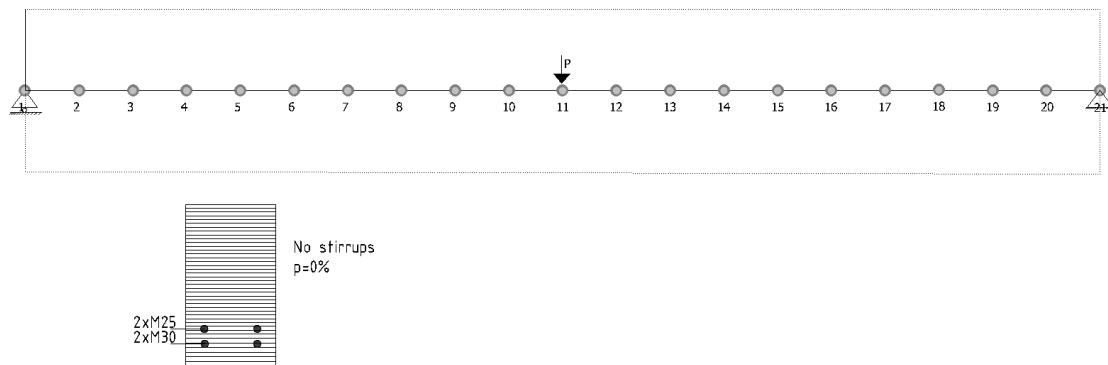


Figure 5.3-3: Case OA1. Mesh of the model

**Table 5.3-1:** Case OA1. Constitutive properties for concrete

	$f_{cm}$ ( $N/mm^2$ )	$f_{ctm}$ ( $N/mm^2$ )	$E_c$ ( $N/mm^2$ )	$\epsilon_{cu}$
Mean measured values	22.6	2.37	36500	0.0035

**Table 5.3-2:** Case OA1. Reinforcement properties

Bar	$\Phi$ (mm)	$A_s$ (mm <sup>2</sup> )	$E_s$ (N/mm <sup>2</sup> )	$f_{ym}$ (N/mm <sup>2</sup> )	$f_{um}$ (N/mm <sup>2</sup> )	$\epsilon_{su}^*$	$E_{sy}^*$ (N/mm <sup>2</sup> )
M25	25.2	500	220000	445	680	0.05	6000
M30	29.9	700	200000	436	700	0.05	6000

\*assumed values

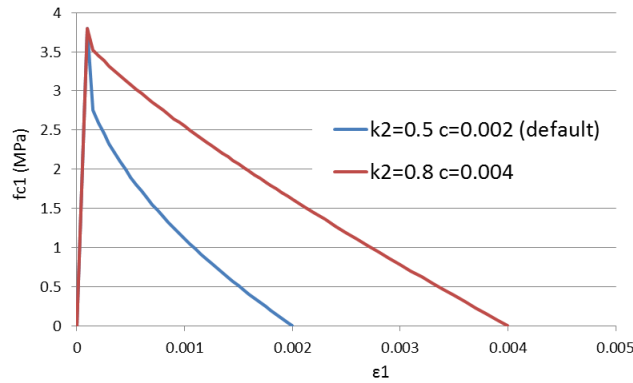


**Figure 5.3-4:** Case OA1. Softening of concrete in tension considered in the model CONSHEAR (Tension stiffening equation of Cervenka)

### 5.3.3 Nonlinear finite element analysis

The load – deflection curve is presented in Figure 5.3-5 and with the experimental curve and calculations with the DSFM method (Vecchio & Shim 2004). The results at failure are resumed in Table 5.3-3.

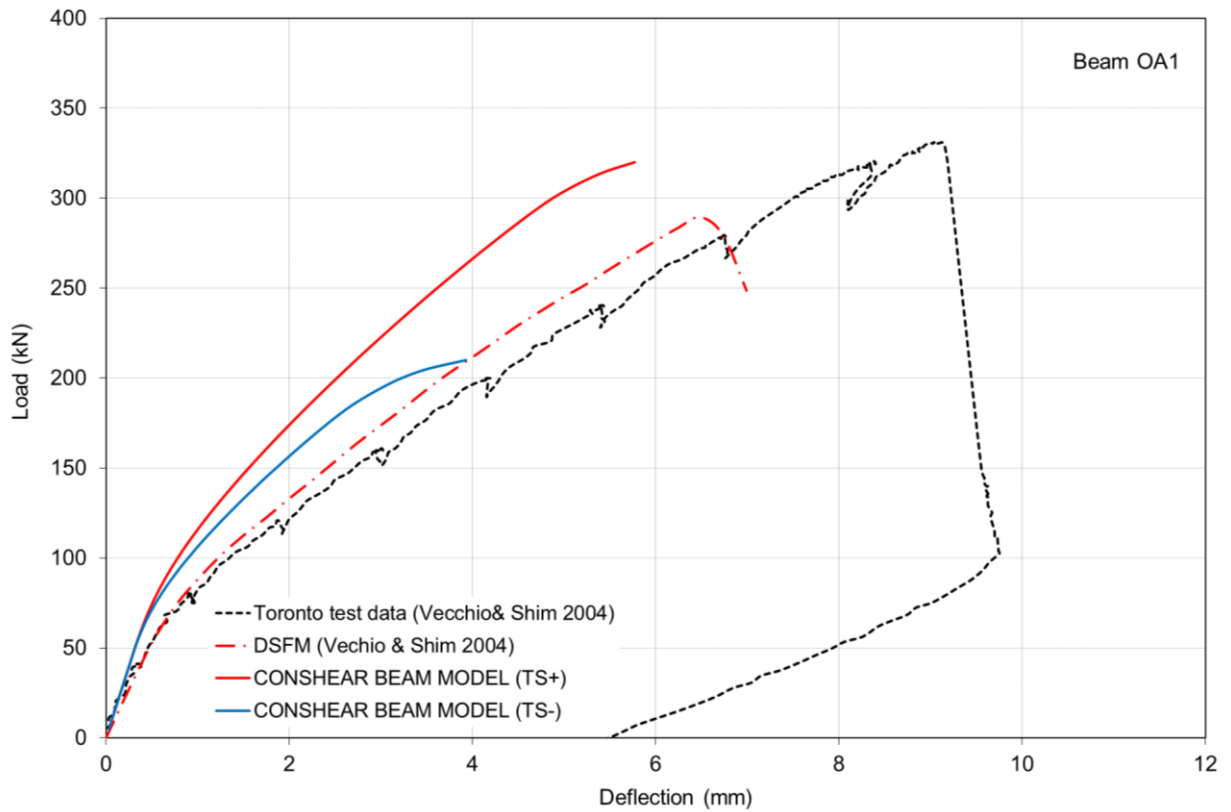


**Figure 5.3-5:** Case OA1. Load-deflection curves

**Table 5.3-3:** Case OA1. Results of the NLFEA

Level of damage	CONSHEAR Beam element (TS+)	CONSHEAR Beam element (TS-)	DSFM (Vecchio & Shim 2004)	Experimental (Vecchio & Shim 2004)
Peak load (kN)	320	210	316	334
Failure	Shear	Shear	Shear	Shear
Computation time	1 minute	1 minute	No data	

It can be observed that the tension stiffening curve has a great influence on the ultimate maximum load computed by the CONSHEAR model; acceptable results of failure load were only achieved with higher values for the tension stiffening curve. CONSHEAR predicted crushing of concrete, with the longitudinal reinforcement remaining elastic. The calculation with the DSFM method (performed by Vecchio and Shim 2004) presented a better fitting with the experimental response. In general, CONSHEAR presented a stiffer response in comparison with the measured behaviour.

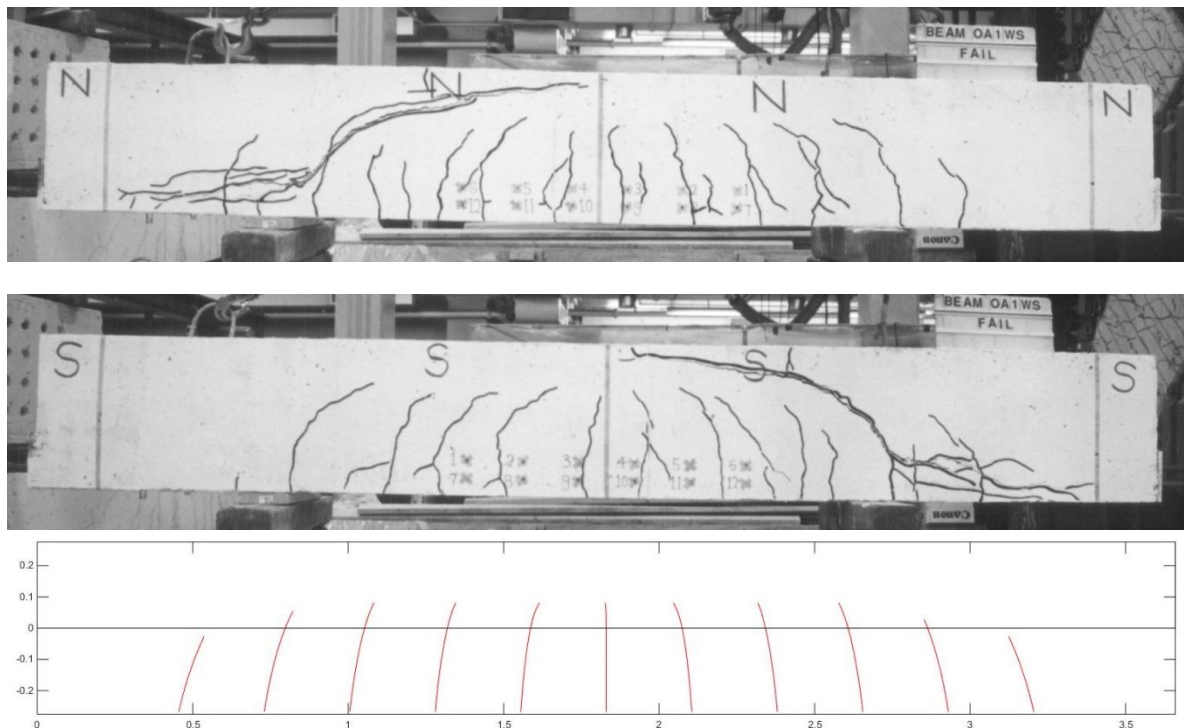
### Crack patterns

Computed cracking patterns at load near failure are compared with experimental observations.

The required information for the algorithm for representation of cracking is considered as:

- $S_{rm}=275$  (EC2  $S_{rmax}=467\text{mm} / 1.7$  (average factor) = 247.7 mm)
- $f_{ct} = 2.37$  MPa
- $E_c = 36500$  MPa
- First crack:  $x = 1.83$  m
- $l = 3.66$  m
- $h = 0.552$  m

It can be observed that the inclination of the cracks predicted by the numerical model is consistent with the observations.

**Figure 5.3-6:** Case OA1. Crack pattern at failure

The predicted crack patterns are represented in Figure 3.3-10 for the load levels of approximately 50%, 70%, 90% of the failure load and ultimate load.

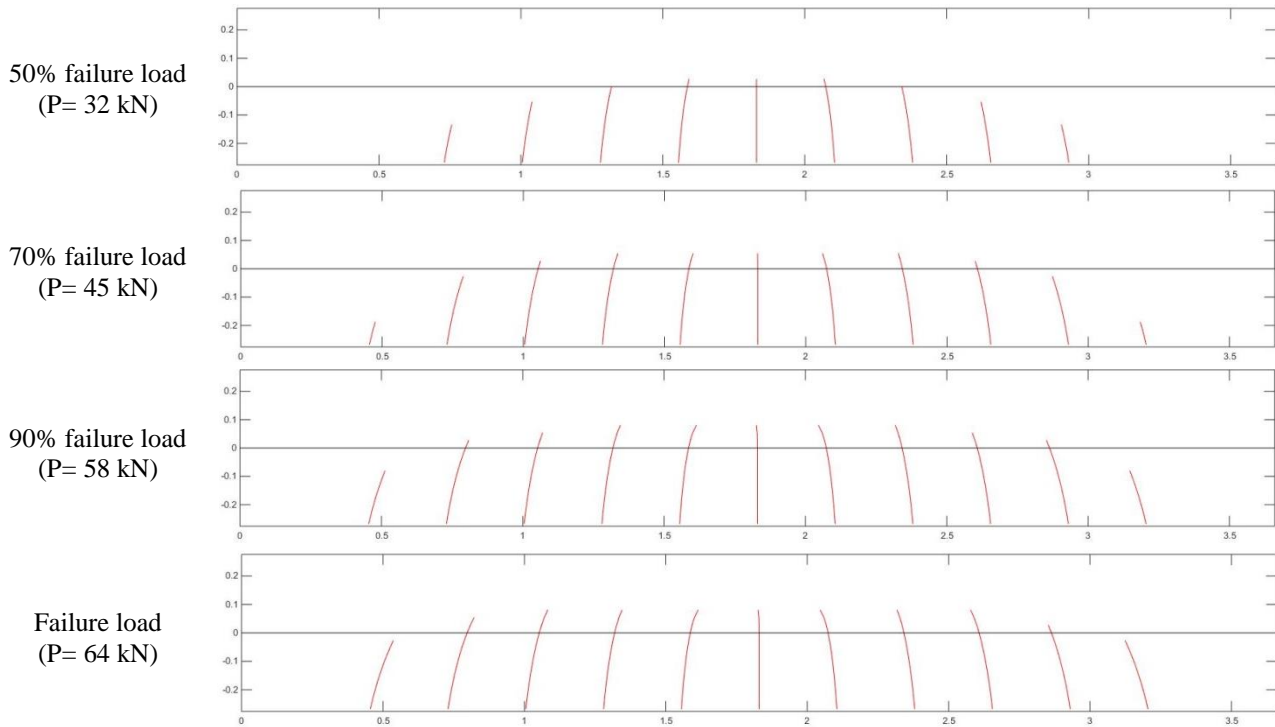


**Figure 5.3-7:** Case OA1. Predicted crack patterns

#### 5.3.4 Concluding remarks

From the analysis of the OA1 test (benchmark failing in brittle shear) with CONSHEAR and comparison with experimental data from (Vecchio & Shim 2004), the following conclusions are pointed out:

- As the beam has no transversal reinforcement and presents brittle shear failure, the results of ultimate load depend on the curve of tension-stiffening adopted in CONSHEAR model;
- This dependency is analogous to the one in 2D / 3D FE models computing beams failing in brittle shear, where the result of ultimate loading will depend on the value considered for the energy of fracture and constitutive treatment of cracking;
- CONSHEAR predicted shear failure by failure of the web around the mid-span cross section;
- For the case of considering higher tension stiffening, the predicted ultimate load is similar to the experimental result;
- The numerical results from CONSHEAR present a stiffer response when compared with the experimental behaviour and also with the DSFM calculations.

### 5.4 Case OA3: Vecchio & Shim (2004)

Specimen OA3 of the series of beams tested by (Vecchio and Shim 2004) in Toronto, is selected because it presents a shear critical failure.

#### 5.4.1 Experimental setup and results

The beam has a total length of 6.840 m (span of 6.4), depth of 0.552 m and width of 0.305 m. The characteristics of the beam in terms of geometry, reinforcement, loading, boundary conditions and

experimental setup are presented in Figure 5.4-1. The bottom longitudinal reinforcement is extended outside the beam and welded to thick plates.

The beam exhibited a diagonal-tension shear failure mode (Figure 5.4-2) with a clear maximum in the load-deflection response. The experimental ultimate value of applied load was equal to  $P_{EXP} = 385$  kN at a deflection of 32.4 mm.

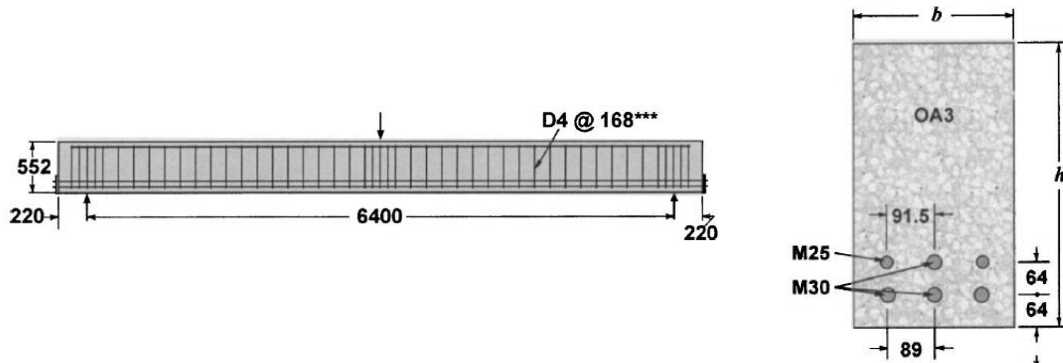


**Figure 5.4-1:** Case OA3. Dimensions, cross section and experimental setup (dimensions in mm), (Vecchio & Shim 2004)



**Figure 5.4-2:** Case OA3. Failure mechanisms observed at ultimate applied load, (Vecchio & Shim 2004)

#### 5.4.2 Finite element model

The characteristics of the model are presented in Figure 5.4-3; the beam was discretized into 32 FEs and 33 nodes (constant length of the beam elements of 0.2 m). The cross section was divided into fibres with 0.013 – 0.016 m of width; steel filaments were simulated according to their positions in the beam (2xM25 and 4xM30) and shear reinforcement is null ( $\rho_{sw}=0.0\%$ ). Apart from the concrete cover, all the fibres were considered shear resistant.

Regarding the material properties, the values given in the paper for the concrete and steel mechanical properties were used in the model as resumed in Table 5.4-1 for concrete and in Table 5.4-2 for steel.

Load (P) was applied as a nodal force, in an incremental form until failure in approximately 90 load steps. Energetic tolerance considered was  $1 \times 10^{-3}$  and updated normal plane switch on in the advanced loading steps. Computation time takes around 1 minute.

As in the same manner as Case OA1, as the beam has no shear reinforcement and is shear critical presenting a brittle failure, the choice of the tension softening curve will be an important factor in the results. Hence, too curves were again considered in the simulations, as presented in Figure 5.4-4.

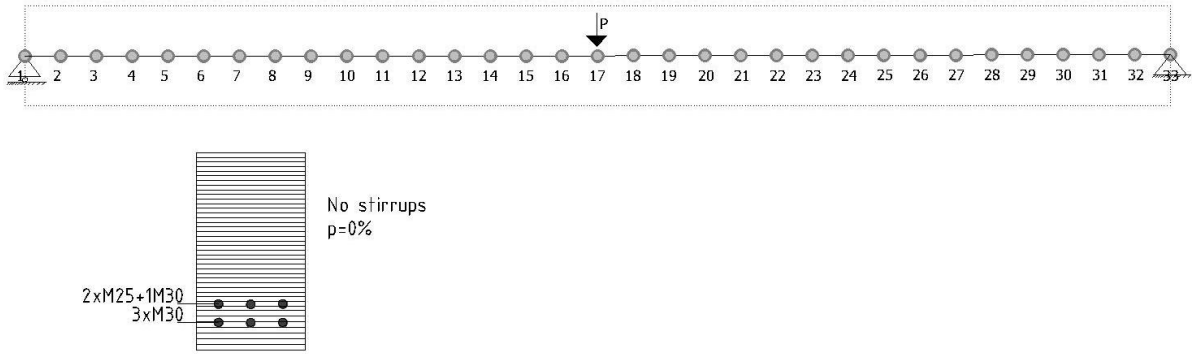


**Figure 5.4-3:** Case OA3. Mesh of the model

**Table 5.4-1:** Case OA3. Constitutive properties for concrete

	$f_{cm}$ (N/mm <sup>2</sup> )	$f_{ctm}$ (N/mm <sup>2</sup> )	$E_c$ (N/mm <sup>2</sup> )	$\epsilon_{cu}$
Mean measured values	43.5	3.13	34300	0.0035

**Table 5.4-2:** Case OA3. Reinforcement properties

Bar	$\Phi$ (mm)	$A_s$ (mm <sup>2</sup> )	$E_s$ (N/mm <sup>2</sup> )	$f_{ym}$ (N/mm <sup>2</sup> )	$f_{um}$ (N/mm <sup>2</sup> )	$\epsilon_{su}^*$	$E_{sy}^*$ (N/mm <sup>2</sup> )
M25	25.2	500	220000	445	680	0.05	6000
M30	29.9	700	200000	436	700	0.05	6000

\*assumed values

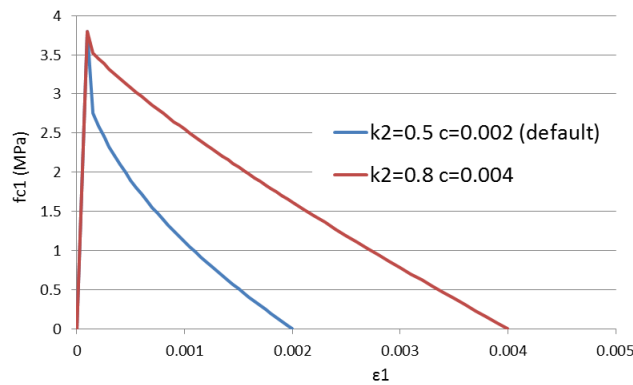


**Figure 5.4-4:** Case OA3. Softening of concrete in tension considered in the model CONSHEAR (Tension stiffening equation of Cervenka)

### 5.4.3 Nonlinear finite element analysis

The load – deflection curve is presented in Figure 5.4-5 and compared with the experimental curve and calculations with the DSFM method (Vecchio & Shim 2004). The results at failure are resumed in Table 5.4-3.

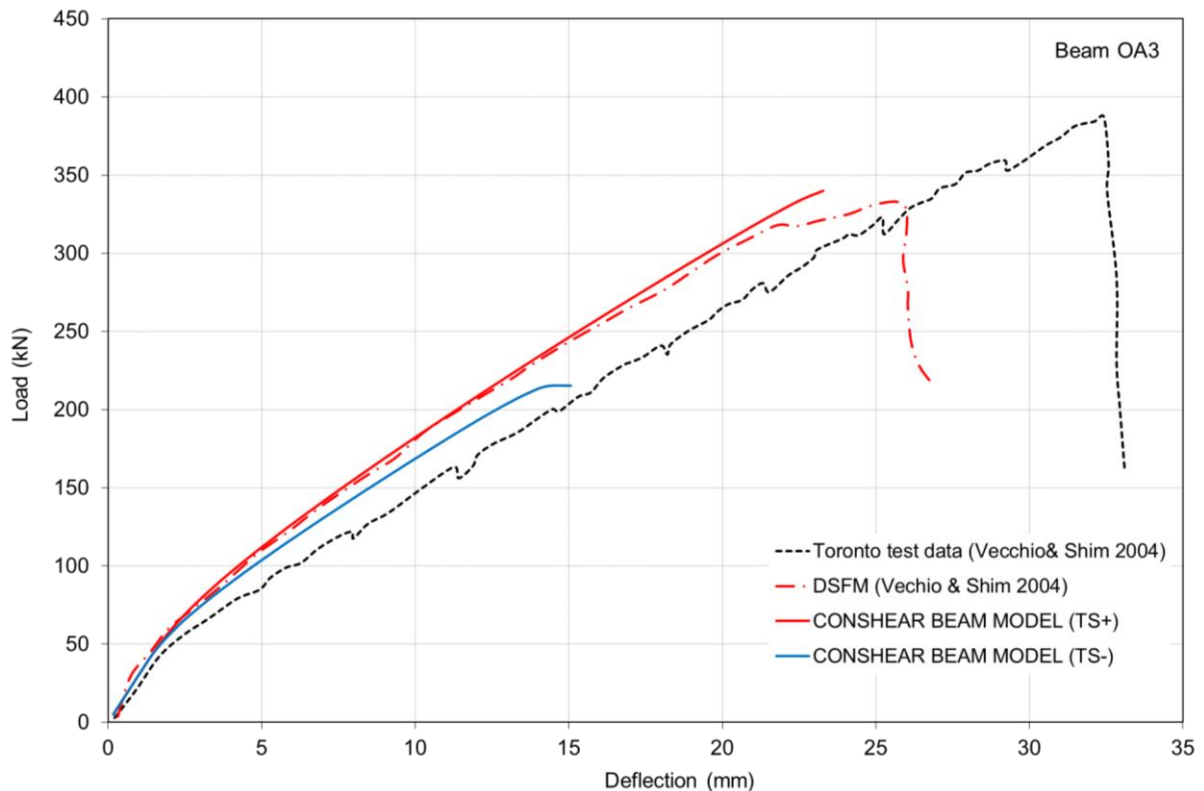


Figure 5.4-5: Case OA3. Load-deflection curves

Table 5.4-3: Case OA3. Results of the NLFEA

Level of damage	CONSHEAR Beam element (TS+)	CONSHEAR Beam element (TS-)	DSFM (Vecchio & Shim 2004)	Experimental (Vecchio & Shim 2004)
Peak load (kN)	340	215.3	294	378
Failure	Shear	Shear	Shear	Shear
Computation time	1 minute	1 minute	No data	

Similarly to what was observed in Case OA1, tension stiffening plays a key role in the ultimate failure load. Again, acceptable results were obtained with higher tension stiffening. In this case, the load-deflection curve was very similar to the one determined by the DSFM method by Vecchio & Collins 2004. Both models predicted lower failure load in comparison with the experimental value. In failure, CONSHEAR presents failure of concrete, with the longitudinal reinforcement remaining elastic until maximum load.

Computed cracking patterns at load near failure are compared with experimental observations. The required information for the algorithm of cracking representation is considered as:

- $S_{rm}=226$  (EC2  $S_{rmax}=384\text{mm} / 1.7$  (average factor) = 384 mm)
- $f_{ct} = 3.13$  MPa
- $E_c = 34300$  MPa
- First crack:  $x = 3.2$  m
- $l = 6.4$  m
- $h = 0.552$  m

It can be observed that the inclination of the cracks predicted by the numerical model is consistent with the observed secondary cracks; the model is not capable of capturing the main diagonal crack that lead to failure.

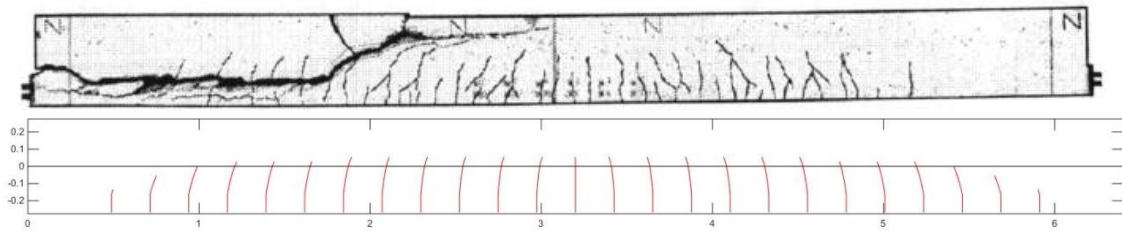


**Figure 5.4-6:** Case OA3. Crack patterns at failure

The predicted crack patterns are represented in Figure 3.3-10 for the load levels of approximately 50%, 70%, 90% of the failure load and ultimate load.

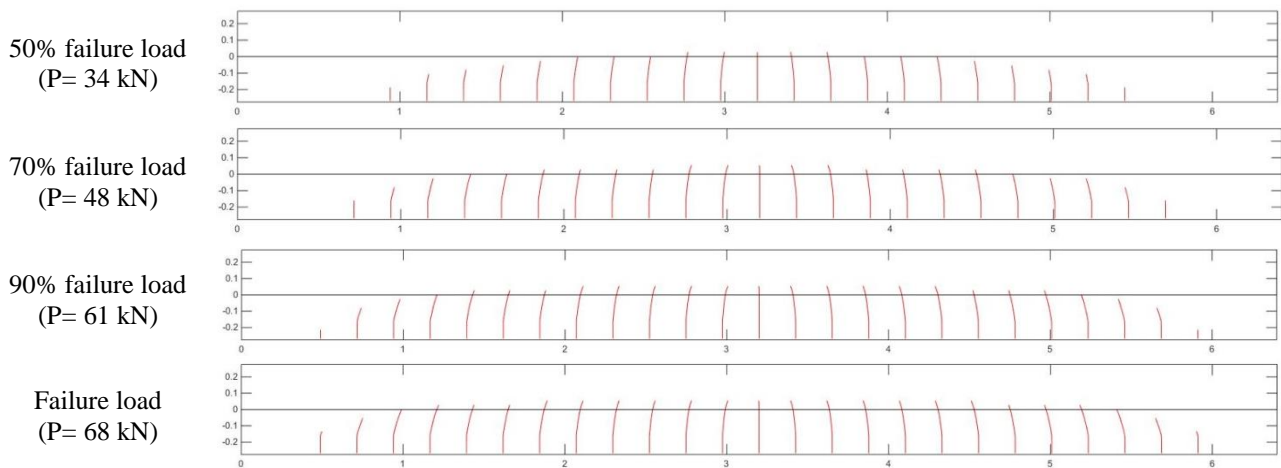


**Figure 5.4-7:** Case OA3. Predicted crack patterns

#### 5.4.4 Concluding remarks

From the analysis of the OA3 test (benchmark failing in shear) with CONSHEAR and comparison with experimental data (Vecchio & Collins) the following conclusions are pointed out:

- CONSHEAR models predicted shear failure by the concrete in the mid shear-span area with longitudinal reinforcement remaining elastic, which is consistent with the experimental observations;
- CONSHEAR model with higher tension stiffening presents very similar results to the DSFM calculations and also similar to the experimental data;
- CONSHEAR with lower tension stiffening predicts shear failure for a lower ultimate load.

## 6 CONCLUSIONS AND FUTURE WORK

### 6.1.1 Summary of results

This report started with a brief insight into the motivations of this research work and the general description of the shear-sensitive fibre beam model. Subsequently, this work presented a systematic comparison between computations of the CONSHEAR beam model (UPC) and the plane stress model in DIANA and experimental data for various cases of beam tests.

The analysed benchmarks include the cases already analysed with DIANA plane stress models by Hendriks, Belletti et al. 2015: four reinforced beams (2 failing in bending and 2 in shear) and three prestressing beams (1 failing in bending and 2 in shear). Also, new benchmarks were studied with the CONSHEAR beam model, that included the prestressed beams from the DIANA User's Contest and two classical beams failing in brittle shear. The comparison was made in terms of load-displacement curves until failure, failure mechanisms, development of damage and, in some cases, crack patterns.

Table 3.4-1 presents a resume of results at failure, comparing numerical and experimental data. Whenever there is more than one experimental result, the average value is considered. Whenever there is more than one model, the best result is considered in this table. The failure mechanism is presented with a symbol representing its fitting with the experimental observations: ✓ in case of correct fitting, ✗ in case of incorrect fitting. Shear DC stands for shear diagonal compression, and Shear DT means shear diagonal tension.

**Table 5.4-1:** Results of simulations at failure

	Case study	Results at failure	CONSHEAR Beam element	DIANA Plane stress	DIANA Beam element
Recalculation RC beams	RB1: Vecchio & Shim 2004	Load ( $P_{u,num}/P_{u,exp}$ )	1.02	1.05	1.06
		Mechanism	Bending✓	Bending✓	Bending✓
		Computation time	1-2 minutes	1h	<1 minute
	RB2: Collins & Kuchma 1999	Load ( $P_{u,num}/P_{u,exp}$ )	0.99	1.00	4.44
		Mechanism	Shear DC✓	Shear DC✓	Bending✗
		Computation time	3 minutes	2h	<1 minute
	RB3: Grace 2001	Load ( $P_{u,num}/P_{u,exp}$ )	1.04	1.05	-
		Mechanism	Bending✓	Bending✓	-
		Computation time	2 minutes	1h	-
RB3A: Grace 2001	Load ( $P_{u,num}/P_{u,exp}$ )	0.86	0.94	-	
	Mechanism	Shear-bending✓	Shear-bending✓	-	
	Computation time	2 minutes	1h	-	
Recalculation PC beams	PB1: Leonhardt, Koch et al. 2007	Load ( $P_{u,num}/P_{u,exp}$ )	1.03	1.03	-
		Mechanism	Bending✓	Bending✓	-
		Computation time	2 minutes	1h30min	-
	PB2/NSEL: Sun and Kuchma 2007	Load ( $P_{u,num}/P_{u,exp}$ )	0.85	1.04	-
		Mechanism	Shear✓	Shear DC✓	-
		Computation time	30 minutes	5h	-
	PB3/MnDOT: Runzell et al. 2007	Load ( $P_{u,num}/P_{u,exp}$ )	0.99	0.91	-
		Mechanism	Shear✓	Shear DT✓	-
		Computation time	15 minutes	1h30min	-

New case studies	DIANA User's Contest (1) Mid-beam	Load ( $P_{u,num}/P_{u,exp}$ )	1.05	-	-
		Mechanism	Shear-bending*	-	-
		Computation time	3 minutes	-	-
	DIANA User's Contest (1) Edge-beam	Load ( $P_{u,num}/P_{u,exp}$ )	1.11	-	-
		Mechanism	Shear-bending*	-	-
		Computation time	3 minutes	-	-
	DIANA User's Contest (2)	Load ( $P_{u,num}/P_{u,exp}$ )	-	-	-
		Mechanism	Shear-bending	-	-
		Computation time	1 minute	-	-
	Case OA1: Vecchio & Shim 2004	Load ( $P_{u,num}/P_{u,exp}$ )	0.96	-	-
		Mechanism	Shear✓	-	-
		Computation time	1 minute	-	-
	Case OA3: Vecchio & Shim 2004	Load ( $P_{u,num}/P_{u,exp}$ )	0.90	-	-
		Mechanism	Shear✓	-	-
		Computation time	1 minute	-	-

From the several analyses performed, the following general conclusions are drawn:

- CONSHEAR gave quite similar predictions of failure load and mechanism in comparison with the plane stress model in DIANA, including different types of failure modes: bending, shear-compression and shear-tension.
- CONSHEAR tend to overestimate the strains and stresses in the transversal reinforcement; which is a direct consequence of the simplification assumption of the fixed shear stress pattern along the cross section considered in the formulation. This fact was observed in the comparisons of results with the plane stress models in DIANA: CONSHEAR presented the start of yielding of stirrups for lower loads in various cases.
- CONSHEAR considers strength enhancement factor for biaxial compression; which was not accounted in the plane stress models in DIANA. This lead to a latter crushing of concrete in CONSHEAR predictions, observed in the majority of the cases studied.
- For the bending cases, CONSHEAR and plane stress models in DIANA gave very similar results of the nonlinear load-displacement curve throughout the loading path and ultimate load (cases RB1, RB3 and PB1).
- For the shear cases, there were some with good fitting with DIANA and with experimental data (cases RB2, RB3A); and other with some differences, where CONSHEAR presented less stiffness then DIANA plane stress models and experimental results for advance load levels (cases PB2, PB3).
- For the new brittle shear cases (OA1 and OA3), CONSHEAR predicted lower failure load in comparison with experimental.
- Softening of concrete in tension is a key factor in CONSHEAR for beams without transversal reinforcement and failing in brittle shear. The model uses a tension stiffening curve based on empirical work (Cervenka equation). This parameter influences the ultimate load and also the load-displacement response along the nonlinear path. This is analogous to the influence of the energy of fracture of concrete in tension in plane stress models.
- CONSHEAR does not capture clearly post-peak behaviour.
- In the bending case (RB1), DIANA 2D beam elements with default integration points (3 points, Simpson integration) underestimated the peak load and the start of the levels of damage. DIANA 2D beam elements of Class II and Class III gave good results, very similar

to DIANA plane stress, CONSHEAR model and experimental results, whenever a higher number of integration points along the height of the cross section is considered (11 points, Simpson integration).

- All beam models in DIANA are pure bending based, hence are not capable of capturing shear failure modes, overpassing it, and continue the analysis until complete bending capacity is achieved; this results into unsafe estimations of ultimate load for beams critical to shear. This was clearly observed in the analysis of case RB2.
- The advantage of CONSHEAR as a ‘quick scan method’ does not only lay in the low computation time, but in the fact that is easy to do the model, handling few parameters and few details. As it is a simplified approach that determines the overall structural response, details on support and load application plates are not modelled. Stirrups are considered as a smeared percentage of transversal steel, and not simulated as individual bar elements. The simplifications used in the beam model allow performing large structural analysis at low modelling effort and computation cost. However, the model is not able to capture localized responses or other mechanisms that are not represented by beam formulations (like strut and tie mechanisms). The model can be attractive for first evaluation of the global structural response by means of nonlinear FE analysis before passing to more sophisticated numerical tools.
- In case of the DIANA contest tests (with load at the original position), the failure mechanism observed was related with local flexural failure around weak points of the top flange of the girders, which is not possible to be predicted with the beam type model.

### 6.1.2 Remarks

In terms of the continuation of the project, and after conclusion of this first stage, the following annotations are made:

#### For the validation:

- Compare one of each shear cases (RB and PB) with DIANA plane stress models, more deeply in terms of strains and stresses in the various materials and, when possible, with experimental data.

#### For the new implementation in DIANA:

- The sectional model will be linked to the various constitutive laws in DIANA; try use tension softening in concrete linked to the energy of fracture and tension stiffening linked to the constitutive law of steel;
- Try to use the advanced solution methods in DIANA to see if the analysis continues in the post-peak regime;
- Use some of cases studied in this report to validate the implementation in DIANA and to evaluate the new enhancements stated above.

#### For the new pre/post processing in DIANA:

- Stirrups will be included in the beam elements in DIANA, which will be a new input, and the strains and stresses in the stirrups along the height of the cross section will be a new output.
- It will be required to print the results along the various integration points (fibres) along the height of the cross section, and not only in the extreme fibres (as it is now, because is the more relevant for bending analysis); this will include principal strains and stresses in concrete.

## **Acknowledgments**

The author would like to thank the funding provided by the Dutch Ministry of Infrastructure and the Environment, Rijkswaterstaat, that allowed the development of this research work.

**REFERENCES**

- Bairán, J. and A. Marí (2006). "Coupled model for the non-linear analysis of anisotropic sections subjected to general 3D loading. Part 1: Theoretical formulation." *Computers & Structures* 84: 2254-2263.
- Bairán, J. and A. Marí (2006). "Coupled model for the non-linear analysis of anisotropic sections subjected to general 3D loading. Part 2: Implementation and validation." *Computers & Structures* 84: 2264-2276.
- Bairán, J. and A. Marí (2007). "Shear-bending-torsion interaction in structural concrete members: a nonlinear coupled sectional approach." *Arch Comput Methods Eng* 14(3): 249-278.
- Bazant, Z. (1983). "Comment on orthotropic models for concrete and geomaterials." *Journal of Eng Mechanics* 109(3): 849-865.
- Bazant, Z. (1988). *Mathematical modeling of creep and shrinkage of concrete.*, John Wiley and Sons.
- Bazant, Z. P. and S. T. Wu (1973). "Dirichlet series creep function for aging concrete." *Journal of Eng Mechanics* 99(2): 367-387.
- Bresler, B. and A. C. Scordelis (1963). "Shear strength of reinforced concrete beams." *Journal American Concrete Institute* 60(1): 51-72.
- CEB Bulletin N0 237 (1997). *Concrete Tension and Size Effects - Utilisation of concrete tension in structural concrete design and relevance of size effect - Contributions from CEB Task Group 2.7.* Lausanne, Switzerland.
- Cervenka, V. (1985). "Constitutive model for cracked reinforced concrete." *ACI Journal* 82(6): 877-882.
- Chong, K. T. C., et al. (2008). "Time-dependent modelling of RC structures using the cracked membrane model and solidification theory." *Computers & Structures* 86: 1305-1317.
- Collins, M. P. and D. Kuchma (1999). "How safe are our large, lightly reinforced concrete beams, slabs and footings?" *ACI Structural Journal* 96(4): 347-358.
- CPH (2008). *Instrucción de Hormigón Estructural (EHE-08).* M. d. Fomento.
- Crisfield, M. A. (1996). *Non-linear finite element analysis of solids and structures, Vol1.*, John Wiley & Sons.
- Ferreira, D. (2013). *A model for the nonlinear, time-dependent and strengthening analysis of shear critical frame concrete structures.* Departament D'Enginyeria de la Construcció. Barcelona, Universitat Politècnica de Catalunya. Escola Tècnica Superior d'Enginyers de Camins, Canals i Ports. PhD Thesis.
- Ferreira, D., et al. (2014). Nonlinear FE analysis of a full scale in situ test on a RC bridge by means of a 1D layered frame model. EURO-C 2014, Computational Modelling of Concrete and Concrete Structures. I. 978-1-138-00145-9. St. Anton am Alberg, Austria: 917-925
- Ferreira, D., et al. (2013). "Numerical simulation of shear-strengthened RC beams." *Engineering Structures* 46: 359-374.
- Ferreira, D., et al. (2015). "Efficient 1D model for blind assessment of existing bridges: simulation of a full scale loading tests and comparison with higher order continuum models." *Structure and Infrastructure Engineering* DOI:10.1080/15732479.2014.964734 (published online).

- Ferreira, D., et al. (2014). "Shear strengthening of RC beams by means of vertical prestressed reinforcement." *Structure and Infrastructure Engineering* DOI: 10.1080/15732479.2015.1019893 (published online).
- Ferreira, D., et al. (2015). "Time-dependent behaviour of shear critical frames." *Materials and Structures*, pre-print under review.
- Ferreira, D., et al. (2014). "Nonlinear analysis of RC beams using a hybrid shear-flexural fibre beam model." *Engineering Computations* 31(7): 1444-1483.
- Ferreira, D., et al. (2014). "Thermo-mechanical simulation of the ConCrack Benchmark RL1 test with a filament beam model." *Engineering Structures* 73: 143-159.
- Ferreira, D., et al. (2013). "Assessment of prestressed concrete bridge girders with low shear reinforcement by means of a non-linear filament frame model." *Structure and Infrastructure Engineering* published in Taylor & Francis Online, DOI:10.1080/15732479.2013.834944, (published online).
- Ferreira, D., et al. (2015). "Shear strain influence in the service response of FRP reinforced concrete beams." *Composite Structures* 121: 142-153.
- Ferreira, D., et al. (2013). "Numerical analysis of shear critical RC beams strengthened in shear with FRP sheets." *Journal of Composites for Construction* 17( 6): Article number, 04013016, pp. 04013011-04013011.
- Grace, N. F. (2001). "Strengthening of Negative Moment Region of Reinforced Concrete Beams Using Carbon Fiber-Reinforced Polymer Strips." *ACI Structural Journal* 98( 3): 347-358.
- Kupfer, H., et al. (1969). "Behavior of concrete under biaxial stresses." *ACI Journal* 66(8): 656-666.
- Leonhardt, F., et al. (1973). *Schubversuche an Spannbetongagern*. D. A. f. Stahlbeton. Berlin.
- Marí, A. R. B. (2000). "Numerical simulation of the segmental construction of three dimensional concrete frames." *Engineering Structures* 22: 585-596.
- Mohr, S., et al. (2010). "A frame element model for the analysis of reinforced concrete structures under shear and bending." *Engineering Structures* 32(12): 3936-3954.
- RTD1016 (2012). *Guidelines for Nonlinear Finite Element Analysis of Concrete Structures. Scope: Girder Members*. D. RTD.
- RTD1016b (2015). *Validating the Guidelines for Nonlinear Finite Element Analysis of Concrete Structures*. D. RTD. Authors: Hendriks, M.A.N., Belletti, B., Damoni, C., de Boer, A.
- Runzell, B., et al. (2007). *Shear capacity of prestressed beams*, Minnesota Department of transportation Research Services Section.
- Sun, S. and D. Kuchma (2007). *Shear behavior and capacity of large- scale prestressed high- strength concrete bulb- tee girders*. N. Report No. NSEL-002, Department of Civil and Environment Engineering University of Illinois at Urbana- Champaign.
- Van Greunen, J. (1979). *Nonlinear geometric, material and time dependent analysis of reinforced and prestressed concrete slabs and panels*. Structures and Materials Research, Department of Civil Engineering. College of Engineering. University of California. Berkeley, California.
- Vecchio, F. J. and M. P. Collins (1986). "The modified compression-tension theory for reinforced concrete elements subjected to shear." *ACI Journal* 83(2): 1357-1417.
- Vecchio, F. J. and M. P. Collins (1993). "Compression response of cracked reinforced concrete." *ASCE Journal of Structural Engineering* 91(2): 261-268.

Vecchio, F. J. and W. Shim (2004). "Experimental and analytical reexaminations of classic concrete beam tests." *Journal of Structural Engineering* 130(3): 460-469.

Zararis, I. P., et al. (2006). "Shear strength of reinforced concrete T-beams." *ACI Journal* 103(5): 693-700.

Zienkiewicz, O. C. and R. L. Taylor (2004). *The finite element method. The basis.* . Barcelona, CIMNE.

Zwicky, D. and T. Vogel (2000). *Failure tests on dismantled prestressed concrete bridge girders* (in German). Institute of Structural Engineering IBK. Zurich, Swiss Federal Institute of Technology ETH.